



Università degli Studi di Palermo

SCUOLA POLITECNICA

Dipartimento di Ingegneria Civile, Ambientale, Aerospaziale, dei Materiali
Dottorato in Ingegneria Civile e Ambientale
Ciclo XXIX
Coordinatore: Prof. Mario Di Paola

PH.D. THESIS

**Mechanical characterisation and
3D fractional viscoelastic modelling of
railway sub-ballast rubberised asphalt**

Candidato:
Ing. Natalia Colinas-Armijo

Relatori:
Ch.mo Prof. Mario Di Paola

Ill.mo Prof. Gaetano Di Mino

NATALIA COLINAS-ARMIJO
Palermo, September 2017
e-mail:natalia.colinasarmijo@unipa.it
e-mail:nataliacolinasarmijo@gmail.com

Thesis of the Ph.D. course in *Roads, Railways and Airports & Structural Engineering*
Dipartimento di Ingegneria Civile Ambientale, Aerospaziale, dei Materiali
Università degli Studi di Palermo
Scuola Politecnica
Viale delle Scienze, Ed.8 - 90128 Palermo, ITALY

Written in L^AT_EX
Examples and figures made with *Wolfram Mathematica 11*[©]

*"- How long is forever?
- Sometimes, just one second."¹*

¹ Lewis Carroll, "Alice in Wonderland".

Contents

Introduction	xiii
1 Fractional calculus	1
1.1 History about fractional calculus and its applications	1
1.2 Fractional derivatives and integrals	3
1.2.1 Riemann-Liouville fractional operators	3
1.2.2 Caputo fractional derivative	5
1.2.3 Grünwald-Letnikov fractional operators	6
1.3 Properties of fractional operators	8
1.3.1 Properties	8
1.3.2 Laplace transform of fractional operators	10
1.3.3 Fourier transform of fractional operators	11
1.4 Step by step integration for fractional operators	13
1.4.1 Step-wise approximation	13
1.4.2 Piece-wise approximation	19
1.4.3 Numerical example	21
1.5 Conclusions	28
2 Linear fractional viscoelasticity	29
2.1 Linear viscoelasticity	29
2.1.1 Boltzmann superposition principle	30
2.2 Linear fractional viscoelasticity	32
2.3 Review of mechanical models	34
2.3.1 Classical models	34
2.3.2 Fractional models	40
2.4 Fractional characteristic times	42
2.4.1 Estimation of fractional characteristic times	45
2.4.2 Elastic and viscous contribution. Dissipated energy.	52

2.5	Conclusions	58
3	Railway sub-ballast rubberised asphalt	59
3.1	The use of recycled rubber in asphalt mixtures	59
3.1.1	Mix design of bituminous mixtures	61
3.1.2	Problem statement and objective	61
3.2	Mix design optimisation of bituminous mixtures with crumb rubber	62
3.2.1	Analytical approach - Correction factor	65
3.3	Maximun rubber content in asphalt mixtures	68
3.3.1	Physical or mathematical limit	68
3.3.2	Design limit	69
3.4	Rubberised asphalt for railway sub-ballast	71
3.4.1	Materials description	71
3.4.2	Correction factor calculation and sample preparation	73
3.4.3	Results and observations	75
3.5	Conclusions	77
4	3D fractional viscoelastic model for bituminous mixtures	79
4.1	3D fractional viscoelasticity	79
4.2	Triaxial tests for bituminous mixtures	83
4.2.1	Measurement and loading	84
4.3	Creep-recovery and cyclic test with triaxial measurements	86
4.3.1	Creep-recovery tests	86
4.3.2	Cyclic test	89
4.4	3D fractional model for crumb rubber asphalt	94
4.4.1	Model parameter fitting	100
4.5	Conclusions	101
5	Temperature effect on railway sub-ballast rubberised asphalt	103
5.1	Time temperature superposition principle	103
5.1.1	Classical horizontal shifting	105
5.1.2	Classical vertical shifting	106
5.2	Mathematical inconsistency of classical shifting in fractional viscoelasticity	107
5.2.1	Mathematical inconsistency of classical shifting in fractional viscoelasticity	108
5.3	Temperature effect on 3D fractional viscoelasticity	110
5.3.1	Time Temperature Superposition Principle approach	110

5.3.2	Step-by-step material parameter variation with temperature	112
5.4	Evaluation of the creep response and the temperature effect on railway sub-ballast rubberised asphalt	115
5.4.1	Material parameters variations with temperature	115
5.4.2	Creep response and temperature effect on railway sub-ballast made of bituminous mixtures	117
5.5	Conclusions	119
Concluding remarks		121
Bibliography		123
Acknowledgements		131

List of Figures

1.1	Step-wise approximation of $f(t)$	14
1.2	Fractional integrals for the step-wise approximation of $f(t)$. . .	15
1.3	Fractional derivatives for the step-wise approximation of $f(t)$. .	18
1.4	Piece-wise approximation of $f(t)$	19
1.5	Fractional derivatives for the piece-wise approximation of $f(t)$.	21
1.6	Fractional integral of $U(t)$	22
1.7	Fractional derivative of $U(t)$	24
1.8	Fractional integral of $\gamma + e^{-\beta t}$, exact solution versus R-L and G-L approaches.	25
1.9	Fractional derivative of $\gamma + e^{-\beta t}$, exact solution versus R-L and G-L approaches.	26
2.1	Boltzmann Superposition Principle.	31
2.2	Linear spring.	34
2.3	Dashpot.	35
2.4	Maxwell and KelvinVoigt models.	35
2.5	Creep and relaxation of the Maxwell model.	36
2.6	Creep and relaxation of the Kelvin Voigt model.	37
2.7	Zener and Standard Solid models.	37
2.8	Springpot element.	40
2.9	Fractional Maxwell and Kelvin Voigt models.	40
2.10	Fractional viscoelastic models for bituminous materials.	41
2.11	Fractional characteristic times versus α	44
2.12	Plot of dimensionless parameters μ_e and E_e versus α	48
2.13	Harmonic excitation (dashed line), response of fractional model (continuous line), equivalent Kelvin-Voigt model (dotted line). $\omega = 1$ rad/s, $\varepsilon_0 = 1$ and $E_\alpha = 1$	49

2.14	Periodic excitation (dashed line), steady-state response of the fractional model (continuous line), equivalent model (dotted line).	51
2.15	Hysteresis loop for harmonic excitation. Continuous line fractional model, dotted line equivalent Kelvin-Voigt model. $\omega = 1$ rad/s, $\varepsilon_0 = 1$ and $E_\alpha = 1$	54
2.17	Hysteresis loop for Periodic excitation. Continuous line fractional model, dotted line equivalent Kelvin-Voigt model. $\omega = 0.5$ rad/s, $n = 15$ and $E_\alpha = 1$	57
3.1	Schematic representation of the mix design of crumb rubber mixtures.	64
3.2	Compaction sample by layers.	65
3.3	Samples with different bitumen content.	75
3.4	Overcompaction problem in the gyratory compactor.	76
3.5	Slab compaction.	76
4.1	3D fractional viscoelastic model.	82
4.2	Triaxial test set-up.	83
4.3	Strain measurement systems.	85
4.4	Triaxial test sample load and measurements.	86
4.5	Creep-recovery test $\sigma_q = 200kPa$ and $\sigma_c = 0kPa$	87
4.6	Creep-recovery test $\sigma_q = 400kPa$ and $\sigma_c = 200kPa$	88
4.7	Longitudinal complex modulus and loss angle without confinement.	90
4.8	Transversal complex modulus and loss angle without confinement.	91
4.9	Longitudinal complex modulus and loss angle with confinement.	92
4.10	Transversal complex modulus and loss angle with confinement.	93
4.11	Imposed stress $\sigma_q(t)$	94
4.12	Longitudinal and transversal strain, $\varepsilon_L(t)$ and $\varepsilon_T(t)$, from triaxial measurements.	95
4.13	Volumetric and deviatoric decomposition of the strain.	96
4.14	Longitudinal and transversal deviatoric strain, $\varepsilon_{d_L}(t)$ and $\varepsilon_{d_T}(t)$	97
4.15	Volumetric strain, $\varepsilon_V(t)$	98
4.16	Poisson's ratio, $\nu(t)$	98
4.17	Experimental versus modelled longitudinal and transversal strain, $\varepsilon_L(t)$ and $\varepsilon_T(t)$	99

5.1	Parameter variation with temperature $\alpha(T)$, $G_\alpha(T)$, $\beta(T)$ and $K_\beta(T)$ for the reference asphalt.	115
5.2	Parameter variation with temperature $\alpha(T)$, $G_\alpha(T)$, $\beta(T)$ and $K_\beta(T)$ for the crumb rubber asphalt.	116
5.3	Temperature variations with time.	117
5.4	Longitudinal and transversal strain response under the temperature history $T(t)$ reported in Figure 5.3.	118

Introduction

Aims and reasons

The aim of this PhD thesis is to provide an advanced mathematical model for the analysis and the design of sustainable bituminous mixtures as railway sub-ballast. This mathematical tool is based on the Fractional Calculus, since this powerful branch of mathematics is used to model viscoelastic materials from the second part of the last century.

Fractional calculus is nothing else than a generalisation of the integer order derivatives and integrals. Fractional derivatives and integrals play an essential role in many branches of the physics and engineering problems (viscoelasticity, dynamical systems, control theory, electrical circuits,...). In the last years, theories of tridimensional viscoelastic constitutive laws based on fractional calculus (3D fractional viscoelasticity) have been proposed. That is the reason why the Fractional calculus is the first pillar of this thesis.

Sustainability is the second pillar of this thesis. Wasted materials and the shortage of some raw materials are becoming a real problem in our society. That is the reason why the Sustainable Pavements & Railways Initial Training Network (SUP&R ITN) project was created, where the aim of this PhD thesis was born. For this reason, this PhD thesis has been focused on the application of a wasted material (as used tyres). In particular, the application is to use a bituminous mixture that contains wasted tyres as railway sub-ballast. The sub-ballast is responsible for protecting the ground from the loads, reducing the vibrations, making the superstructure more resistant and increasing the comfort of the passengers inside the train.

Therefore, the challenge of the present PhD thesis is to combine Fractional Calculus and Sustainability. In particular, a methodology to design sustainable rubberised asphalt and a sophisticated mathematical model that allows to predict its mechanical response are proposed.

SUP&R ITN

Sustainable Pavements & Railways Initial Training Network (SUP&R ITN) is part of the Marie Curie Initial Training Network (ITN) action, FP7-PEOPLE-2013-ITN and is funded from the European Union under grant agreement number 607524. SUP&R ITN is a four years project that started at the beginning of October 2013 and has offered training-through-research for 15 young researchers with a consortium of universities, research centres and companies/industries from five EU countries (UK, Italy, France, Ireland and Spain).

The aim of the SUP&R ITN is: “To setup a multidisciplinary and multi-sectorial network in order to form a new generation of engineers versed in sustainable technologies and to provide, to both academia and industry, design procedures and sustainability assessment methodologies to certify the sustainability of the studied technologies to the benefit of the European community”.

The developed research by the fellows of the SUP&R ITN has been focused on planning and executing sustainable road and railway infrastructures, and deliver longterm benefits in terms of:

- Eco-designed road and rail infrastructure that maximises the recycling of waste materials and ensures best performance characteristics to suit the diverse set of European environments;
- Reduced installation, maintenance and operating costs as well as long term sustainable solutions;
- A bespoke sustainability assessment tool, tailored to the needs of product development in the road pavement and rail infrastructure sector.

Fractional Calculus

Fractional calculus is the generalisation of the ordinary differential and integral calculus to the non-integer derivatives and integrals. This may be easily evidenced since all the properties of the classic integro-differential operators still hold for the so-called fractional operators.

The theory of non-integer order derivation goes back to seventeenth century, when in 1695 Leibniz, in his letter, asked about the meaning of half derivative to l’Hôpital. With this event the study of derivatives and integrals

with arbitrary order began, and this study has been continued at the end of nineteenth century by Liouville, Grünwald, Letnikov and Riemann.

Despite the fractional calculus exists from more than two hundred years, in the engineering and physics fields its application has been relatively limited. Probably, the main reason of this limitation is due to the fact that this kind of operators have no geometrical meaning. This implies that in some physical application there is no mechanical interpretation of the analytical law which involves fractional operators. In the presented work this powerful tool is used to describe the tridimensional viscoelastic behaviour of bituminous mixtures.

Crumb rubber asphalt as Railway sub-ballast

Sub-ballast is the layer of the railway track-bed structure, interposed between the ballast and the blanket. The blanket is a layer, or several layers, of granular material laid over the subgrade to conform to the formation and create its desired properties. Frequently, unbound granular materials are replaced by bituminous sub-ballast, which may provide additional benefits to the subgrade protection and track performance. For instance, the bituminous sub-ballast, being almost completely water-resistant, protects the subgrade from the seasonal variations of moisture and atmospheric actions. This has an important effect in slowing down the deterioration process over the track's service life. Moreover, the bituminous sub-ballast plays an important role in distributing the load and reducing the solicitations on the subgrade. It dissipates the stress transmitted by passing trains, ensuring a higher protection of the formation compared to a granular sub-ballast. Overall, the use of bituminous sub-ballasts has the potential to improve the track quality and durability, leading to a reduction of maintenance interventions.

The re-use of crumb rubber in asphalt mixtures can lead not only to the reduction of the natural resources employed in the construction and maintenance/rehabilitation of railway track-bed, but also to mitigate the need for the disposal of a solid waste. Rubber grains can be incorporated into the preparation of bituminous mixtures by the so-called "wet" and "dry" production processes. The wet process envisages the dissolution of the crumb rubber in the bitumen as a modifying agent. The dry process envisages the replacement of a small portion of aggregates with the same fractions of rubber grains. Recent studies on the life cycle assessment of bituminous mixtures incorporating crumb rubber produced by both processes showed the benefits of using such

technologies in reducing the Gross Energy Requirement and the emissions of greenhouse gasses. Moreover, incorporating crumb rubber as aggregate could enhance damping properties, due to the capability of the rubber to absorb vibrations.

3D Fractional viscoelasticity

Fractional viscoelasticity has been widely studied from two different theoretical points of view: mathematicians and engineers. Many experimental results of monodimensional tests are available in literature and they confirm that in 1D conditions fractional viscoelasticity is the best approach to model the mechanical behaviour of viscoelastic materials. However, 1D models are not enough when there is the need to study real engineering components. The fitting of tridimensional experimental tests needs the definition of a proper 3D constitutive law as well as the structural analysis of complex engineering components. In the last years some 3D fractional viscoelastic models have been proposed, but the behaviour has never been experimentally investigated in simple 3D conditions and in real applications. For these reasons, in this thesis a theory of 3D linear isotropic fractional viscoelasticity, based on the generalisation of Hooke's law, is presented. This theory may be used to model the mechanical behaviour of bituminous mixtures as the experimental tests are properly performed. In this thesis, it is shown how to obtain the model coefficients from tridimensional experimental tests, and the theory of 3D fractional viscoelasticity is validated for bituminous mixtures.

Temperature effect on viscoelastic materials

It is well known, from the experimental and theoretical point of view, that the properties of viscoelastic materials are strongly dependent on the temperature. In the decade of 1950's the so called Time-Temperature Superposition Principle was experimentally observed in a study of the viscoelastic behaviour of polymers. This principle defines the relationship between time or frequency and temperature in the mechanical properties of viscoelastic materials under constant or dynamic stress conditions.

The application of this principle is based on modifying the time scale by multiplying by the so-called shift factor. Different techniques, based on experimental observations, to calculate the shift factor have been proposed for

the classical mechanical models. Unfortunately, when fractional operators are involved in the material constitutive laws, it has been observed that the classical shifting technique has some inconsistencies. For this reason, in this thesis it is studied how to deal with the Time-Temperature Superposition Principle when the material is modelled by means of fractional constitutive laws.

Organisation of the thesis

This PhD thesis is organised in five chapters. Each chapter includes original work developed during the three years of the PhD programme at the *Università degli Studi di Palermo* (Italy) and during the six month secondment at *IFSTTAR* (Institut français des sciences et technologies des transports, de l'aménagement et des réseaux) in Nantes (France).

Chapter 1 presents the so called *Fractional Calculus*, a branch of mathematical analysis that extends the classical integro-differential calculus to non-integer order operators. In particular, the derivatives and integrals of fractional order, their fundamental properties are introduced in this chapter. Moreover, a step by step integration technique for the fractional operators is presented in order to expand the capabilities of this operators in discrete form.

Chapter 2 introduces the *linear fractional viscoelasticity*. It starts with the theory of linear viscoelasticity, founded on the Boltzmann superposition principle that includes the constitutive laws of linear viscoelasticity. Then, the theory of linear fractional viscoelasticity is introduced. Moreover, a review of the classical and fractional mechanical models is reported. Furthermore an approach to separate the elastic and the viscous phase in the fractional stress-strain is provided in order to calculate the fractional characteristic times.

Chapter 3 presents the use of recycled rubber on asphalt mixtures. The main problem on *crumb rubber asphalt*, using rubber of a certain size, is the compaction. It has been demonstrated experimentally that the void content increases after the compaction. In this chapter an analytical approach is proposed to the mix design optimisation of bituminous mixtures containing crumb rubber using a gyratory compactor. The method takes into account the deformation release of the rubber after compaction for the calculation of the expected void content. The analytical approach is validated by the results of experimental tests.

Chapter 4 introduces the theory of the *3D fractional viscoelasticity*. The experimental set up used to perform the triaxial test for the asphalt mixtures is presented. Then the mechanical behaviour of the reference asphalt and the

rubber asphalt designed in the Chapter 3 is compared by the experimental creep and cyclic test performed. Finally, both asphalts are modelled as 3D fractional viscoelastic materials. The novelty in this Chapter arises on the validation of the 3D fractional viscoelasticity theory by means experimental triaxial test.

Chapter 5 deals with the *temperature effect* on viscoelastic materials. The chapter starts with the introduction of the Time-Temperature Superposition Principle, which deals with the strong relationship that time and temperature have in viscoelastic materials. Once the Time-Temperature Superposition Principle is introduced, its mathematical inconsistency is demonstrated when fractional elements appear in the mechanical model . Furthermore, the mechanical response of the bituminous mixtures presented and characterised in the previous Chapters 3 and 4 is evaluated taking into account the temperature effect. To conclude, the response of the two bituminous mixtures (reference and crumb rubber) used as railway sub-ballast it is compared based on the discrete fractional operators presented in Chapter 1.

Chapter 1

Fractional calculus

This Chapter presents the *Fractional Calculus*, a branch of mathematical analysis that extends the classical integro-differential calculus to non-integer order operators. In particular, the derivatives and integrals of fractional order, their fundamental properties are introduced in this chapter. The fractional operators introduced in this Chapter are those required to understand the concepts of fractional viscoelasticity. Further details can be found in [Oldham and Spanier, 1974, Miller and Ross, 1993, Samko et al., 1993, Podlubny, 1998, Kilbas et al., 2006]. Moreover, a step by step integration technique for the fractional operators is presented in order to expand the capabilities of this operators in discrete form [Colinas-Armijo and Di Paola, 2017].

1.1 History about fractional calculus and its applications

The Fractional Calculus was born after a postal conversation between *Gottfried Wilhelm von Leibniz* and his French colleague *Guillaume de L'Hôpital*. The conversation was started by Leibniz asking to L'Hôpital "*Can the meaning of derivatives with integer order be generalised to derivatives with non-integer orders?*". L'Hôpital was somewhat curious with the question and replied with another question "*What if the order be 1/2?*". Leibniz on a letter dated on the 30th September 1695 answer "*Thus it follows that $d^{1/2}x$ will be equal to $x\sqrt{dx} : x$, an apparent paradox, from which one day useful consequences will be drawn.*", and that has been the date set for the origin of fractional calculus. Only half century later, the first systematic studies were made and they involved several mathematicians such as *Fourier, Laplace, Lacroix* and *Euler*.

Probably, the first one who used fractional calculus in a mathematical problem was *N. H. Abel*. He studied in 1823 the tautochrone curve by the integral

$$\int_a^t (t - \tau)^{-\frac{1}{2}} f(\tau) d\tau, \quad (1.1)$$

which is similar to the fractional integral that will be introduced by *Riemann* later. But the main breakthrough has been made by the French mathematician *Joseph Liouville*, who in 1832 formulates the first definition of fractional derivative. He defined a non-integer order derivative using exponential series expansion of the function. In particular, Liouville considered the derivative of exponential function:

$$\frac{d^n}{dt^n} e^{at} = a^n e^{at} \quad n \in \mathbb{N}, \quad (1.2)$$

and he extended the derivation considering an order $n = \alpha$ with α being a non-integer number, and obtaining

$$\frac{d^\alpha}{dt^\alpha} e^{at} = a^\alpha e^{at}, \quad \alpha \in \mathbb{R}^+. \quad (1.3)$$

Subsequently, around 1835, he expressed the generic function $f(t)$ as a summation of exponential functions with infinity terms, and he defined the derivative of fractional order as series

$$(D^\alpha f)(t) = \sum_{j=0}^{\infty} c_j a_j^\alpha e^{a_j t}, \quad (1.4)$$

where $f(t) = \sum_{j=0}^{\infty} a_j^\alpha e^{a_j t}$.

An important contribution was provided in 1847 by the 22-years-old *George Friedrich Bernhard Riemann*, who introduced a definition of fractional integration by generalizing the Taylor series. That is,

$$(\mathbb{I}_{a^+}^\alpha f)(t) = \frac{d^{-\alpha}}{dt^{-\alpha}} f(t) = \frac{1}{\Gamma(\alpha)} \int_a^t (t - \tau)^{\alpha-1} f(\tau) d\tau. \quad (1.5)$$

The definitions of Liouville and Riemann have been unified with the aid of Cauchy integration formula in the manuscript of 1869 by *N. Ya. Sonin* entitled “*On Differentiation with Arbitrary Index*”. This is probably the first document in which the two definitions appear unified. Other contributions to this unification were provided by *A. Krug*, and *Aleksey Vasilievic Letnikov*, the latter one

in 1872 extended the work of Sonin in his paper “*An Explanation of the Theory of Differentiation of Arbitrary Index*”.

Next, during the collaboration with *Letnikov*, in 1867 *Anton Karl Grünwald* overcame the limits of Liouville definition, obtaining a more complete definition. Indeed, the Grünwald-Letnikov derivative has been obtained with the aid of the *difference quotient*. In 1930 the mathematician *Emil Leon Post* extended the definition of Grünwald and Letnikov.

Recently, around 1967, *Michele Caputo* provided a new mathematical formulation that represents a good tool to solve physical and engineering problems.

1.2 Fractional derivatives and integrals

In this section, the Riemann-Liouville fractional operators, the Caputo fractional derivative and the Grünwald-Letnikov fractional operators are presented. This operators are well known and extended information of them may be found for example in [Samko et al., 1993, Podlubny, 1998].

1.2.1 Riemann-Liouville fractional operators

The definition of the integral by *Cauchy* (*Augustin-Louis*, French mathematician and engineering, 1789-1857) is

$$\begin{aligned} (I_{a^+}^n f)(t) &= \frac{d^{-n} f(t)}{d(t-a)^{-n}} = \int_a^t \int_a^{\tau_{n-1}} \cdots \int_a^{\tau_1} f(\tau) d\tau d\tau_1 \cdots d\tau_{n-1} \\ &= \frac{1}{(n-1)!} \int_a^t (t-\tau)^{n-1} f(\tau) d\tau. \end{aligned} \quad (1.6)$$

In this way the multiple integral is represented as a convolution integral in which the kernel is $(t-\tau)^{n-1}$. By using the property of the Euler gamma function the Cauchy multiple integral formula can be generalised to the non-integer order case, obtaining the *Riemann-Liouville* (R-L) definition. In this regard, by replacing the factorial $(n-1)!$ with the gamma function, and the integer order n with generic order α (real or complex), the following relation holds:

$$(I_{a^+}^\alpha f)(t) = \frac{d^{-\alpha} f(t)}{d(t-a)^{-\alpha}} = \frac{1}{\Gamma(\alpha)} \int_a^t (t-\tau)^{\alpha-1} f(\tau) d\tau. \quad (1.7)$$

Eq. (1.7) is known as *Riemann-Liouville fractional integral*, since $\Re(\alpha) > 0$, and it holds true for $\alpha \in \mathbb{C}$. According the Davis notation, the integral is also

denoted as ${}_a I_t^\alpha f(t)$. In particular, this integral represents the *left-sided integral*, since the lower bound is the parameter a , and then $t > a$. The *right-sided integral* can be obtained chosen as lower bound the integration variable t . That is,

$$({}_b I_-^\alpha f)(t) = \frac{1}{\Gamma(\alpha)} \int_t^b (\tau - t)^{\alpha-1} f(\tau) d\tau, \quad (1.8)$$

in this case the parameter b is such that $b > t$. For the Davis notation the right-sided integral is also denoted as ${}_t I_b^\alpha f(t)$.

Provided that $\dot{f}(t)$ exists Eq. (1.7) may be written as

$$({}_a I_{a+}^\alpha f)(t) = \frac{1}{\Gamma(1+\alpha)} \int_a^t (t-\tau)^\alpha \dot{f}(\tau) d\tau. \quad (1.9)$$

The *Riemann-Liouville fractional derivative* can be readily obtained from the definition of the R-L fractional integral. In particular, by considering that the derivative of order n can be represented as the derivative of order $n+m$ of the m -order primitive function, the non-integer order the definition is obtained:

$$(D_{a+}^\alpha f)(t) = \frac{1}{\Gamma(n-\alpha)} \left(\frac{d}{dt} \right)^n \int_a^t \frac{f(\tau)}{(t-\tau)^{\alpha-n+1}} d\tau, \quad (1.10)$$

where $(n-1) < \mathbb{R}(\alpha) < n$.

Eq. (1.10) represents the *left-sided derivative*, since $t > a$. Instead, chosen an upper bound $t < b$, the *right-sided derivative* is defined as

$$(D_b^\alpha f)(t) = \frac{1}{\Gamma(n-\alpha)} \left(-\frac{d}{dt} \right)^n \int_t^b \frac{f(\tau)}{(\tau-t)^{\alpha-n+1}} d\tau. \quad (1.11)$$

For the Davis notation the right-sided and left-sided derivative are denoted as ${}_a D_t^\alpha f(t)$ and ${}_t D_b^\alpha f(t)$ respectively.

In the previous definitions the backward difference $(t-\tau)$ appear in the convolution integral. If the forward difference $(t+\tau)$ is chosen, then another definition, known as *Weil differintegral operator*, is obtained.

Observe that the R-L derivative of a constant is not zero, indeed:

$$D_{0+}^\alpha c = \frac{c t^{-\alpha}}{\Gamma(1-\alpha)}. \quad (1.12)$$

1.2.2 Caputo fractional derivative

Another definition has been provided by *Michele Caputo*, and it is applied to solve several physical problems.

The Riemann-Liouville definition represents an accurate mathematical tool, but often it is unsuitable to solve and/or to model real physical problems. In particular, the solution of fractional differential equations with R-L derivatives can be found if the initial conditions are expressed as the involved fractional operators. Such derivatives, having no physical meaning, are unknown in physical problems, and they do not permit to represent the initial condition of those problems.

The Caputo's approach [Caputo, 1967, Caputo, 1969] overcomes the limitations of the R-L definition, since it permits to define the fractional derivative and/or integral of the function $f(t)$ by using initial conditions expressed as integer-order derivative. In this manner, when there is a fractional differential equation with Caputo's fractional operators, the solution can be evaluated by the knowledge of a certain number of initial conditions expressed as in the classical way. To model the mechanical behaviour of real materials, the fractional derivation is commonly used in rheology. In this physical field there are some problems in which the initial conditions are known in terms of integer-order derivatives (e.g. the deformation rate is the first-order derivative in time of the strain history). The Caputo's formulation permits to solve this kind of problems, providing an accurate modelling of the phenomena.

M. Caputo, around 1967, provided the a new definition of the fractional operator

$$\left({}^C D_{a^+}^\alpha f\right)(t) = \frac{1}{\Gamma(n-\alpha)} \int_a^t \frac{f^{(n)}(\tau)}{(t-\tau)^{\alpha+1-n}} d\tau, \quad (1.13)$$

which is known as *Caputo's differintegral* and it is valid for $n-1 < \alpha < n$. Eq. (1.13) is obtained as a kind of interpolation of the integer-order derivative. Indeed, if $\alpha \rightarrow n$, Eq. (1.13) leads to n -order derivative of the function $f(t)$. In this case, the Caputo's derivative of a constant is zero.

In certain cases, in which the function $f(t)$ has particular properties when $t \rightarrow -\infty$, and under specific initial conditions, the R-L derivative and the Caputo's one coincide.

1.2.3 Grünwald-Letnikov fractional operators

The Grünwald-Letnikov (G-L) definition of fractional operators consists of a discretisation of the time axis into small steps of equal length Δt . The approximation of the derivatives of integer order at the time step $t_j = j\Delta t$ is given as

$$\begin{aligned} \dot{f}(t_j) &\cong (t_j - t_{j-1})\Delta t^{-1}; \quad \ddot{f}(t_j) \cong (t_j - 2t_{j-1} + t_{j-2})\Delta t^{-2}; \\ \frac{d^n f(t_j)}{dt^n} &= \left(\sum_{r=0}^{j-1} (-1)^r \binom{n}{r} f(t_j - r\Delta t) \right) \Delta t^{-n}; \quad n = 1, 2, \dots \end{aligned} \quad (1.14)$$

and the n -th integral is approximated as

$$\frac{d^{-n} f(t_j)}{dt^{-n}} = \left(\sum_{r=0}^{j-1} \binom{r+n-1}{r} f(t_j - r\Delta t) \right) \Delta t^n; \quad n = 1, 2, \dots \quad (1.15)$$

The G-L fractional derivatives and integrals are obtained by a proper substitution of the order $n \in \mathbb{N}$ with $\alpha \in \mathbb{R}^+$ (or also $\alpha \in \mathbb{C}$ with $Re(\alpha) \in \mathbb{R}^+$), thus obtaining the fractional derivatives and integrals in the form

$$(\nabla^\alpha f)(t_j) = \Delta t^{-\alpha} \sum_{r=0}^{j-1} \frac{\Gamma(r-\alpha)}{\Gamma(r+1)\Gamma(-\alpha)} f(t_j - r\Delta t); \quad Re(\alpha) > 0 \quad (1.16)$$

and

$$(\nabla^{-\alpha} f)(t_j) = \Delta t^\alpha \sum_{r=0}^{j-1} \frac{\Gamma(r+\alpha)}{\Gamma(r+1)\Gamma(\alpha)} f(t_j - r\Delta t); \quad Re(\alpha) > 0 \quad (1.17)$$

where the symbols $\nabla^\alpha f$ and $\nabla^{-\alpha} f$ denote the G-L fractional derivative and integral, respectively.

The G-L approach is very attractive since $\Delta t \rightarrow 0$ Eqs. (1.16) and (1.17) tend toward Eq. (1.10) and Eq. (1.7), respectively. For this reason the G-L derivative and integral are considered as a discretisation of the Riemann-Liouville fractional operators. Moreover, the various coefficients in Eqs. (1.16) and (1.17) may be constructed in recursive form. By denoting $\omega_r(\alpha) = \Gamma(r-\alpha)/(\Gamma(r+1)\Gamma(-\alpha))$ and $\omega_r(-\alpha) = \Gamma(r+\alpha)/(\Gamma(r+1)\Gamma(\alpha))$ it is obtained

$$\begin{aligned} \omega_0(\alpha) &= 1, \quad \omega_1(\alpha) = -\alpha, \quad \omega_2(\alpha) = \omega_1(\alpha) \frac{(1-\alpha)}{2}, \quad \dots, \\ \omega_{j-1}(\alpha) &= \omega_{j-2}(\alpha) \frac{(j-2-\alpha)}{(j-1)}, \quad \dots \quad \alpha > 0 \end{aligned} \quad (1.18)$$

and $\omega_r(-\alpha)$ is obtained simply by substituting $-\alpha$ in the Eq. (1.18). Eqs. (1.16) and (1.17) may be rewritten in the following form (see [Podlubny, 1998])

$$\nabla^\alpha f_N = \Delta t^{-\alpha} \mathbf{A}_N(\alpha) f_N, \quad (1.19a)$$

$$\nabla^{-\alpha} f_N = \Delta t^\alpha \mathbf{B}_N(\alpha) f_N. \quad (1.19b)$$

By denoting $f(t_r) = f_r$, inserting f_r into a vector f_N

$$f_N^T = [f_1 \ f_2 \ \dots \ f_N] \quad (1.20)$$

and writing Eq. (1.19a) at each temporal step, it is recognised that \mathbf{A}_N is a lower triangular strip matrix defined as

$$\mathbf{A}_N(\alpha) = \begin{bmatrix} 1 & 0 & 0 & \dots & 0 & 0 \\ \omega_1(\alpha) & 1 & 0 & \dots & 0 & 0 \\ \omega_2(\alpha) & \omega_1(\alpha) & 1 & \dots & 0 & 0 \\ \vdots & \vdots & \vdots & \ddots & \vdots & \vdots \\ \omega_{N-2}(\alpha) & \omega_{N-3}(\alpha) & \omega_{N-4}(\alpha) & \dots & 1 & 0 \\ \omega_{N-1}(\alpha) & \omega_{N-2}(\alpha) & \omega_{N-3}(\alpha) & \dots & \omega_1(\alpha) & 1 \end{bmatrix}, \quad (1.21)$$

and the matrix \mathbf{B}_N is obtained as $\mathbf{B}_N(\alpha) = \mathbf{A}_N(-\alpha)$.

Semigroup properties for R-L and G-L operators are preserved, that is

$$\begin{aligned} \mathbf{A}_N(-\alpha) &= \mathbf{B}_N(\alpha) = \mathbf{B}_N^{-1}(\alpha); \quad \mathbf{B}_N(-\alpha) = \mathbf{A}_N^{-1}(\alpha) \\ \mathbf{A}_N^2(\alpha) &= \mathbf{A}_N(2\alpha); \quad \mathbf{B}_N^2(\alpha) = \mathbf{B}_N(2\alpha); \dots \end{aligned} \quad (1.22)$$

With all these informations it seems that the G-L operators may be used without any care. However, in some circumstances the use of G-L operators may lead to errors in the approximate solutions of practical problems in physics and engineering. The problem arises because in the approximation of Eq. (1.15) implicitly is assumed that $f(t)$ is continuous with the all the derivatives up to the order $d^n t/dt^n$, $\forall t$ including the value at $t = 0$. It follows that Eq. (1.19) remains valid provided that the derivative of order n exists in all the real axis for $Re(\alpha) \leq n$ including the value in zero. Such an example, let $f(t) = exp(-t)$ this function belong to the class $C_\infty \forall t > 0$, excluding the point $t = 0$ in which the function exhibits a jump, then in the proximity of $t = 0$ Eq. (1.19a) fails.

1.3 Properties of fractional operators

The properties of classical derivation and integration can be extended to the fractional operators. This shows that the integer-order differential/integral calculus is nothing else than a subset of the fractional calculus. The properties of fractional operators presented in this section are well known, see for example in [Samko et al., 1993, Podlubny, 1998].

1.3.1 Properties

This subsection introduces just three fundamental properties of the fractional operators, that are, the *linearity* that concerns the summation of two operators, the *Leibniz rule* that affects the product, and the *semigroup property*, which is useful for multiple integration and derivation.

The linearity

The fractional derivative is a linear operator. Considering two function $f(t)$ and $g(t)$, and two parameters $\lambda, \mu \in \mathbb{C}$, the relation

$$D^\alpha (\lambda f + \mu g) (t) = \lambda (D^\alpha f) (t) + \mu (D^\alpha g) (t) \quad (1.23)$$

holds. This property of fractional derivative is a consequence of its definition.

In order to show this property, considering the Grünwald-Letnikov definition, for which

$$\begin{aligned} D_{a^+}^\alpha (\lambda f + \mu g) (t) &= \lim_{\substack{h \rightarrow 0 \\ nh=t-a}} h^{-\alpha} \sum_{r=0}^n (-1)^r \binom{\alpha}{r} [\lambda f(t-rh) + \mu g(t-rh)] \\ &= \lambda \lim_{\substack{h \rightarrow 0 \\ nh=t-a}} h^{-\alpha} \sum_{r=0}^n (-1)^r \binom{\alpha}{r} f(t-rh) + \mu \lim_{\substack{h \rightarrow 0 \\ nh=t-a}} h^{-\alpha} \sum_{r=0}^n (-1)^r \binom{\alpha}{r} g(t-rh), \end{aligned} \quad (1.24)$$

that leads to

$$(D_{a^+}^\alpha \lambda f + \mu g) (t) = \lambda (D_{a^+}^\alpha f) (t) + \mu (D_{a^+}^\alpha g) (t). \quad (1.25)$$

The property can be proved considering the other definitions.

The Leibniz rule

Take two function $f(t)$ and $\varphi(t)$, the Leibniz rule permits to evaluate the n -derivative of their product:

$$\frac{d^n}{dt^n} [\varphi(t)f(t)] = \sum_{r=0}^n \binom{n}{r} \varphi^{(r)}(t) f^{(n-r)}(t), \quad (1.26)$$

where $\binom{n}{r}$ represents the binomial coefficient, and $\varphi^{(r)}(t)$ is the r -order derivative.

In order to demonstrate that the Leibniz rule is still available for fractional operators, consider the Grünwald-Letnikov derivative of order $\alpha \in \mathbb{R}$:

$$(\mathbb{D}_{a^+}^\alpha \varphi f)(t) = \sum_{r=0}^n \binom{\alpha}{r} \varphi^{(r)}(t) (\mathbb{D}_{a^+}^{\alpha-r} f)(t) - \mathbb{R}_n^\alpha(t), \quad (1.27)$$

which is obtained under the assumptions that $n \geq \alpha + 1$, that the function $f(\tau)$ is continuous in the range $[a, t]$, and that $\varphi(\tau)$ admits $n + 1$ continuous derivatives in the domain $[a, t]$. The second term of Eq. (1.27) is

$$\mathbb{R}_n^\alpha(t) = \frac{1}{n! \Gamma(-\alpha)} \int_a^t (t - \tau)^{-\alpha-1} f(\tau) d\tau \int_\tau^t \varphi^{(n+1)}(\xi) (\tau - \xi)^n d\xi, \quad (1.28)$$

and represents a sort of *remainder*, which is due to the fact that the summation in Eq. (1.27) does not have infinite terms, but it is truncated at finite number n . By using infinite terms in the summation, the Leibniz rule for fractional derivatives becomes:

$$(\mathbb{D}_{a^+}^\alpha \varphi f)(t) = \sum_{r=0}^{\infty} \binom{\alpha}{r} \varphi^{(r)}(t) (\mathbb{D}_{a^+}^{\alpha-r} f)(t). \quad (1.29)$$

Also in this case, the shown property can be proved by other definitions of fractional derivative.

The semigroup rule

Considering a function $f(t)$, which is integrable for both order α_1 and α_2 , with $\mathbb{R}(\alpha_1) > 0$ and $\mathbb{R}(\alpha_2) > 0$, then the relation

$$(\mathbb{I}_{a^+}^{\alpha_1} \mathbb{I}_{a^+}^{\alpha_2} f)(t) = (\mathbb{I}_{a^+}^{\alpha_2} \mathbb{I}_{a^+}^{\alpha_1} f)(t) = (\mathbb{I}_{a^+}^{\alpha_1 + \alpha_2} f)(t), \quad (1.30)$$

holds. This property is still available for right-sided integration, then:

$$(\mathbb{I}_b^{\alpha_1} \mathbb{I}_b^{\alpha_2} f)(t) = (\mathbb{I}_b^{\alpha_2} \mathbb{I}_b^{\alpha_1} f)(t) = (\mathbb{I}_b^{\alpha_1 + \alpha_2} f)(t). \quad (1.31)$$

Eq. (1.30) is known as *semigroup property*. Observe that the integration is also *commutative*.

Take an $\Re(\alpha) > 0$, then:

$$\begin{aligned} (D_{a^+}^\alpha \mathbb{I}_{a^+}^\alpha f)(t) &= f(t), \\ (D_{b^-}^\alpha \mathbb{I}_{b^-}^\alpha f)(t) &= f(t). \end{aligned} \quad (1.32)$$

The Eqs. (1.32) can be proved by the R-L definition. Indeed, by using this definition from the first of Eqs. (1.32), the equality

$$(D_{a^+}^\alpha \mathbb{I}_{a^+}^\alpha f)(t) = \frac{d^n}{dt^n} \{ (D_{a^+}^{-n+\alpha} \mathbb{I}_{a^+}^\alpha f)(t) \} = f(t), \quad \text{with } n = \Re(\alpha) + 1 \quad (1.33)$$

holds true. The latter operation, between derivative and integral, is not commutative. Therefore,

$$\begin{aligned} (\mathbb{I}_{a^+}^\alpha D_{a^+}^\alpha f)(t) &\neq f(t), \\ (\mathbb{I}_{b^-}^\alpha D_{b^-}^\alpha f)(t) &\neq f(t). \end{aligned} \quad (1.34)$$

Another particular case can be obtained if $\Re(\alpha) > \Re(\gamma) > 0$:

$$\begin{aligned} (D_{a^+}^\gamma \mathbb{I}_{a^+}^\alpha f)(t) &= (\mathbb{I}_{a^+}^{\alpha-\gamma} f)(t), \\ (D_{b^-}^\gamma \mathbb{I}_{b^-}^\alpha f)(t) &= (\mathbb{I}_{b^-}^{\alpha-\gamma} f)(t) \end{aligned} \quad (1.35)$$

Moreover, considering an $\Re(\alpha) > 0$ and an $n \in \mathbb{N}$, then,

$$\begin{aligned} \frac{d^n}{dt^n} (D_{a^+}^\alpha f)(t) &= (D_{a^+}^{\alpha+n} f)(t), \\ \frac{d^n}{dt^n} (D_{b^-}^\alpha f)(t) &= (-1)^n (D_{b^-}^{\alpha+n} f)(t). \end{aligned} \quad (1.36)$$

1.3.2 Laplace transform of fractional operators

In this subsection the concepts about the Laplace transform are extended to the fractional operators.

Laplace transform of Riemann-Liouville fractional derivative

The Laplace transform of the Riemann-Liouville fractional derivative of order $\mathbb{R}(\alpha) > 0$ with lower bound $a = 0$ is

$$\mathcal{L} \{ (D_{0+}^{\alpha} f)(t); s \} = s^{\alpha} \hat{F}(s) - \sum_{r=0}^{n-1} s^r \left[(D_{0+}^{\alpha-r-1} f)(t) \right]_{t=0}, \quad (1.37)$$

where $n - 1 \leq \alpha < n$ and $\hat{F}(s)$ is the Laplace transform of $f(t)$.

In this mathematical transformation the values of the R-L fractional derivatives appear at the origin. In physical problems described by fractional differential equations, the R-L formulation cannot be used, since this fractional derivative at the origin has no physical meaning.

Laplace transform of Caputo's fractional derivative

The Laplace transform of the Caputo's fractional derivative leads to

$$\mathcal{L} \{ ({}_C D_{0+}^{\alpha} f)(t); s \} = s^{\alpha} \hat{F}(s) - \sum_{r=0}^{n-1} s^{\alpha-r-1} f^{(r)}(0), \quad (1.38)$$

where $n - 1 \leq \alpha < n$.

Observe that in this case the integer derivatives appear at the origin. This is an important characteristic of this kind of fractional derivatives, since Eq. (1.38) can be applied to solve physical problems in which the Caputo's fractional derivatives appear, and when the initial conditions are given in terms of integer derivative. In a physical point of view, the difference of Eq. (1.37) and Eq. (1.38) is crucial, since the integer-order derivative at the origin has a physical meaning (e.g.: if $x(t)$ is the displacement function, $\dot{x}(0)$ is the initial velocity, $\ddot{x}(0)$ is the initial acceleration).

1.3.3 Fourier transform of fractional operators

In some physical problems, expressed by fractional differential equations, it is useful to apply the Fourier transform. In this section the previous concepts about this mathematical transformation are extended to fractional derivatives and integrals.

Fourier transform of fractional integral

Considering the R-L fractional integrals on the whole real axis, that is with lower bound $a = -\infty$, and order $0 < \alpha < 1$, the previous definition leads to

$$(I_+^\alpha f)(t) = (D_+^{-\alpha} f)(t) = \frac{1}{\Gamma(\alpha)} \int_{-\infty}^t (t - \tau)^{\alpha-1} f(\tau) d\tau, \quad (1.39)$$

by performing the Fourier transform of (1.39), the relation

$$\mathcal{F} \{ (D_+^{-\alpha} f)(t); \omega \} = (i\omega)^{-\alpha} \tilde{F}(\omega) \quad (1.40)$$

holds, where $\alpha \in \mathbb{R}$ and \tilde{F} is the Fourier transform of $f(t)$.

By using the Eq. (1.40) to left and right-sided fractional integrals $(I_\pm^\alpha f)(t)$, the Fourier transform becomes

$$\mathcal{F} \{ (I_\pm^\alpha f)(t); \omega \} = (\mp i\omega)^{-\alpha} \tilde{F}(\omega), \quad (1.41)$$

where

$$(\mp i\omega)^{-\alpha} = \left[\cos\left(\frac{\alpha\pi}{2}\right) \pm i \operatorname{sgn}(\omega) \sin\left(\frac{\alpha\pi}{2}\right) \right] |\omega|^{-\alpha}. \quad (1.42)$$

Eq. (1.41), obtained from the R-L definition, is still available for the Grünwald-Letnikov $(D_+^{-\alpha} f)(t)$ and the Caputo's definition $({}^C D_+^{-\alpha} f)(t)$.

Fourier transform of fractional derivative

Similarly to the previous case, consider the fractional derivative with lower bound $a = -\infty$. That is,

$$(D_+^\alpha f)(t) = \frac{1}{\Gamma(n - \alpha)} \int_{-\infty}^t \frac{f^{(n)}(\tau)}{(t - \tau)^{\alpha+1-n}} d\tau = \left(D_+^{\alpha-n} f^{(n)} \right)(t), \quad (1.43)$$

under the assumption that the function $f(t)$ is derivable n -times, and where $n - 1 < \alpha < n$.

Taking into account Eq. (1.40) the Fourier transform of Eq. (1.43) is

$$\mathcal{F} \{ (D_+^\alpha f)(t); \omega \} = (-i\omega)^\alpha \tilde{F}(\omega). \quad (1.44)$$

That expression is commonly used to solve several physical problems.

1.4 Step by step integration for fractional operators

In this section, an approach based on the definition of the Riemann-Liouville fractional operators is proposed in order to provide a different discretisation technique as alternative to the Grünwald-Letnikov operator (see [Colinas-Armijo and Di Paola, 2017]). The proposed R-L discretisation consists of a step-by-step integration schema based upon the discretisation of the function $f(t)$ as step-wise or piece-wise function. Applications to unit step function and exponential function are presented to show the accuracy and capabilities of the R-L discretisation proposed and the G-L discrete operators.

1.4.1 Step-wise approximation

The step-by-step approximation is evaluated for Riemann-Liouville fractional integral and derivative discretising of the function $f(t)$ as step-wise function.

Riemann-Liouville integral for the step-wise approximation

The R-L integral defined in Eq. (1.8) may be easily evaluated by a proper discretisation of the time axis into small intervals of equal length Δt . In each step the function $f(t)$ is assumed to be constant as depicted in Figure 1.1.

The step-wise approximation of $f(t)$ may be written in the form

$$f(t_N) \simeq \sum_{j=1}^N (f_j - f_{j-1})U(t - t_{j-1}); \quad t_{N-1} \leq t \leq t_N \quad (1.45)$$

where $f_j = f(j\Delta t)$ and $U(\cdot)$ is the unit step function. By inserting Eq. (1.45) in Eq. (1.8) the exact solution of the R-L fractional integral for the step-wise approximation is obtained in the form

$$D^{-\alpha} f(t) = \frac{1}{\Gamma(1+\alpha)} [f_1 t^\alpha + \dots + (f_N - f_{N-1})(t - (N-1)\Delta t)^\alpha] \quad (1.46)$$

By particularising t as $j\Delta t$ and by collecting f_j into $f_N^T = [f_1 f_2 \dots f_3]$ the R-L fractional integral may be represented in matrix form as follows

$$D^{-\alpha} f_N = \Delta t^\alpha P_N(\alpha) A_N(1) f_N = \Delta t^\alpha V_N(\alpha) f_N \quad (1.47)$$

where $A_N(1)$ is the G-L operator particularised for $\alpha = 1$ and $P_N(\alpha)$ is the lower triangular strip matrix defined as

$$P_N(\alpha) = \frac{1}{\Gamma(1+\alpha)} \begin{bmatrix} 1 & 0 & 0 & \dots & 0 & 0 \\ 2^\alpha & 1 & 0 & \dots & 0 & 0 \\ 3^\alpha & 2^\alpha & 1 & \dots & 0 & 0 \\ \vdots & \vdots & \vdots & \ddots & \vdots & \vdots \\ (N-1)^\alpha & (N-2)^\alpha & (N-3)^\alpha & \dots & 1 & 0 \\ N^\alpha & (N-1)^\alpha & (N-2)^\alpha & \dots & 2^\alpha & 1 \end{bmatrix}, \quad (1.48)$$

and in Eq. (1.47) $V_N(\alpha) = P_N(\alpha)A_N(1)$.

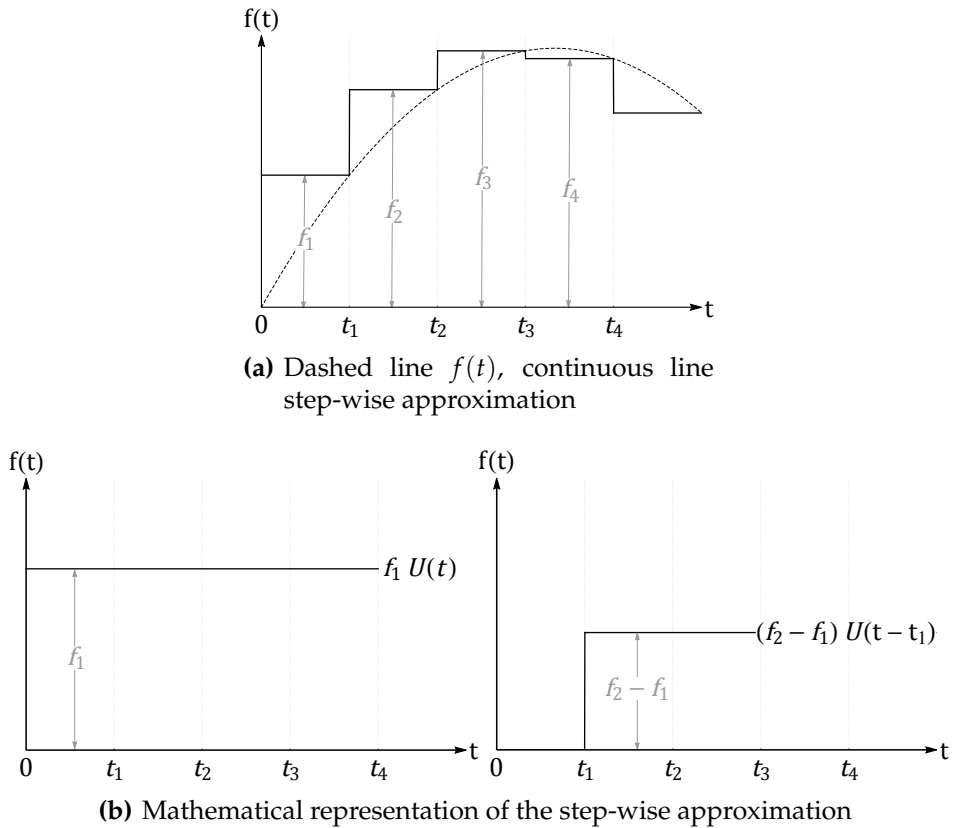


Figure 1.1: Step-wise approximation of $f(t)$.

Eq. (1.47) provides an exact R-L fractional integral in t_j for a step-wise function $f(t)$, moreover from Eq. (1.46) the values in the intermediate points may be evaluated for the step-wise approximation.

It may be observed that $D^{-\alpha}f(t)$ for the step-wise approximation of $f(t)$ is continuous for every $\alpha > 0$, and for $0 < \alpha < 1$ the slope in t_j^+ , that is the derivative in $t_j + \varepsilon$ as $\varepsilon \rightarrow 0$, is ∞ . On the contrary, for $\alpha \geq 1$ the R-L fractional integral is continuous with all the derivatives up to the order $int(\alpha) - 1$, being $int(\alpha)$ the integer part of α . These two situations are depicted in Figures 1.2(a) and 1.2(b), respectively. Furthermore, for $1 < \alpha < 2$ the R-L fractional integral is continuous $\forall t$ and the first derivatives in t_j are discontinuous, that is $d(D^{-\alpha}f(t))/dt|_{t_j-\varepsilon} \neq d(D^{-\alpha}f(t))/dt|_{t_j+\varepsilon}$ with ε arbitrarily small. For $2 < \alpha < 3$ the term $D^{-\alpha}f(t)$ is continuous with first order derivatives in all the time axis, and so on.

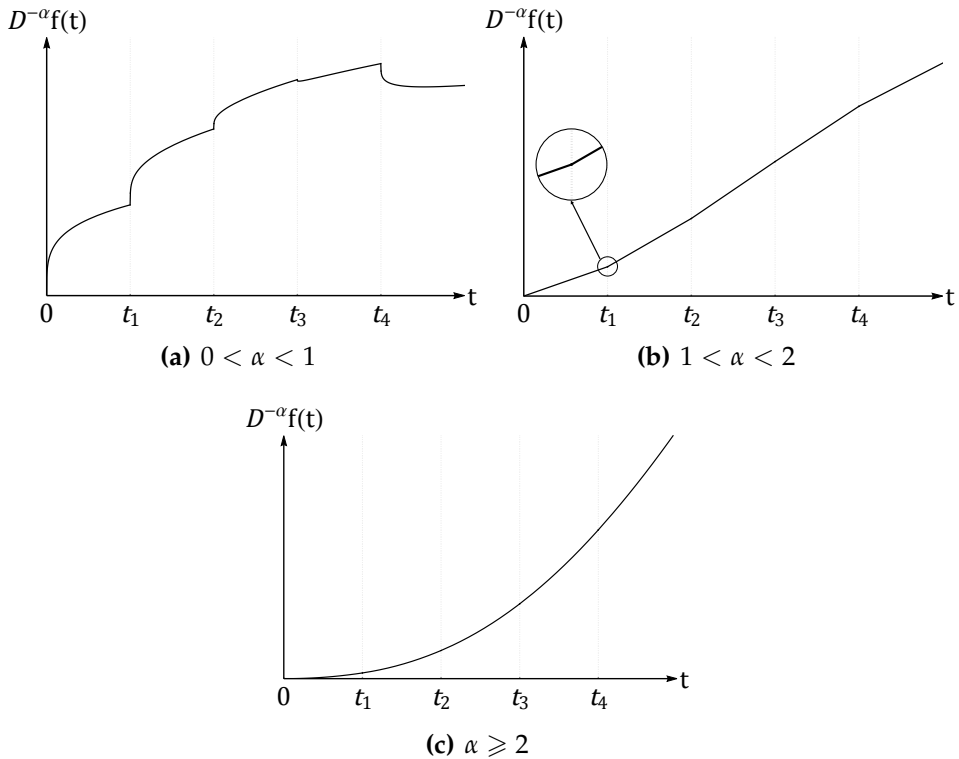


Figure 1.2: Fractional integrals for the step-wise approximation of $f(t)$.

It may be easily seen that the semigroup properties for the operator $V_N(\alpha)$ is not fulfilled, such an example is

$$D^{-2\alpha} f_N \neq \Delta t^{2\alpha} V_N^2(\alpha) f_N \quad (1.49)$$

and then $D^{-2\alpha} f_N$ has to be evaluated in the form

$$D^{-2\alpha} f_N = \Delta t^{2\alpha} V_N(2\alpha) f_N. \quad (1.50)$$

The lack of the semigroup properties is due to the fact that the term $D^{-\alpha} f(t)$ for the step-wise function is, in each step, a power law (see Eq. (1.46)). It follows that $D^{-\alpha} f(t)$ may not be considered constant especially for α small and then $D^{-\alpha} D^{-\alpha} f_N = \Delta t^{\alpha+\alpha} V_N(\alpha + \alpha) f_N \neq \Delta t^{\alpha+\alpha} V_N(\alpha) V_N(\alpha) f_N$.

A direct comparison between the G-L operator $B_N(\alpha)$ and the R-L operator $V_N(\alpha)$ for the step-wise approximation reveals that both are lower triangular strip matrices but the corresponding elements $\omega_j(\alpha)$ and the corresponding elements of the matrix $V_N(\alpha)$ are quite different each another as in fact

$$\omega_j(\alpha) = \omega_{j-1}(\alpha) \frac{j-1+\alpha}{j-1} \neq \frac{1}{\Gamma(\alpha+\alpha)} [(j+1)^\alpha - j^\alpha]. \quad (1.51)$$

Moreover looking at the diagonal elements of the matrix $B_N(\alpha)$ and those of $V_N(\alpha)$ the difference is immediately evident since the diagonal elements of $B_N(\alpha)$ are 1 while the diagonal elements of $V_N(\alpha)$ are $1/\Gamma(1+\alpha)$. It may be easily shown that $B_N(\alpha) = V_N(\alpha)$ for $\alpha = 1$.

A very instructive case that highlights the difference between the G-L operator $A_N(\alpha)$ and the R-L operator $V_N(\alpha)$ is the integration of the unit step function. In this case, following the R-L step-by-step integration scheme (see Eq. (1.47)) the response at every time step coalesces with the exact one no matter the time Δt selected, while the G-L integration scheme is an approximation for the first few time instants.

Riemann-Liouville derivative for the step-wise approximation

As $f(t) = 0, \forall t < 0$ the R-L fractional derivative (Eq. (1.10)) and the Caputo's fractional derivative coalesce each another, then for the step-wise approximation of $f(t)$ it may be used both Eq. (1.10) or Eq. (1.13). In order to show this, lets suppose $0 \leq \text{Re}(\alpha) \leq 1$. Then Eq. (1.13), particularised for $n = 1$, is written as

$$\left({}^C D^\alpha f\right)(t) = \frac{1}{\Gamma(1-\alpha)} \int_0^t (t-\tau)^{-\alpha} \dot{f}(\tau) d\tau; \quad 0 \leq \alpha \leq 1. \quad (1.52)$$

The step-wise approximation reads

$$\dot{f}(t) \simeq \sum_{j=1}^N (f_j - f_{j-1}) \delta(t - t_{j-1}); \quad t_N \leq t \leq t_{N+1} \quad (1.53)$$

where $\delta(\cdot)$ is the Dirac's delta function. By inserting Eq. (1.53) in Eq. (1.52) in the various time steps it is obtained

$$\begin{aligned} ({}^C D^\alpha f)(t) &= \frac{f_1}{\Gamma(1-\alpha)} t^{-\alpha}; \quad 0 \leq t \leq \Delta t \\ ({}^C D^\alpha f)(t) &= \frac{f_1 t^{-\alpha}}{\Gamma(1-\alpha)} + \frac{(f_2 - f_1)}{\Gamma(1-\alpha)} (t - t_1)^{-\alpha}; \quad \Delta t \leq t \leq 2\Delta t \\ &\vdots \\ ({}^C D^\alpha f)(t) &= \frac{1}{\Gamma(1-\alpha)} \sum_{j=1}^N (f_j - f_{j-1}) (t - t_{j-1})^{-\alpha}; \quad (N-1)\Delta t \leq t \leq N\Delta t \end{aligned} \quad (1.54)$$

Particularisation of Eq. (1.54) in $t_j = j\Delta t$, the Caputo's fractional derivative at $j\Delta t$ is obtained in the form

$${}^C D^\alpha f_N = \Delta t^{-\alpha} P_N(-\alpha) A_N(1) f_N = \Delta t^{-\alpha} \mathbf{U}_N(\alpha) f_N; \quad 0 \leq \alpha \leq 1, \quad (1.55)$$

where $P_N(-\alpha)$ is derived by a simple substitution of $-\alpha$ in the matrix in Eq. (1.48). It follows that the identity

$$\mathbf{U}_N(\alpha) = \mathbf{V}_N(-\alpha) \quad (1.56)$$

holds true. For $\alpha = 1$, $\Gamma(1-\alpha) = \infty$ that represents the fact that the first derivative is a series of impulses.

Exactly the same result are achieved following the R-L definition of the derivative for $0 \leq \alpha \leq 1$. In this case, according to Eq. (1.10), the R-L fractional derivative is given as

$$({}^R D^\alpha f)(t) = \frac{1}{\Gamma(1-\alpha)} \frac{d}{dt} \int_0^t (t-\tau)^{-\alpha} f(\tau) d\tau; \quad 0 \leq \alpha \leq 1, \quad (1.57)$$

and by using Eq. (1.45) leads to

$$\begin{aligned} (D^\alpha f)(t) &= \frac{1}{\Gamma(1-\alpha)} \frac{d}{dt} \left[\frac{f_1 t^{-\alpha}}{\Gamma(1-\alpha)} + \dots + \frac{(f_N - f_{N-1})}{\Gamma(1-\alpha)} (t - t_{N-1})^{-\alpha} \right] = \\ &= \frac{f_1 t^{-\alpha}}{\Gamma(1-\alpha)} \sum_{j=1}^N \frac{(f_j - f_{j-1})}{\Gamma(1-\alpha)} (t - t_{j-1})^{-\alpha}; \quad (N-1)\Delta t \leq t \leq N\Delta t. \end{aligned} \quad (1.58)$$

Then, Eq. (1.55) is exactly obtained by particularising Eq. (1.58) for $t = j\Delta t$.

In Figures 1.3 the R-L (or the Caputo) fractional derivative for the step-wise approximation is plotted for $0 \leq \alpha < 1$ and for $\alpha > 1$.

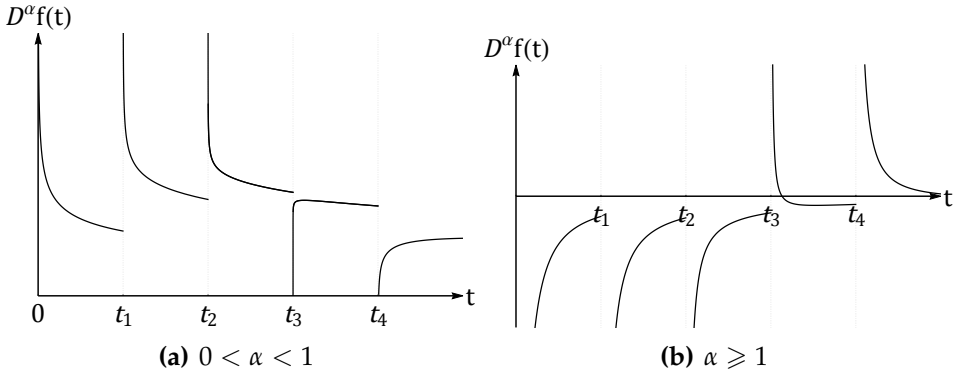


Figure 1.3: Fractional derivatives for the step-wise approximation of $f(t)$.

Also in this case the semigroup properties for $\mathbf{U}_N(\alpha)$ are not preserved. The motivation is the same already exploited for the fractional integral. In this case it is more evident that the step-wise approximation for the fractional derivative exhibits hyper-singularities at the beginning of each step. Subsequently, assuming that $(D^\alpha f)$ may be represented as a step-wise function is a mistake. As a consequence $D^\beta (D^\alpha f)$ in which $(D^\alpha f)$ is supposed to be constant at each step may not be represented as the product of $\mathbf{A}_N(\beta)\mathbf{B}_N(\alpha)$. Nevertheless also in this case the equality

$$D^{\alpha+\beta} f_N = \Delta t^{-(\alpha+\beta)} \mathbf{U}_N(\alpha + \beta) f_N; \quad \alpha \geq 0, \beta \geq 0, (\alpha + \beta) \leq 1. \quad (1.59)$$

remains still valid. The rules for the derivative of the integral are as follows

$$D^\alpha (D^{-\beta} f_N) = \Delta t^{(\alpha-\beta)} \mathbf{U}_N(\alpha - \beta) f_N. \quad (1.60)$$

Because of the singularities in the fractional operator for $\alpha > -1$ another possibility to get the step-by-step integration schemes of the fractional operators in the Riemann-Liouville sense yields a more accurate description of $f(t)$ such as a piece-wise approximation. This issue will be developed in the next section.

1.4.2 Piece-wise approximation

The step-by-step approximation is evaluated for the Riemann-Liouville fractional integral and derivative discretising the function $f(t)$ as a piece-wise function. For simplicity sake's it is supposed that $f(0) = f_0 = 0$, and the hypothesis of quiescent system in $t = 0$ will be removed later on once the main results are achieved.

Riemann-Liouville integral for the piece-wise approximation

This approximation mainly assumes that $\dot{f}(t)$ remains constant during each step as shown in Figure 1.4.

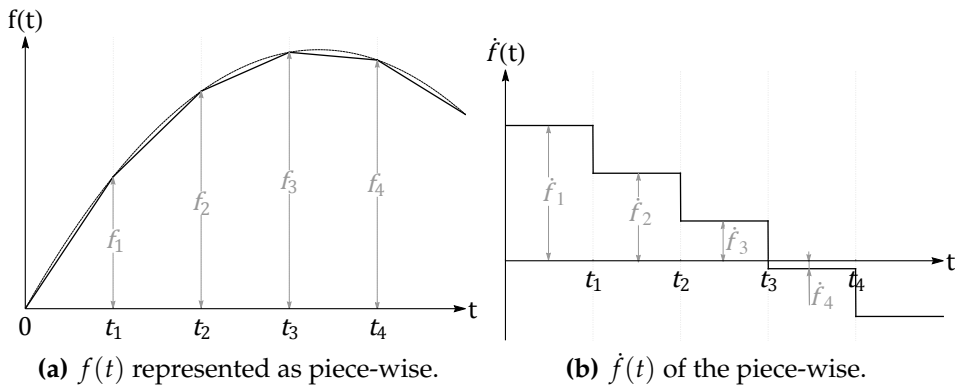


Figure 1.4: Piece-wise approximation of $f(t)$.

$f(t_j)$ is indicated as $f_j, j = 1, 2, \dots, N$ and \dot{f}_j is the rate of $f(t)$ in the interval $t_{j-1} < t < t_j$. By means of Eq. (1.9), taking into account that for the piece-wise approximation

$$\dot{f}(t) \simeq \sum_{j=1}^N (\dot{f}_j - \dot{f}_{j-1}) U(t - t_{j-1}); \quad t_{N-1} \leq t \leq t_N, \quad (1.61)$$

and inserting Eq. (1.61) into Eq. (1.47) yields

$$\begin{aligned} \Gamma(2 + \alpha) (D^{-\alpha} f) (t) &= \dot{f}_1 t^{\alpha+1} + (\dot{f}_2 - \dot{f}_1)(t - \Delta t)^{\alpha+1} + \dots \\ &+ (\dot{f}_N - \dot{f}_{N-1})(t - (N - 1)\Delta t)^{\alpha+1}. \end{aligned} \quad (1.62)$$

It follows that

$$D^{-\alpha} f_N = \Delta t^{\alpha+1} \mathbf{P}_N(\alpha + 1) \mathbf{A}_N(1) \dot{f}_N = \Delta t^\alpha \mathbf{P}_N(\alpha + 1) \mathbf{A}_N(2) f_N \quad (1.63)$$

where $\mathbf{P}_N(\alpha + 1)$ is the strip matrix already defined in Eq. (1.48) in which α is substituted by $\alpha + 1$ and $\mathbf{A}_N(2)$ is the G-L operator particularised for $\alpha = 2$.

In Eq. (1.63) the piece-wise approximation $\dot{f}_j = \Delta t^{-1}(f_j - f_{j-1})$ has been used. From Eq. (1.62) it is seen that in t_j^+ the slope is not infinity for $0 < \alpha < 1$ as it happens in the step-wise approximation. It follows that it may be asserted that for $0 < \alpha < 1$ the fractional R-L integral is continuous with bounded discontinuity in the slope at time instants t_1, t_2, \dots, t_N . For $\alpha > 1$ the R-L fractional integral is continuous with the derivatives up to the order $\text{int}(\alpha)$. If $f(0) = f_0$ is different from zero, that is $f(t)$ exhibits a jump in $t = 0$ (as for example $\cos(t)$), Eq. (1.63) has to be modified in the form

$$D^{-\alpha} f_N = \Delta t^\alpha \left[\mathbf{P}_N(\alpha + 1) \mathbf{A}_N(2) \tilde{f}_N^{(1)} + f_0 \mathbf{P}_N(\alpha) \mathbf{A}_N(1) e_N \right] \quad (1.64)$$

where $\tilde{f}_N^{(1)}$ is a vector with the components $\tilde{f}_j^{(1)} = f_j - f_0, j = 1, 2, \dots, N$, and e_N is a N vector where all components are 1.

Riemann-Liouville derivative for the piece-wise approximation

For the R-L fractional derivative both the R-L and Caputo's fractional definition lead to the same result. Following the Caputo's definition given in Eq. (1.13) yields for $0 < \alpha < 1$

$$\begin{aligned} (D^\alpha f) (t) &= \frac{1}{\Gamma(2 - \alpha)} [\dot{f}_1 t^{1-\alpha} + (\dot{f}_2 - \dot{f}_1)(t - \Delta t)^{1-\alpha} + \dots \\ &+ (\dot{f}_N - \dot{f}_{N-1})(t - (N - 1)\Delta t)^{1-\alpha}]. \end{aligned} \quad (1.65)$$

By evaluating Eq. (1.64) in $t_j = j\Delta$ leads to

$$D^\alpha f_N = \Delta t^{1-\alpha} \mathbf{P}_N(1 - \alpha) \mathbf{A}_N(1) \dot{f}_N = \Delta t^{-\alpha} \mathbf{P}_N(1 - \alpha) \mathbf{A}_N(2) f_N \quad (1.66)$$

From Eq. (1.64) it is observed that for $0 < \alpha < 1$ the R-L fractional derivative of the piece-wise approximation is continuous $\forall t$ while the slope in t_j^+ is ∞ . It may be easily demonstrated that Eq. (1.64) and Eq. (1.66) remain still valid for $\alpha > 1$, and the R-L fractional derivative exhibits unbounded variation in t_j^+ , namely at the beginning of each new interval. This situation is depicted in Figure 1.5.

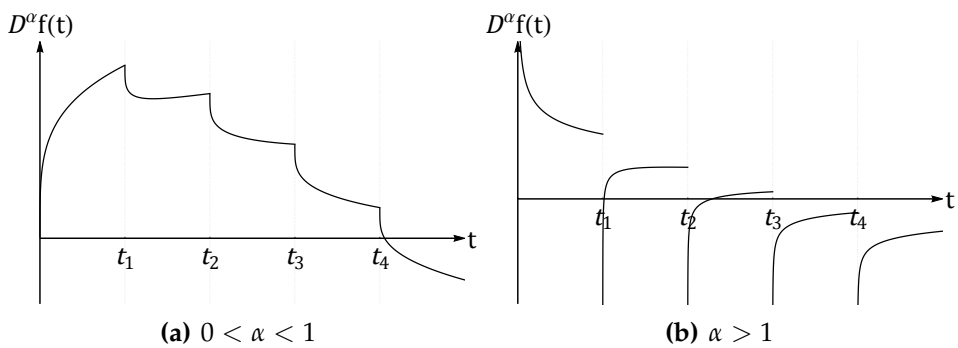


Figure 1.5: Fractional derivatives for the piece-wise approximation of $f(t)$.

If $f_0 \neq 0$, Eq. (1.66) may be rewritten as

$$D^\alpha f_N = \Delta t^{-\alpha} \left[\mathbf{P}_N(1 - \alpha) \mathbf{A}_N(2) \tilde{f}_N^{(1)} + f_0 \mathbf{P}_N(-\alpha) \mathbf{A}_N(1) e_N \right] \quad (1.67)$$

Since Eq. (1.67) is exact if the function $f(t)$ is actually a piece-wise linear function, and for $0 \leq \alpha \leq 1$ the fractional derivative is continuous, then Eq. (1.67) does not require any care. For $\alpha > 1$ Eq. (1.67) remains still valid but since in t_j^+ the fractional derivative exhibits an unbounded jump, Eq. (1.67) predicts the value in t_j^- , and in t_j^+ the response may be $\pm\infty$ depending on the value $\text{sgn}(\dot{f}_j - \dot{f}_{j-1})$.

1.4.3 Numerical example

In this subsection, a direct comparison between the G-L fractional operators and the step by step R-L (step-wise and piece-wise approximation) is evaluated.

Unit step function

The first example is very simple and illuminating, $f(t) = U(t)$ where $U(t)$ stands for unit step function. In this case, the fractional integral of $U(t)$ in exact form may be calculated by means of Eq. (1.7) and yields

$$D^{-\alpha}U(t) = t^\alpha / \Gamma(1 + \alpha). \tag{1.68}$$

For $U(t)$ function, the R-L step-wise approximation integral in Eq. (1.47) gives the exact solution and coalesces with the R-L piece-wise approximation in Eq. (1.63). In this case the solution is exact, no matter the temporal step Δt and on the α selected. The G-L fractional integral approximation is performed by using Eq. (1.19b), notice that the G-L approach does not give the exact solution.

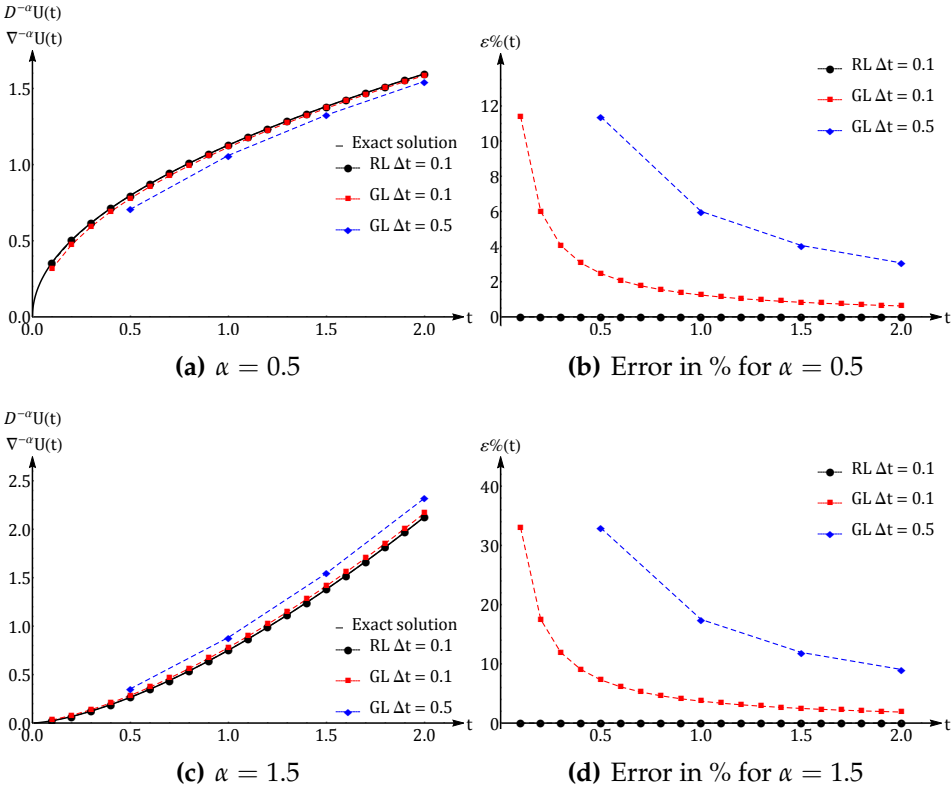


Figure 1.6: Fractional integral of $U(t)$.

In Figure 1.6 it is compared the exact form of the fractional integral of the unit step function calculated in Eq. (1.68) (continuous black line), the R-L step-wise and piece wise approximation for $\Delta t = 0.1$ (dotted dashed black line) that coalesce with the exact solution and the G-L fractional integral approximation of the unit step function for $\Delta t = 0.1$ and $\Delta t = 0.5$ (squared red and triangular blue dashed lines respectively). The comparison is shown for two different values of α , namely $\alpha = 0.5$ and $\alpha = 1.5$.

From Figure 1.6 it appears that the present R-L integral evaluated for each approximation, $f(t) = \text{const}$ into the step, $\tilde{f}(t) = \text{const}$ into the step and so on. The G-L operator gives approximate solutions and the smaller Δt , higher the accuracy is. Moreover, as t increases the G-L approximation tends asymptotically to the exact solution. Furthermore higher accuracy is achieved when α increases for the G-L integration scheme.

The relative error $\varepsilon\%(t)$, at each time instant, evaluated with the expression

$$\varepsilon\%(t) = \left| \frac{D^\alpha f(t) - \tilde{D}^\alpha f(t)}{D^\alpha f(t)} \right| \cdot 100 \quad (\alpha < 0 \& \alpha > 0), \quad (1.69)$$

where $\tilde{D}^\alpha f(t)$ stands for the the approximation (G-L or R-L step-by-step).

From Figures 1.6(b) and 1.6(d), it has to be remarked that the error of the R-L approximation (step-wise and piece-wise) is zero no matter the time step selected as previously stated. In the case of the G-L fractional integral approach, this relative error is very sensible to both the time step selected and the order of integration α .

The fractional derivative of the unit step function, obtaining by solving Eq. (1.10) yields

$$D^\alpha U(t) = D^\alpha U(t) = t^{-\alpha} / \Gamma(1 - \alpha). \quad (1.70)$$

As in the case of the fractional integral, the R-L step-wise and the piece-wise derivative approximations, in Eq. (1.55) and Eq. (1.66) respectively, provide the exact solution of the fractional derivative of $U(t)$. Also, the G-L fractional derivative approximation, performed by using Eq. (1.19a) does not provide the exact solution.

In order to evaluate the difference between the exact solution and the R-L and G-L approaches, in Figure 1.7 the fractional derivative of $U(t)$ is evaluated for two different values of α , that are $\alpha = 0.5$ and $\alpha = 1.5$. Figure 1.7 compares the exact form of the fractional derivative of the $U(t)$ calculated in Eq. (1.70) (continuous black line), the R-L step-wise and piece wise approximation for $\Delta t = 0.1$ (dotted dashed black line) that coalesce with the exact

solution and the G-L fractional derivative approximation of the unit step function for $\Delta t = 0.1$ and $\Delta t = 0.5$ (squared red and triangular blue dashed lines respectively).

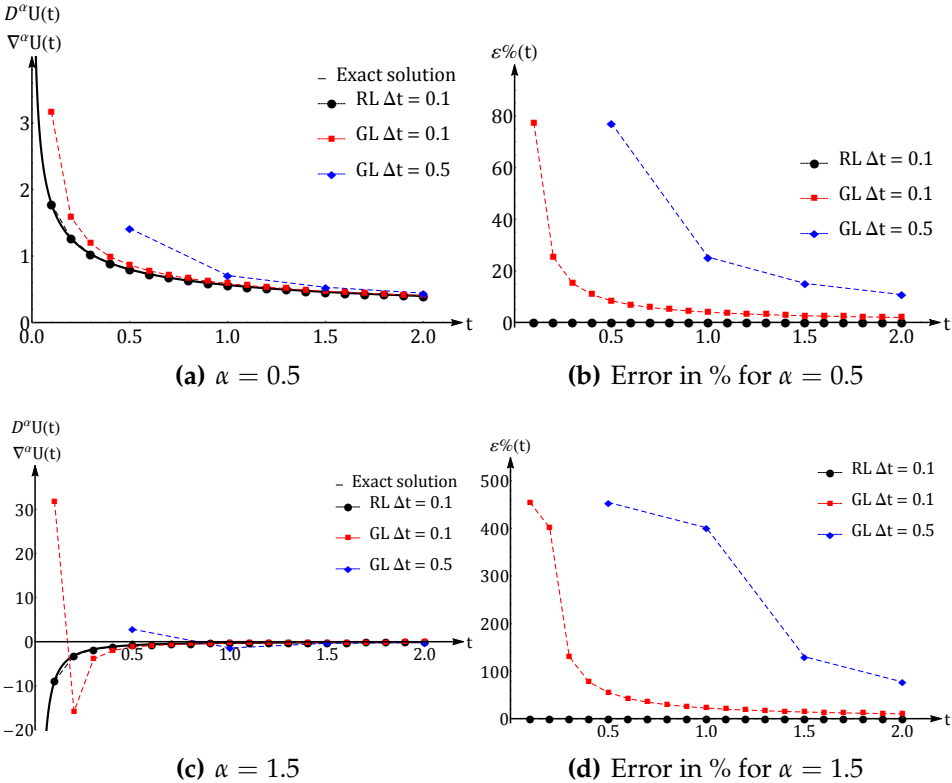


Figure 1.7: Fractional derivative of $U(t)$.

From Figure 1.7 it is evident that, by using G-L derivative, the $D^\alpha U(t)$ depends on the temporal step selected, and as α increases the accuracy decreases and as Δt decreases the accuracy of the G-L approximation increases. From Figures 1.7(b) and 1.7(d), it has to be remarked that the relative error of the R-L is zero, no matter the time step selected, since the R-L derivative approximations (step-wise and piece-wise) are equal to the exact solution.

Exponential function

As second example the function $f(t) = \gamma + e^{-\beta t}$ with $\beta > 0$ and $\gamma > 0$ is examined.

In Figure 1.8 the comparison between the G-L fractional integral and the step by step R-L fractional integral discretised as step-wise and piece-wise for $\alpha = 0.5$ and $\alpha = 1.5$ for $\Delta t = 0.1$ and $\alpha = 1$ is reported.

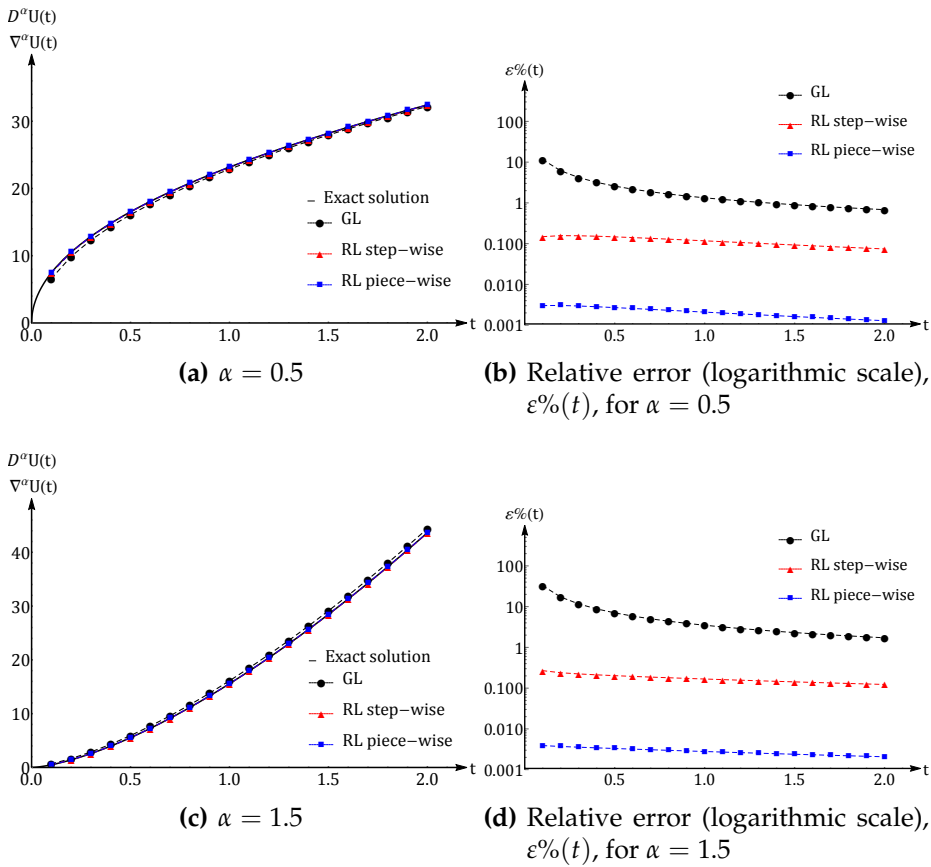


Figure 1.8: Fractional integral of $\gamma + e^{-\beta t}$, exact solution versus R-L and G-L approaches.

In Figure 1.8 the comparison between the G-L fractional integral and the step by step R-L fractional integral discretised as step-wise and piece-wise for $\alpha = 0.5$ and $\alpha = 1.5$ with $\Delta t = 0.1$, $\beta = 1$ and $\gamma = 20$ is reported.

In Figure Figure 1.8 the exact solution of the fractional integral $f(t) = \gamma + e^{-\beta t}$ calculated by means of Eq. (1.7) (continuous black line), the G-L integral approximation (dotted dashed black line) obtained using Eq. (1.19b), R-L step-wise integral approximation in Eq. (1.47) (triangular red dashed line) and R-L piece-wise integral approximation in Eq. (1.63) (squared blue dashed line).

From Figure 1.8, it is clear that by using the R-L piece-wise integral approximation in Eq. (1.63) the relative error is the smallest one in comparison. Moreover, it may be observed that the relative error of the three approaches decreases as t increases.

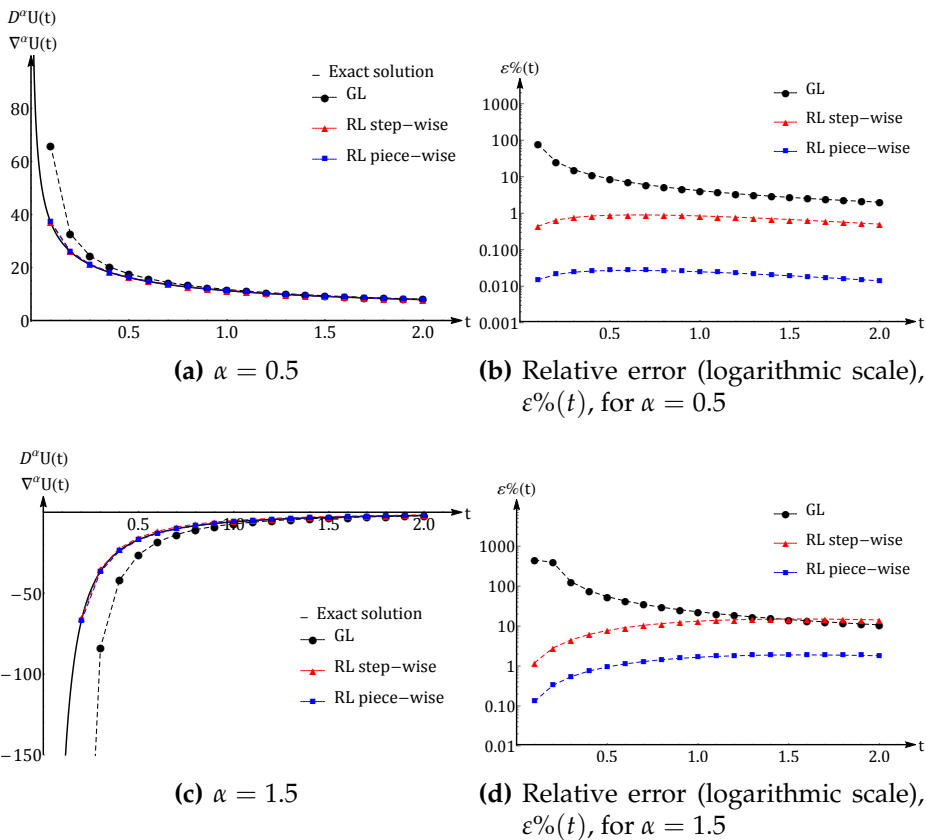


Figure 1.9: Fractional derivative of $\gamma + e^{-\beta t}$, exact solution versus R-L and G-L approaches.

In Figure 1.9 the comparison between the G-L fractional derivative and the step by step R-L fractional derivative discretised as step-wise and piece-wise for $\alpha = 0.5$ and $\alpha = 1.5$ with $\Delta t = 0.1$, $\beta = 1$ and $\gamma = 20$ is reported. In Figure 1.9 the exact solution of the fractional derivative of $f(t) = \gamma + e^{-\beta t}$ calculated by means of Eq. (1.10) (continuous black line), the G-L integral approximation (dotted dashed black line) obtained using Eq. (1.19b), the R-L step-wise derivative approximation in Eq. (1.55) (triangular red dashed line) and the R-L piece-wise derivative approximation in Eq. (1.66) (squared blue dashed line).

From Figure Figure 1.9, it may be observed that the accuracy of the piece-wise approximation of the R-L derivative is higher than the accuracy the of G-L and step-wise approximation. The relative error of the three approaches is shown in Figures 1.9(c) and 1.9(d), it may be concluded that the relative error for the R-L piece-wise is the smallest one, as in the case of the integral. By the other hand the R-L step wise and the G-L approach tend to the same relative error when t increases, but the G-L approach still has worst results at the first time steps.

1.5 Conclusions

In this chapter, some well known concepts of fractional calculus have been presented. Riemann-Liouville operators have been defined showing that for such operators all the rules of classical derivatives and integrals remain valid. In this sense it may be asserted that fractional operators may be considered as the extension of derivatives and integrals of integer order to derivatives and integrals of arbitrary order (real or complex).

Furhtermore, an approach based on the definition of the Riemann-Liouville fractional operators is proposed in order to provide a different discretisation technique as alternative to the Grünwald-Letnikov operator. The proposed R-L discretisation consists in making a step-by-step integration based upon the discretisation of the function $f(t)$. It has been shown that as $f(t)$ is discretised as step-wise or piece-wise function the R-L fractional integral and the R-L fractional derivative are ruled by operators very similar to that present in the G-L approach. The aforementioned R-L discrete operators are lower band strip matrices like the the operator in the G-L one, but the various entries are quite different each another giving the exact solution as the temporal step decreases.

It has been demonstrated that, for a truly step-wise or truly piece-wise function, the provided results by the R-L step-wise and piece-wise approximations, proposed in Section 1.4, are exact. That is, the only limitation on the accuracy of the fractional integral or derivative, by means of the R-L step-wise or piece-wise approximation proposed in the manuscript, for a generic function $f(t)$ is in the approximation done on the function $f(t)$ as step-wise or piece-wise. Moreover it has been evidenced that if the given function $f(t)$ is discontinuous in some points the G-L approach fails. It has been also proved that the R-L operators presented in this paper coalesce with the G-L and the classical operators for integer order derivatives and integrals.

Applications to unit step function and exponential function have been presented in order to show the accuracy and capabilities of the R-L step-by-step approaches (step-wise and piece-wise).

Chapter 2

Linear fractional viscoelasticity

This chapter deals with the theory of *linear fractional viscoelasticity*. It starts with the theory of linear viscoelasticity, founded on the Boltzmann superposition principle that includes the constitutive laws of linear viscoelasticity. Then, the theory of linear fractional viscoelasticity is introduced in time and frequency domain. Moreover, a review of the classical and fractional mechanical models is reported.

The novelty in this Chapter is to provide an approach to separate the elastic and the viscous phase in the fractional stress-strain relation with the aid of an equivalent classical model, [Colinas-Armijo et al., 2016]. For such equivalent model the parameters are selected by an optimisation procedure. Once the parameters of the equivalent model are defined, characteristic times of fractional viscoelasticity may be easily calculated.

2.1 Linear viscoelasticity

Viscoelastic materials are those materials that exhibit a mechanical behaviour intermediate between those of elastic solids and viscous fluids. Solids are characterised by the fact that they have their own shape; in particular elastic solids are those solids that experience deformations proportional to external applied loads through a material parameter, the modulus of elasticity, and that return to their initial configuration once the loads are removed. Fluids, instead, do not possess an own shape and are characterised by the fact that the internal stress is proportional to the deformation gradient through the so-called viscosity, a parameter of the liquid itself; in particular for Newtonian

fluids the viscosity is a constant that does not depend on the gradient of deformation. Because of the presence of the viscous part in their behaviour, mechanical behaviour of viscoelastic materials is time dependent. Many materials exhibit viscoelastic behaviour: polymers, biological tissues, bones, asphalt mixtures, concrete, soils and also some kind of rocks. For this reason in civil and industrial construction the characterisation of viscoelastic properties of materials is very important because it allows to predict long term effects of loads which if neglected can lead to erroneous design of engineering components and structures.

The time dependent nature of the mechanical behaviour of viscoelastic material imposes to take into account the time variable for viscoelastic models. For this reason in viscoelasticity the terms stress history and strain history are used, and relaxation and creep functions are necessary, instead of the simple elastic moduli used in linear elasticity.

Linear viscoelasticity is based on the knowledge of two fundamental functions: creep function and relaxation function. The relaxation function, denoted as $R(t)$, is the stress response under an unitary stress excitation. The creep function, denoted as $C(t)$, represents the time response in terms of deformation due to a constant imposed stress-history. The creep and the relaxation functions are able to completely describe the time dependent linear behaviour of viscoelastic materials since they are involved in the viscoelastic constitutive laws.

Theory of viscoelasticity is well known, the concepts presented in this section may be found in books like for example [Flügge, 1967, Christensen, 1971].

2.1.1 Boltzmann superposition principle

Consider an ideal test in which a tensile stress is applied to a linear viscoelastic material. At time $t = t_1 > 0$ a stress of magnitude $\Delta\sigma_1$ is applied. At time $t = t_2 > t_1$ the stress is instantaneously increased to the value $\Delta\sigma_1 + \Delta\sigma_2$. The stress history may be written as follows:

$$\sigma(t) = \Delta\sigma_1 U(t - t_1) + \Delta\sigma_2 U(t - t_2) \quad (2.1)$$

The presence of the unitstep function $U(t)$ in Eq. (2.1) suggests that in t_1 and in t_2 the history of the applied stress has two jumps, thus it is discontinuous, as shown in Figure 2.1(a). In the range $0 \leq t \leq t_1$ the applied stress is zero and nothing happens. In the range $t_1 \leq t \leq t_2$, the applied stress is $\Delta\sigma_1$, then the response in terms of strain history can be evaluated.

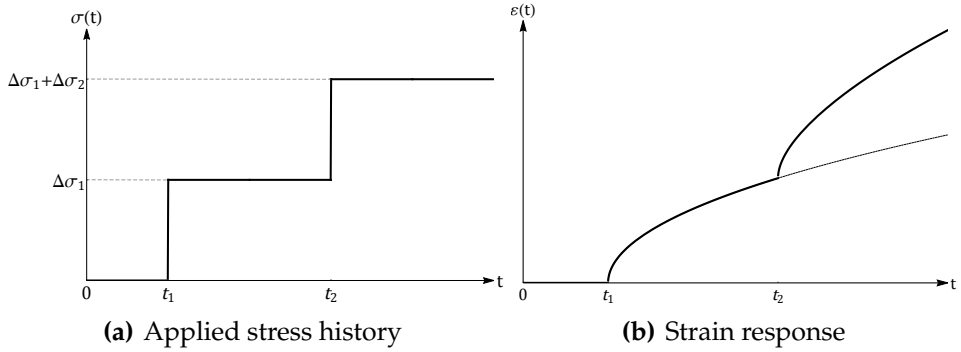


Figure 2.1: Boltzmann Superposition Principle.

Finally, for $t \leq t_2$ the applied stress is $\Delta\sigma_1 + \Delta\sigma_2$ and since the material is linear, it is possible to superimpose the responses due to the two stresses $\Delta\sigma_1$ and $\Delta\sigma_2$ separately taken, that is:

$$\varepsilon(t) = \Delta\sigma_1 C(t - t_1) + \Delta\sigma_2 C(t - t_2) \quad (2.2)$$

Since $C(t - t_1) = 0$ for $t < t_1$, in Eq. (2.2) $\varepsilon(t) = 0$ for $t < t_1$ and in the range $t_1 < t \leq t_2$ only the stress $\Delta\sigma_1$ contributes to the strain as it is shown in Figure 2.1(b), while for $t > t_2$ the new term $\Delta\sigma_2(t - t_2)$ appears and so on. The same approach described above can be used with n jumps in the stress history. In this case the response in terms of strain history can be written as

$$\varepsilon(t) = \sum_{k=1}^n \Delta\sigma_k C(t - t_k) \quad (2.3)$$

Eq. (2.3) expresses the superposition principle that is valid in linear viscoelasticity. If the applied stress history is continuous, it can be discretised as a series of steps of duration Δt in which the stress is constant. If $\Delta t \rightarrow 0$ then $\Delta\sigma \rightarrow d\sigma$ and the sum in Eq. (2.3) is rewritten in the following integral form

$$\varepsilon(t) = \int_0^t C(t - \tau) d\sigma(\tau) = \int_0^t C(t - \tau) \dot{\sigma}(\tau) d\tau. \quad (2.4)$$

Eq. (2.4) is a convolution integral that gives the response in terms of strain history to a certain applied stress history and represents the integral formulation of viscoelasticity. It is evident that at every time instant the strain depends on

all the past stress history. Moreover if $\sigma(0) \neq 0$ it is necessary to add another term in 2.4 as follows

$$\varepsilon(t) = \int_0^t C(t - \tau) \dot{\sigma}(\tau) d\tau + \sigma(0)C(t). \quad (2.5)$$

It is possible to define a dual formulation of the integral formulation of viscoelasticity. Then for an assigned strain history $\varepsilon(t)$, using the same approach as above, the stress history $\sigma(t)$ results

$$\sigma(t) = \int_0^t R(t - \tau) \dot{\varepsilon}(\tau) d\tau + \varepsilon(0)R(t). \quad (2.6)$$

Boltzmann superposition formulation in Eqs. (2.5) and (2.6) is a cornerstone of the linear viscoelasticity and it immediately shows the time-dependance of the stress-strain relation.

By virtue of the linear formulation in Eqs. (2.5) and (2.6) the Laplace transform of the two kernels are related each other. That is,

$$\hat{R}(s)\hat{C}(s) = s^{-2}, \quad (2.7)$$

where $\hat{R}(s)$ and $\hat{C}(s)$ are the Laplace transforms of $R(t)$ and $C(t)$, respectively.

2.2 Linear fractional viscoelasticity

In order to obtain a correct modelling of the viscoelastic phenomenon with the aid of the integral formulation in Eqs. (2.5) and (2.6), at least one of the two kernel functions must be determined by experimental investigations. In this context, Nutting [Nutting, 1921], on the basis of experimental investigations, stated that the creep function for any material is well fitted by a power-law. An appropriate creep function according to Nutting's experience is

$$C(t) = \frac{t^\alpha}{E_\alpha \Gamma(1 + \alpha)}, \quad (2.8)$$

where E_α and $\alpha \in \mathbb{R}^+ : 0 \leq \alpha \leq 1$ are coefficients obtained from the best fitting of experimental data, and $\Gamma(\cdot)$ denotes the Euler gamma function. Once the creep function in Eq. (2.8) is defined, the relaxation function can be immediately obtained by the relationship in Eq. (2.7). That is,

$$R(t) = \frac{E_\alpha t^{-\alpha}}{\Gamma(1 - \alpha)}. \quad (2.9)$$

By using the power-law functions in Eqs. (2.8) and (2.9) as kernels of the two convolution integrals in Eqs. (2.5) and (2.6), the stress history $\sigma(t)$ and the strain history $\varepsilon(t)$ are

$$\sigma(t) = \frac{E_\alpha}{\Gamma(1-\alpha)} \int_0^t (t-\tau)^{-\alpha} \dot{\varepsilon}(\tau) d\tau, \quad (2.10a)$$

$$\varepsilon(t) = \frac{1}{E_\alpha \Gamma(\alpha+1)} \int_0^t (t-\tau)^\alpha \dot{\sigma}(\tau) d\tau. \quad (2.10b)$$

Eq. (2.10a) contains a particular convolution integral that is known as *Caputo's fractional derivative* of the strain history. Usually, such derivation operator is denoted as $({}^C D_{0^+}^\alpha \varepsilon)(t)$, and it is defined as

$$({}^C D_{0^+}^\alpha \varepsilon)(t) = \frac{1}{\Gamma(n-\alpha)} \int_0^t (t-\tau)^{n-\alpha-1} \frac{d^n \varepsilon(\tau)}{d\tau} d\tau, \quad (2.11)$$

where 0^+ denotes the right handed derivative with lower bound 0, and the order $\alpha \in \mathbb{R}^+ : n-1 \leq \alpha \leq n$. In linear viscoelasticity, the order α is such that $0 \leq \alpha \leq 1$, then the Caputo's definition yields

$$({}^C D_{0^+}^\alpha \varepsilon)(t) = \frac{1}{\Gamma(1-\alpha)} \int_0^t (t-\tau)^{-\alpha} \dot{\varepsilon}(\tau) d\tau. \quad (2.12)$$

From Eq. (2.10b) an integration by parts leads to

$$\varepsilon(t) = \frac{1}{E_\alpha \Gamma(\alpha)} \int_0^t (t-\tau)^{\alpha-1} \sigma(\tau) d\tau, \quad (2.13)$$

where $E_\alpha \varepsilon(t)$ represents the *Riemann-Liouville fractional integral* of the stress history, denoted as $(I_{0^+}^\alpha \sigma)(t)$. With the aid of the fractional operators definitions, Eqs. (2.10) may be rewritten as

$$\sigma(t) = E_\alpha ({}^C D_{0^+}^\alpha \varepsilon)(t), \quad (2.14a)$$

$$\varepsilon(t) = \frac{1}{E_\alpha} (I_{0^+}^\alpha \sigma)(t). \quad (2.14b)$$

Eqs. (2.14) represent the constitutive laws of linear fractional viscoelasticity. Observe that for the two limit values of α ($\alpha = 0$ and $\alpha = 1$), since $({}^C D_{0^+}^0 \varepsilon)(t) = \varepsilon(t)$ and $({}^C D_{0^+}^1 \varepsilon)(t) = \dot{\varepsilon}(t)$ the purely elastic and the purely viscous behaviours are recovered, respectively. Thus, when $0 < \alpha < 1$ both elastic and viscous phase are present simultaneously, and the viscoelastic behaviour is captured. Such fractional stress-strain relations contain a coefficient E_α with anomalous dimensions, $[E_\alpha] = [FT^\alpha L^{-2}]$.

2.3 Review of mechanical models

This section provides a review of the mechanical models representing viscoelasticity. The first part introduces the classical models, composed of combinations of springs and dashpots. The second subsection presents more sophisticated models that include the fractional element presented in Section 2.2, focusing on the mechanical models used for asphalt mixtures.

2.3.1 Classical models

Traditionally, linear viscoelasticity has been modelled by different arrangements of springs (that represent the purely elastic behaviour) and dashpots (that behave like pure Newtonian fluids).

The linear elastic model is characterised by the so called Hooke's law in which the stress is linearly proportional to the strain, that is

$$\sigma(t) = E\varepsilon(t) \quad (2.15)$$

where E is Young modulus which measures the attitude of a material to be strained under the application of some stress. The higher the Young modulus the greater has to be the stress to induce a given strain, or the smaller is the strain to induce a given stress. The elastic behaviour is graphically represented as a spring (see Figure 2.2).

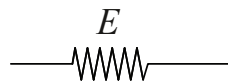


Figure 2.2: Linear spring.

For the viscous model, the Newton-Petroff model is used. The constitutive law of this model is

$$\sigma(t) = \mu\dot{\varepsilon}(t), \quad (2.16)$$

where μ is the viscosity of the fluid. The viscosity parameter μ plays a role in analogy to Young modulus. If it is higher a smaller strain rate $\dot{\varepsilon}(t)$ is needed to obtain a given stress. Differently from Young modulus, the dimension of μ is a stress multiplied by time and the dimension of the strain rate is the inverse of time. The Newton-Petroff model is represented as a dashpot as depicted in Figure 2.3.

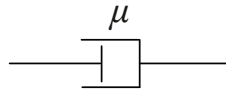


Figure 2.3: Dashpot.

Even if the constitutive laws of the spring and the dashpot are similar, they describe very different behaviours. In fact, Hooke's law does not depend on time. Any stress/strain applied to the solid immediately causes a correspondent strain/stress and when the cause is removed also the consequence immediately disappears. This also means that the Hooke material is able to store the work done by external load and to give it back when the loads are removed, without any loss of energy. The Newton-Petroff model, instead, is not able to store energy and all the work done by the external load is transformed into heat. As a consequence, the viscous fluid flows and does not return to the initial configuration when the loads are removed. For this reason this model is usually used to represent the damping or dissipation of materials.

The Hooke and the Newton-Petroff models are mathematical models that represent ideal solids respectively ideal fluids. Although some materials can be very satisfactory approximated with one of these ideal models, as for example many metals in their linear elastic range, in the real world neither of the limiting behaviours above described exist. Indeed, all real materials combine properties of those limit cases and for this reason in classical viscoelasticity they are modelled as combinations of springs and dashpots.

The most simple classical viscoelastic models are the Maxwell model and the Kelvin-Voigt model. The first is constituted by a spring and a dashpot in series while the second is a spring connected in parallel with a dashpot, as depicted in Figure 2.4.

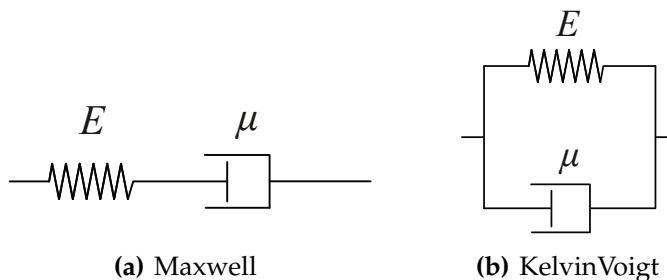


Figure 2.4: Maxwell and KelvinVoigt models.

The Maxwell model (Figure 2.4(a)) is characterised by the fact the both the spring and the dashpot experience the same stress, while the strain is the sum of the strains of the spring and of the dashpot. Although the relaxation function, depicted in Figure 2.5(b), function is acceptable to fit experimental data (but it is not the best fitting possible for many viscoelastic material), the creep function is in contrast to experimental evidence, because the strain increases linearly indefinitely, as it may be observed in Figure 2.5(a). For this reason this model is not suitable to reproduce the mechanical behaviour of real viscoelastic material.

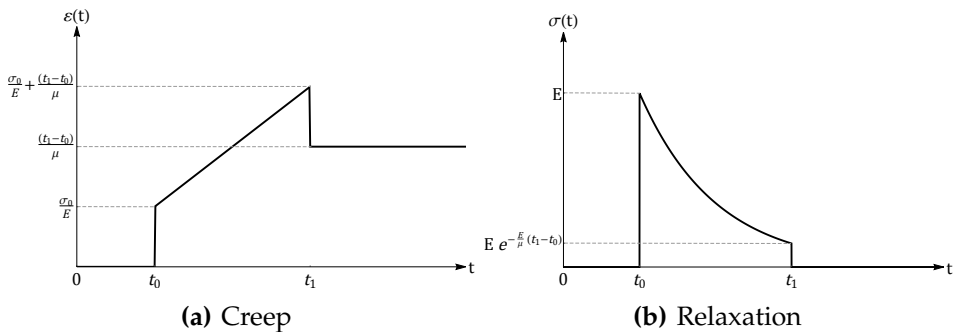


Figure 2.5: Creep and relaxation of the Maxwell model.

The Kelvin Voigt model (see (Figure 2.4(b))) is the dual of the Maxwell one, since the elements are connected in parallel. Differently from the Maxwell model, in this case the creep function (depicted in Figure 2.6(a)) can be considered acceptable to fit experimental data, although it is not the best choice for correct fitting. The relaxation function, instead, is totally in disagreement with experiments, because it is constant, see Figure 2.6(b).

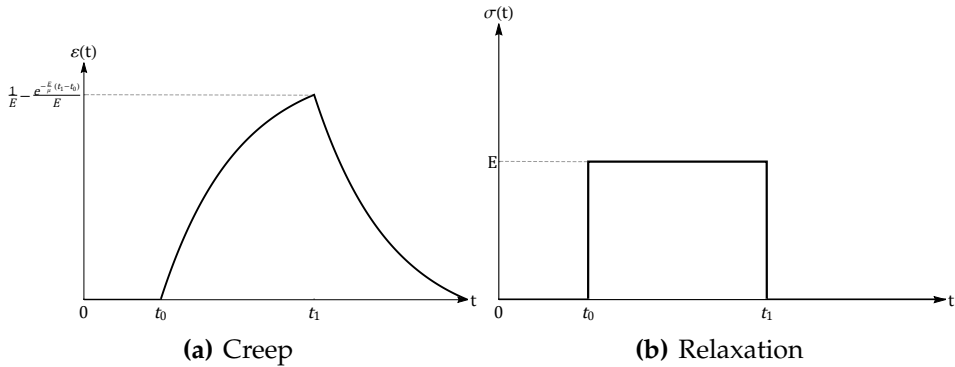


Figure 2.6: Creep and relaxation of the Kelvin Voigt model.

The Maxwell and the Kelvin Voigt are not able to reproduce both the creep and relaxation behaviours. Indeed, the Maxwell model is acceptable only to simulate relaxation while the Kelvin Voigt model is acceptable only to reproduce creep behaviour. For this reason other viscoelastic models composed of more elements have been developed.

Using more than two simple elements it is possible to define viscoelastic mechanical models that are able to reproduce both the creep and the relaxation behaviour. Changing the way the springs and the dashpots are linked, different viscoelastic behaviours may be represented. The most simple of these models are the Standard Linear Solid (SLS) and Zener model, shown in Figure 2.7.

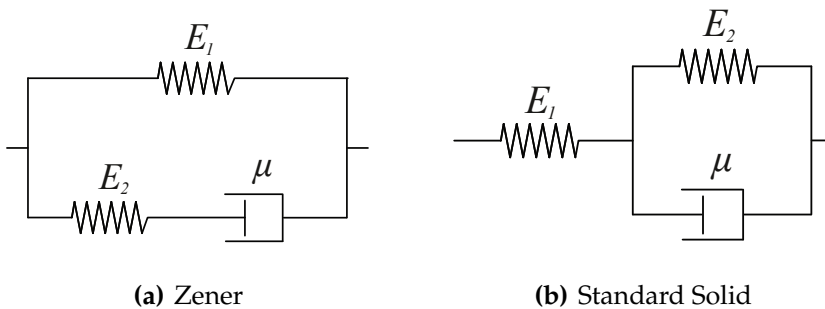


Figure 2.7: Zener and Standard Solid models.

All the response of these models are governed by exponential functions that ensure acceptable approximation of the creep and relaxations functions, especially when short term responses have to be simulated. Furthermore, these models have only three parameters each, and then the best fitting of experimental results is still easy to perform.

However, when simulation of long term behaviour is needed these models are not sufficiently accurate. For this reason viscoelastic models with more than three elements exist. The generic constitutive equation of these models is

$$\sum_{k=0}^n a_k \frac{d^k}{dt^k} \sigma(t) = \sum_{k=0}^m b_k \frac{d^k}{dt^k} \varepsilon(t). \quad (2.17)$$

In Eq. (2.17) a_k and b_k are coefficients that depend on the mechanical parameters of the springs and dashpots. When n and m increase, the accuracy of the model improves both in the short and in long term behaviour. This is due to the fact that real viscoelastic materials exhibit power law type creep and relaxation functions. Since the models of Eq. (2.17) have exponential type creep and relaxation functions, a good fitting of experimental data can be performed only with the superposition of many exponential functions, and then using models with many elements. However, many elements in the model means many coefficients to be defined with the best fitting of the experimental results. This can lead to practical difficulties in performing the best fitting and sometimes also to unexpected results. Despite all the disadvantages classical viscoelastic models are still used for some engineering applications, for the simplicity of mathematical manipulation and also for simple implementation in finite element software. However, many researchers in the field switched in the last decades their attention to something more rigorous and consistent with experimental results, that is fractional viscoelasticity.

Table 2.1 summarises the creep and the relaxation functions of the models presented in this subsection.

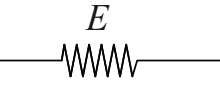
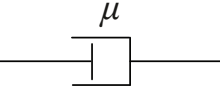
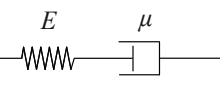
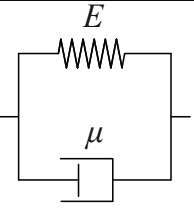
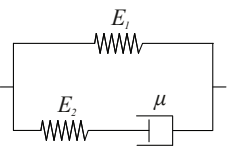
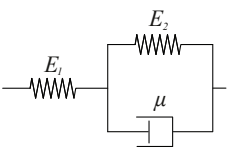
Element	Creep $C(t)$	Relaxation $R(t)$
	$\frac{1}{E}$	E
	$\frac{1}{\mu}t$	0
	$\frac{1}{E} + \frac{1}{\mu}t$	$Ee^{-t\frac{E}{\mu}}$
	$\frac{1}{E} \left(1 - e^{-t\frac{E}{\mu}}\right)$	E
	$\frac{1}{E_1} \left(1 - \frac{E_2 e^{-t\frac{E_1 E_2}{(E_1 + E_2)\mu}}}{E_1 + E_2}\right)$	$E_1 + E_2 e^{-t\frac{E_2}{\mu}}$
	$\frac{1}{E} \left(\frac{E_1 + E_2}{E_1} - e^{-t\frac{E_2}{\mu}}\right)$	$\frac{E_1}{E_1 + E_2} \left(E_2 + E_1 e^{-t\frac{E_1 + E_2}{\mu}}\right)$

Table 2.1: Creep and Relaxation response of different classical mechanical models.

2.3.2 Fractional models

Fractional models have the advantage of having a small number of parameters associated to some physical properties of the material. Apart from this, the main advantage associated with the fractional concept is due to the fact that it allows for the establishment of a new component named "Springpot" (or fractional dashpot or parabolic element or fractional Newton element). This element is depicted in Figure 2.8. The springpot was introduced by Scott Blair and Caffyn in 1949 [Scott Blair and Caffyn, 1949, Scott Blair, 1966, Scott Blair, 1974]. The constitutive laws of this element have been presented in Section 2.2 and they are characterised by the two parameters α and E_α .

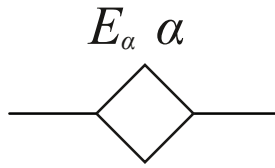


Figure 2.8: Springpot element.

The Springpot interpolates between the pure elastic behaviour (represented by the spring) and the viscous behaviour (represented by the dashpot). Unlike the conventional differential equations that use integer order differentiation, the fractional dashpot is achieved by using non-integer order of differentiation, as shown in the constitutive laws of Eq. (2.14).

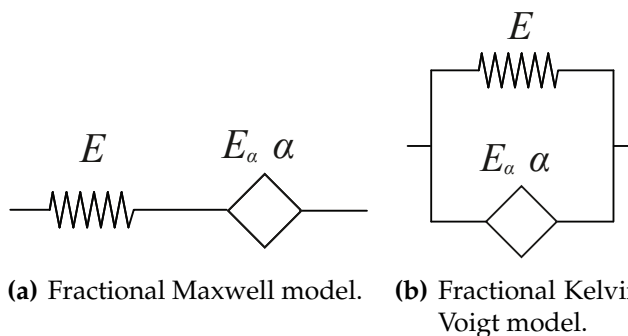


Figure 2.9: Fractional Maxwell and Kelvin Voigt models.

Even the Springpot element models well the viscoelastic behaviour of some materials for both the creep and the relaxation, it has been experimentally observed for other materials that the Springpot element is not enough. For this reason, it have been proposed model that combine the Springpot with springs and dashpots. The more simple ones are the fractional Maxwell and Kelvin Voigt models represented in Figure 2.9.

For bituminous materials and mixtures, the first fractional model developed was the Huet model (Figure 2.10(a)), published in 1963 [Huet, 1963]. In 1965 Sayegh presented the Huet-Sayegh (Figure 2.10(b)) model [Sayegh, 1965]. The Huet and the Huet-Sayegh models are Figure 2.10.

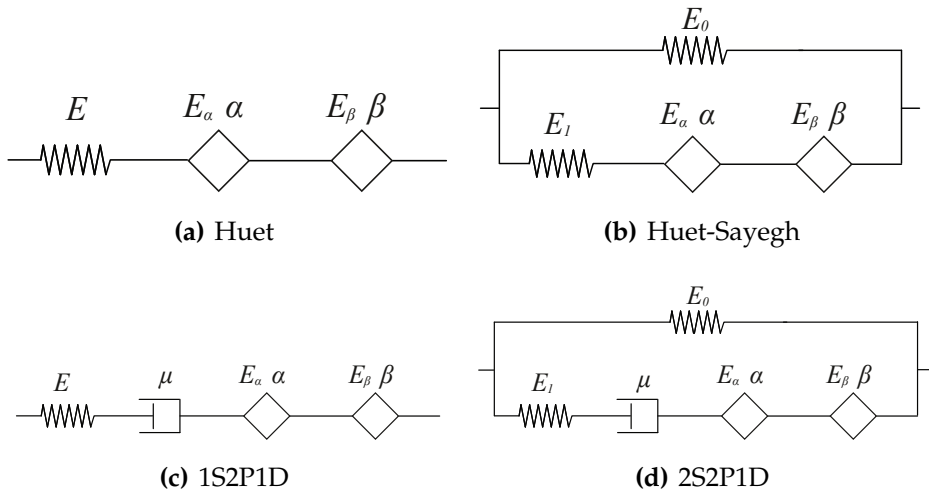


Figure 2.10: Fractional viscoelastic models for bituminous materials.

Recent developments have been introduced by Olard and Di Benedetto [Olard and Di Benedetto, 2003]. This models are the 1S2P1D (Figure 2.10(c)) and the 2S2P1D (Figure 2.10(d)) model, which overcomes some problems encountered with Huet and the Huet-Sayegh models. In the publication [Oeser and Pellinien, 2012], an wider review of the mechanical models for bituminous materials and mixtures is presented.

2.4 Fractional characteristic times

This section introduces the so-called fractional characteristic times and evaluates the equivalent elastic and viscous contribution of the fractional element, as proposed in [Colinas-Armijo et al., 2016].

Eqs. (2.14) represent the constitutive laws of linear fractional viscoelasticity. It has to be observed that for the two limit values of α ($\alpha = 0$ and $\alpha = 1$), the purely elastic and the purely viscous behaviours are recovered, respectively, since $({}^C D_{0+}^0 \varepsilon)(t) = \varepsilon(t)$ and $({}^C D_{0+}^1 \varepsilon)(t) = \dot{\varepsilon}(t)$. Thus, when $0 < \alpha < 1$ both elastic and viscous phase are present simultaneously, and the viscoelastic behaviour is captured. Such fractional stress-strain relations contain a coefficient E_α with anomalous dimension. In fact, this parameter is not a stiffness nor a viscosity quantity, and its dimension is

$$[E_\alpha] = [FT^\alpha L^{-2}], \quad (2.18)$$

that means that as α changes, the dimensions of E_α will change. This fact leads to some problems when a comparison is needed or a classification of different mechanical behaviour of materials is necessary. In fact, different materials with different values of α will have proportional parameters E_α depending on α (see Eq. (2.18)), and their comparison would be meaningless. An approach to solve this problem may be obtained by modifying temporal scale removing the presence of the dimension $[T^\alpha]$ on the coefficient E_α and obtaining a classical parameter from E_α .

In order to clarify this issue it is convenient to consider the classical models of viscoelasticity in which only two kinds of parameters appear (stiffnesses and viscosities). Classical viscoelastic models are obtained by different arrangements of springs and dashpots. Springs are characterised by stiffness parameter E and dashpots by a viscosity coefficient μ . The most well-known mechanical models are the Maxwell model and Kelvin-Voigt one.

The relaxation function of the Maxwell model is

$$R(t) = E \exp\left(-\frac{t}{\tau_\sigma}\right), \quad (2.19)$$

where $\tau_\sigma = \mu/E$ is the so-called the *relaxation time*, that is, the time such that $R(\tau_\sigma) = E/e$. The Maxwell model is commonly used to perform the best fitting of the relaxation tests by Eq. (2.19). Unfortunately, the corresponding creep function does not follow the experimental evidence of the creep test.

Another classical model that is able to characterise the creep behaviour is the Kelvin-Voigt model. For the Kelvin-Voigt model commonly the creep function is

$$C(t) = [1 - \exp(-t/\tau_\varepsilon)]/E \quad (2.20)$$

where $\tau_\varepsilon = \mu/E$ is known as *retardation time*, and it may be defined as the time such that $C(\tau_\varepsilon) = (eE)^{-1}/(e-1)$. Relaxation τ_σ and retardation τ_ε times are defined as characteristic times, and they are given by the same ratio μ/E . These two temporal parameters of classical viscoelasticity are important since they define at what instant it is possible to reach a purely elastic behaviour.

Now, it is useful to define two characteristic times for fractional models, that are the *fractional relaxation time* τ_σ defined as the time for which the relaxation function is equal to the stiffness $R(\tau_\sigma) = E$, and the *fractional creep time* τ_ε , that is defined as the time such that the creep function becomes a compliance, $C(\tau_\varepsilon) = 1/E$. Unfortunately, for the case in which the creep function and the relaxation function are power laws, these two times may not be defined uniquely. In order to show this issue it is necessary to define a time parameter η as the ratio of the viscous and the elastic contribution,

$$\eta = \frac{\mu}{E} [\text{sec}]. \quad (2.21)$$

Clearly, both μ and E are unknown since the fractional model is characterised by the coefficients E_α and α . Formerly introduced η , fractional creep and relaxation times are

$$\tau_\varepsilon = \eta \sqrt[\alpha]{\Gamma(1+\alpha)}, \quad (2.22a)$$

$$\tau_\sigma = \frac{\eta}{\sqrt[\alpha]{\Gamma(1-\alpha)}}. \quad (2.22b)$$

For the aforementioned definitions, and from the fractional stress-strain relations in Eqs. (2.14), the stress $\sigma(t)$ and the deformation $\varepsilon(t)$, due to a constant deformation ε_0 and a constant stress σ_0 at the time $t = 0$, are

$$\sigma(t) = \varepsilon_0 E \left(\frac{t}{\tau_\sigma} \right)^{-\alpha}, \quad (2.23a)$$

$$\varepsilon(t) = \sigma_0 \frac{1}{E} \left(\frac{t}{\tau_\varepsilon} \right)^\alpha. \quad (2.23b)$$

Setting $\varepsilon_0 = 1$ and $\sigma_0 = 1$, Eqs. (2.23) yields

$$R(t) = E \left(\frac{t}{\tau_\sigma} \right)^{-\alpha}, \quad (2.24a)$$

$$C(t) = \frac{1}{E} \left(\frac{t}{\tau_\varepsilon} \right)^\alpha. \quad (2.24b)$$

Observe that the two fractional characteristic times in Eq. (2.22) are such that $R(\tau_\sigma) = E$ and $R(\tau_\varepsilon) = 1/E$, as it has been previously established.

By introducing the fractional characteristic times in the fractional constitutive laws, the coefficient E_α with anomalous dimensions disappears and the issue of comparing mechanical properties at different conditions is not ambiguous. Figure 2.11 shows the ratios τ_ε/η and τ_σ/η versus α .

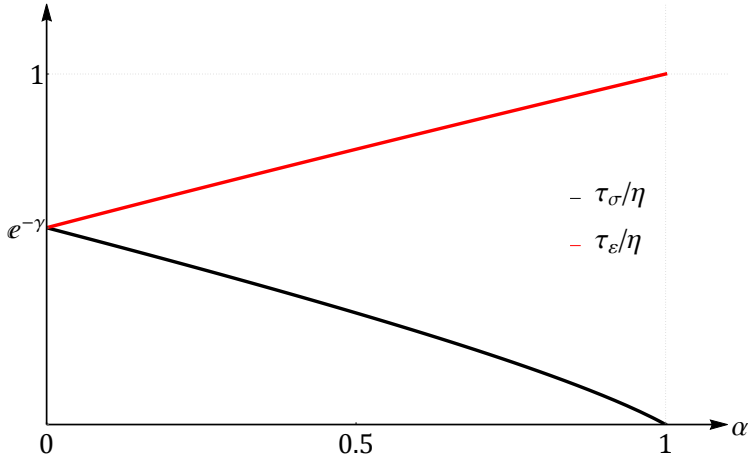


Figure 2.11: Fractional characteristic times versus α

From Figure 2.11, observe that $\tau_\varepsilon \geq \tau_\sigma$, the two curves share a common point at $\alpha = 0$, and this value is equal to $e^{-\gamma}$ (being $\gamma = 0.577215\dots$ the Euler-Mascheroni constant).

From the fractional characteristic times, two remarkable relations can be derived. The first one is that the two curves are almost linear, then the subtraction of τ_ε and τ_σ yields

$$\tau_\varepsilon - \tau_\sigma = \eta \left[\sqrt[\alpha]{\Gamma(1 + \alpha)} - \frac{1}{\sqrt[\alpha]{\Gamma(1 - \alpha)}} \right] \approx \eta \alpha. \quad (2.25)$$

The second relation is given by the product of $R(t)C(t)$, that is,

$$R(t)C(t) = \left(\frac{\tau_\sigma}{\tau_\varepsilon} \right)^\alpha = [\Gamma(1 + \alpha)\Gamma(1 - \alpha)]^{-1} = \frac{\sin(\alpha\pi)}{\alpha\pi}. \quad (2.26)$$

It is observed that the fundamental relationship in the Laplace domain in Eq. (2.7) may be rewritten in the time domain as Eq. (2.26). Unfortunately, taking into account the relationships (2.25) and (2.26), there is not enough information to define clearly τ_σ , τ_ε and η since there are two equations and three unknown variables.

At this point, the necessity to distinguish the elastic and the viscous contribution inside the fractional model arises. In some previous papers [Di Paola and Zingales, 2012, Di Paola et al., 2013a, Di Paola et al., 2013b], some efforts to clarify the lack of an unambiguous separation of the elastic and the viscous contribution in the fractional model have been performed by introduction of a mechanical model of the fractional stress-strain relation. Such mechanical model is composed by a proper arrangements of perfect elastic springs and purely viscous dashpots. However, also the mechanical model of the fractional viscoelasticity still contains the same lack of uniqueness in the determination of the involved parameters. In other words, there is one arrangement of the fractional viscoelasticity but more than one model to describe the same fractional stress-strain relation [Di Paola et al., 2013b]. This fact implies that the time parameters τ_ε and τ_σ cannot be unequivocally defined. Moreover, in a previous work [Deseri et al., 2014], it was shown that with energetic considerations about the dissipated energy of the fractional mechanical model, the separation of the elastic and viscous contribution is impossible. For these reasons, in the next section a new approach to obtain the elastic and the viscous contribution on the fractional model is presented.

2.4.1 Estimation of fractional characteristic times

As it has been shown, in fractional viscoelasticity the coefficients μ and E may not be defined unambiguously, and as a consequence τ_σ and τ_ε may not be determined. In order to overcome this difficulty, a new method to calculate equivalent elastic and viscous contributions is developed with the aid of an equivalent classical viscoelastic model. The proposed method is based on the definition of an equivalent Kelvin-Voigt model of fractional viscoelasticity. In this way only classical parameters appear in the stress-strain relation, that is, the stiffness coefficient of the equivalent spring E_e , and the viscous coefficient of the dashpot μ_e (where the subscript e stands for *equivalent*). Similarly to the method of linearisation, the equivalent classical model is obtained by the definition of a proper functional and by a minimisation of the error due to the difference between the response of the given fractional model and the re-

sponse of the equivalent classical one. In this way the equivalent stress-strain relation becomes a classical integer order differential equation, and the elastic and viscous contribution can be readily obtained. The procedure may be developed as soon as the external input in terms of deformation history is defined. In particular, three classes of excitations are considered below, namely, purely harmonic, periodic and pseudo-stochastic deformation history.

Hereinafter, since the strain history $\varepsilon(t)$ is assigned and the corresponding stress history is determined by the fractional stress-strain relation in Eq. (2.14a), then the equivalent classical model that is able to describe such relation is the Kelvin-Voigt one. On the contrary, if the stress history $\sigma(t)$ is assigned and the corresponding strain history is obtained by Eq. (2.14b), then the equivalent model is of Maxwell type.

Harmonic excitation

Suppose an harmonic excitation in terms of deformation history,

$$\varepsilon(t) = \varepsilon_0 \sin(\omega t). \quad (2.27)$$

The steady state solution in terms of stress history $\sigma(t)$ can be found by using Eq. (2.10a) and by putting $-\infty$ as lower bound. For the imposed strain input in Eq. (2.27), such solution can be found in closed form [Samko et al., 1993, Miller and Ross, 1993, Podlubny, 1998], that is,

$$\sigma(t) = E_\alpha \left({}^C D_+^\alpha \varepsilon \right) (t) = E_\alpha \varepsilon_0 \omega^\alpha \sin \left(\frac{\pi\alpha}{2} + \omega t \right), \quad \omega > 0. \quad (2.28)$$

where the subscript $+$ denotes the left-handed derivative with lower bound $-\infty$ (according to the notation in [Samko et al., 1993]). The response of the fractional stress-strain relation in Eq. (2.28) can be obtained as the solution of an *equivalent model*, that is ruled by an integer-order differential equation in the form

$$\mu_e \dot{\varepsilon}(t) + E_e \varepsilon(t) = \sigma(t), \quad (2.29)$$

where μ_e and E_e are equivalent coefficients. These coefficients have to be chosen in such a way that the difference between Eq. (2.28) and Eq. (2.29) is minimum in some sense. It is noted that Eq. (2.29) represents the stress-strain relationship of the Kelvin-Voigt model.

As in the classical linearisation technique it is necessary to define a functional $F(\mu_e, E_e)$ that is related to the difference between the original and the

equivalent system. In particular, taking into account Eqs. (2.28) and (2.29), such functional is

$$F(\mu_e, E_e) = \int_0^{2\pi/\omega} \left[E_\alpha \left({}^C D_{+}^\alpha \varepsilon \right) (t) - \mu_e \dot{\varepsilon}(t) - E_e \varepsilon(t) \right]^2 dt. \quad (2.30)$$

Now, in order to find the coefficients of the equivalent systems, the squared error due to the two response must be the minimum with respect to the equivalent parameters μ_e and E_e . This fact implies that coefficients are given by the following two partial differential equations,

$$\partial F(\mu_e, E_e) / \partial \mu_e = 0, \quad (2.31a)$$

$$\partial F(\mu_e, E_e) / \partial E_e = 0. \quad (2.31b)$$

In particular, by performing the variations, the equivalent coefficients μ_e and E_e are

$$\mu_e = \omega^{\alpha-1} E_\alpha \sin\left(\frac{\pi\alpha}{2}\right), \quad (2.32a)$$

$$E_e = \omega^\alpha E_\alpha \cos\left(\frac{\pi\alpha}{2}\right). \quad (2.32b)$$

From Eq. (2.21) the equivalent ratio η_e is

$$\eta_e = \frac{\mu_e}{E_e} = \frac{\omega^{\alpha-1} E_\alpha \sin\left(\frac{\pi\alpha}{2}\right)}{\omega^\alpha E_\alpha \cos\left(\frac{\pi\alpha}{2}\right)} = \frac{1}{\omega} \tan\left(\frac{\pi\alpha}{2}\right). \quad (2.33)$$

Eqs. (2.32) and (2.33) show that μ_e , E_e and η_e depend on the frequency of the strain history ω , and on the parameters of the fractional law E_α and α . Once η_e is obtained then the fractional creep and relaxation times (τ_ε and τ_σ) may be calculated by the definition in Eq. (2.22), that is,

$$\tau_\varepsilon = \frac{1}{\omega} \tan\left(\frac{\pi\alpha}{2}\right) \sqrt[\alpha]{\Gamma(1+\alpha)}, \quad (2.34a)$$

$$\tau_\sigma = \frac{1}{\omega} \tan\left(\frac{\pi\alpha}{2}\right) \frac{1}{\sqrt[\alpha]{\Gamma(1-\alpha)}}. \quad (2.34b)$$

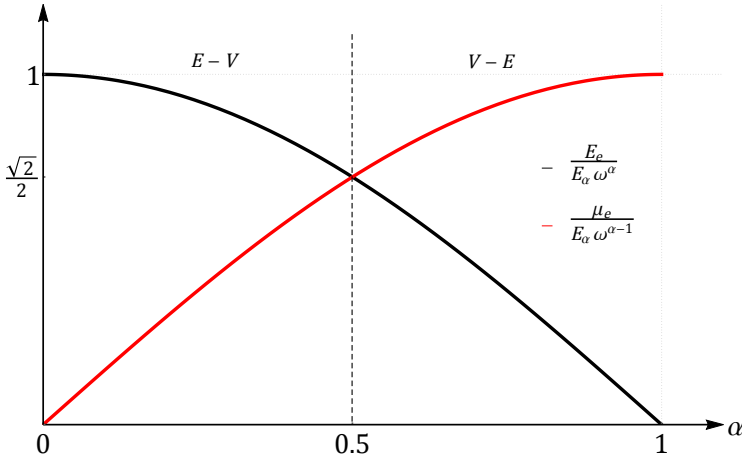


Figure 2.12: Plot of dimensionless parameters μ_e and E_e versus α .

Figure 2.12 shows the dimensionless coefficients μ_e and E_e versus α . In other words, in such figures the trends of $\mu_e/(E_\alpha\omega^{\alpha-1})$ and $E_e/(E_\alpha\omega^\alpha)$ are represented for different values of the order α . Thus, in that graphical representation the influence of α on the viscoelastic behaviour appears. Specifically, for $0 < \alpha < 1/2$ the ratio $E_e/(E_\alpha\omega^\alpha)$ is greater than $\mu_e/(E_\alpha\omega^{\alpha-1})$, and the elastic behaviour prevails with respect to the viscous one, when $\alpha = 0$ the viscous term disappears and only the purely elastic contribution is present. For $1/2 < \alpha < 1$ the viscous behaviour prevails and for $\alpha = 1$ the elastic component disappears and only the purely viscous phase remains. For $\alpha = 1/2$ the two curves share a common point and the two contributions, elastic and viscous, are equal.

By inserting μ_e and E_e in Eq. (2.29) and solving with respect to the excitation of Eq. (2.27), the solution gives exactly the same response, at steady-state, as the one evaluated with Eq. (2.28). It follows that the response of the two models, the fractional and the equivalent, under harmonic excitation is equal at steady-state. This fact is shown in Figure 2.13.

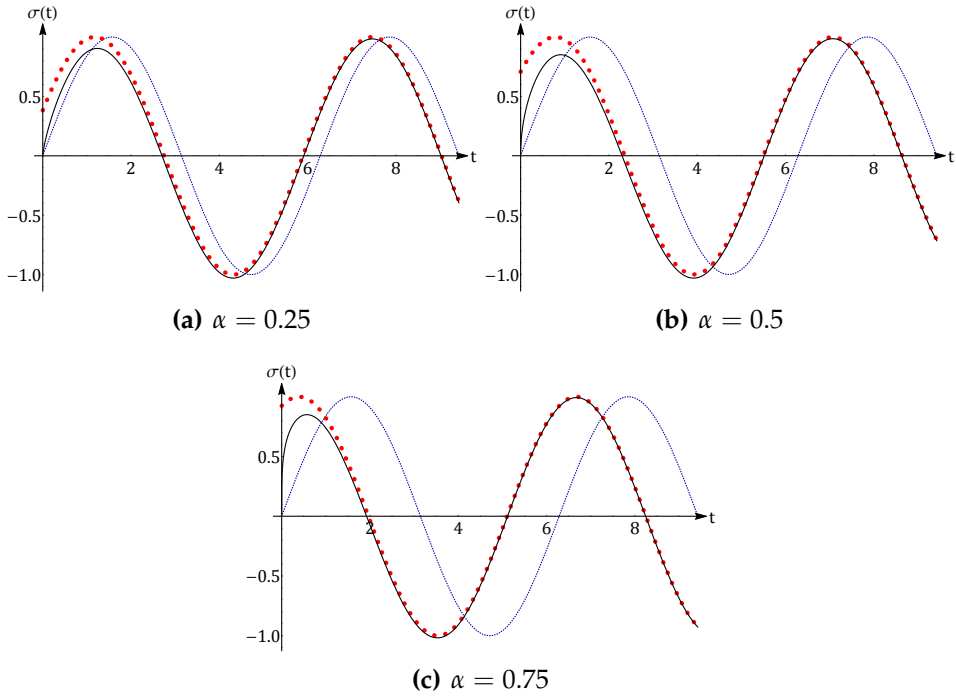


Figure 2.13: Harmonic excitation (dashed line), response of fractional model (continuous line), equivalent Kelvin-Voigt model (dotted line).
 $\omega = 1$ rad/s, $\varepsilon_0 = 1$ and $E_\alpha = 1$.

From Figure 2.13, it can be observed that in the transient state (in the first few seconds) the responses of the fractional and the equivalent models are different, but, as soon as both models reach the steady-state, the responses tend to overlap each other and, for $t \rightarrow \infty$ the two responses exactly coincide.

Periodic excitation

Hereinafter, the concepts exploited for the harmonic function are generalised for any periodic function with the shape

$$\varepsilon(t) = \sum_{j=1}^n \varepsilon_j \sin(j\omega t), \quad j = 1, 2, \dots, n, \quad (2.35)$$

where ω is the fundamental frequency and ε_j are the coefficients of the Fourier series.

The steady-state response due to the generic periodic excitation of Eq. (2.35) is calculated by solving Eq. (2.14a) and by putting as lower integration bound $-\infty$ to t . Therefore, such response is

$$\sigma(t) = E_\alpha \sum_{j=1}^n \varepsilon_j(j\omega)^\alpha \sin\left(\frac{\pi\alpha}{2} + j\omega t\right). \quad (2.36)$$

As it has been done in the previous case, in order to obtain μ_e and E_e the minimisation of the functional in Eq. (2.30) for the periodic excitation of Eq. (2.35) has to be performed. In particular, for this case the coefficients may be readily found in the form

$$\mu_e = E_\alpha \sin\left(\frac{\pi\alpha}{2}\right) \frac{\lambda_\varepsilon(\alpha + 1)}{\lambda_\varepsilon(2)}, \quad (2.37a)$$

$$E_e = E_\alpha \cos\left(\frac{\pi\alpha}{2}\right) \frac{\lambda_\varepsilon(\alpha)}{\lambda_\varepsilon(0)}, \quad (2.37b)$$

where $\lambda_\varepsilon(\rho)$ are the spectral moments of order ρ of the power associated to each harmonic component in Eq. (2.35), that is,

$$\lambda_\varepsilon(\rho) = \sum_{j=1}^n \varepsilon_j^2(j\omega)^\rho, \quad \rho = 0, 2, \alpha, \alpha + 1. \quad (2.38)$$

In this way the ratio $\eta_e = \mu_e/E_e$ is

$$\eta_e = \tan\left(\frac{\pi\alpha}{2}\right) q(\alpha), \quad (2.39)$$

where $q(\alpha) = \lambda_\varepsilon(0) \lambda_\varepsilon(\alpha + 1) / \lambda_\varepsilon(2) \lambda_\varepsilon(\alpha)$ accounts for the distribution of the power due to each harmonic component.

The fractional characteristic times result as

$$\tau_\varepsilon = \tan\left(\frac{\pi\alpha}{2}\right) q(\alpha) \sqrt[\alpha]{\Gamma(1 + \alpha)}, \quad (2.40a)$$

$$\tau_\sigma = \tan\left(\frac{\pi\alpha}{2}\right) q(\alpha) \frac{1}{\sqrt[\alpha]{\Gamma(1 - \alpha)}}. \quad (2.40b)$$

The comparison between Eqs. (2.34) and Eqs. (2.40) shows that in the case of periodic excitation the fractional characteristic times are modified by the factor $q(\alpha)$, in which the distribution of ε_j^2 is considered.

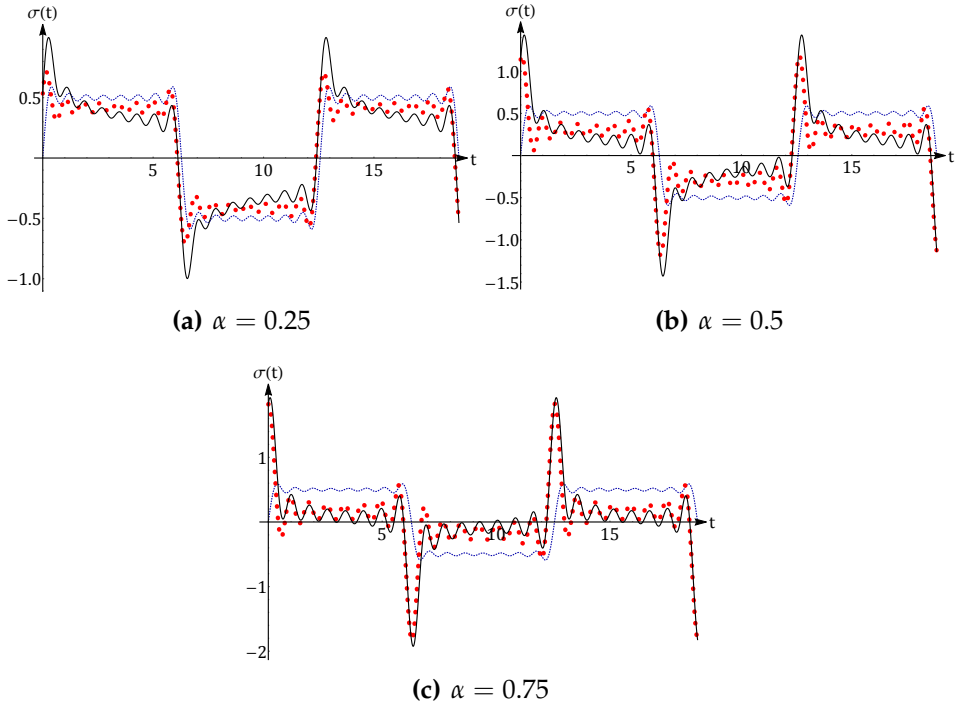


Figure 2.14: Periodic excitation (dashed line), steady-state response of the fractional model (continuous line), equivalent model (dotted line).

Figure 2.14 shows the periodic excitation and the response evaluated by direct integration of the fractional and the equivalent models. In this example, $\varepsilon(t)$ is a periodic square wave, approximated by fifteen terms in the Fourier series, with unitary amplitude and period $T = 2\pi/\omega$ (where $\omega = 0.5$ rad/s), and ε_j follows the equation

$$\varepsilon_j = \int_0^{2\pi/\omega} u(t) \sin(j\omega t) dt = \frac{\cos(j\pi) - 1}{j\pi}, \quad (2.41)$$

where $u(t)$ is the periodic square wave.

From Figure 2.14 it may be seen that the responses due to a periodic excitation for the fractional and for the equivalent model do not coincide, both in the transient phase and at steady-state.

2.4.2 Elastic and viscous contribution. Dissipated energy.

Once the fractional characteristic times have been obtained for any harmonic or periodic function, the elastic and viscous contribution and the dissipated energy may be calculated.

Harmonic excitation

By using the convolution theorem and the properties of fractional operators (see [Samko et al., 1993, Miller and Ross, 1993, Podlubny, 1998]), the Fourier transform of Eq. (2.14a) yields

$$\hat{\sigma}(\omega) = E_\alpha (i\omega)^\alpha \hat{\varepsilon}(\omega) = E_\alpha |\omega|^\alpha \left[\cos\left(\frac{\pi\alpha}{2}\right) + i \operatorname{sign}(\omega) \sin\left(\frac{\pi\alpha}{2}\right) \right] \hat{\varepsilon}(\omega), \quad (2.42)$$

where $\hat{\sigma}(\omega)$ and $\hat{\varepsilon}(\omega)$ are the Fourier transform of $\sigma(t)$ and $\varepsilon(t)$ respectively, and ω is the frequency of the Fourier transform. The complex modulus, denoted $E^*(i\omega)$, is defined as the ratio between stress and strain in the Fourier domain. That is,

$$E^*(i\omega) = \frac{\hat{\sigma}(\omega)}{\hat{\varepsilon}(\omega)} = E_\alpha |\omega|^\alpha \left[\cos\left(\frac{\pi\alpha}{2}\right) + i \operatorname{sign}(\omega) \sin\left(\frac{\pi\alpha}{2}\right) \right]. \quad (2.43)$$

$E^*(i\omega)$ can be also written as

$$E^*(i\omega) = E'(\omega) + i E''(\omega), \quad (2.44)$$

where $E'(\omega) \in \mathbb{R}$ is the *storage modulus*, and $E''(\omega) \in \mathbb{R}$ is the *loss modulus*. By comparing Eqs. (2.32) with Eq. (2.43), μ_e and E_e may be written in terms of $E'(\omega)$ and $E''(\omega)$ as follows

$$E_e = E'(\omega), \quad (2.45a)$$

$$\mu_e = \frac{E''(\omega)}{\omega}. \quad (2.45b)$$

This is a remarkable result because it gives a different perspective of $E'(\omega)$ and $E''(\omega)$ and links the creep and relaxation functions with the complex modulus. As in fact, the former is the stiffness and the latter is related to the viscosity of the equivalent model.

Clearly, the dissipated energy of the fractional model at steady-state and of the equivalent model are equal, since $\sigma(t)$ and $\varepsilon(t)$ coincide for both models. Nevertheless, it is useful to evaluate the dissipated energy in one cycle, which

is denoted by $\mathcal{D}(T)$. The energy balance for Eq. (2.28) is obtained by multiplying both members of such equation by $\dot{\varepsilon}(t)dt$, and performing the time integration. From the obtained equation the distinction between dissipated and stored energy may not be done. However, if the integration is performed in one cycle the stored energy becomes zero and then the dissipated energy coincides with the entire energy, that is,

$$\mathcal{D}(T) = \int_{t_1}^{t_1+T} \sigma(t)\dot{\varepsilon}(t)dt, \quad (2.46)$$

where the selected T is the period of the harmonic excitation ($T = 2\pi/\omega$) and t_1 is such that the transitory effects may be neglected. Substituting Eq. (2.27) and (2.28) in Eq. (2.46) the dissipated energy in one cycle for the fractional model becomes

$$\mathcal{D}(T) = E_\alpha \varepsilon_0^2 \pi \omega^\alpha \sin\left(\frac{\pi\alpha}{2}\right). \quad (2.47)$$

For the equivalent Kelvin-Voigt model, the stored and the dissipated energy is readily obtained by multiplying both members of Eq. (2.29) by $\dot{\varepsilon}(t)dt$ and integrating over one period. In this way the term $E_e \int_{t_1}^{t_1+T} \varepsilon(t)\dot{\varepsilon}(t)dt$, which represents the stored energy, becomes zero, and the dissipated energy is

$$\mathcal{D}_e(T) = \mu_e \int_{t_1}^{t_1+T} \dot{\varepsilon}^2(t)dt = \varepsilon_0^2 \mu_e \pi \omega. \quad (2.48)$$

By substituting the coefficient μ_e , obtained by Eq. (2.32a), into Eq. (2.48) the same fractional model calculated by Eq. (2.47) is obtained. In other words, in the case of harmonic excitation, at steady-state, the dissipated energy of the fractional and of the equivalent models are equivalent and the hysteresis loops are coincident.

Figure 2.15 shows the hysteresis loops for the equivalent and for the fractional models at steady-state for different values of α (both lines exactly coincide and may not be distinguished). It has to be emphasised that the hysteresis loop of the fractional model under a pure harmonic input is an ellipse.

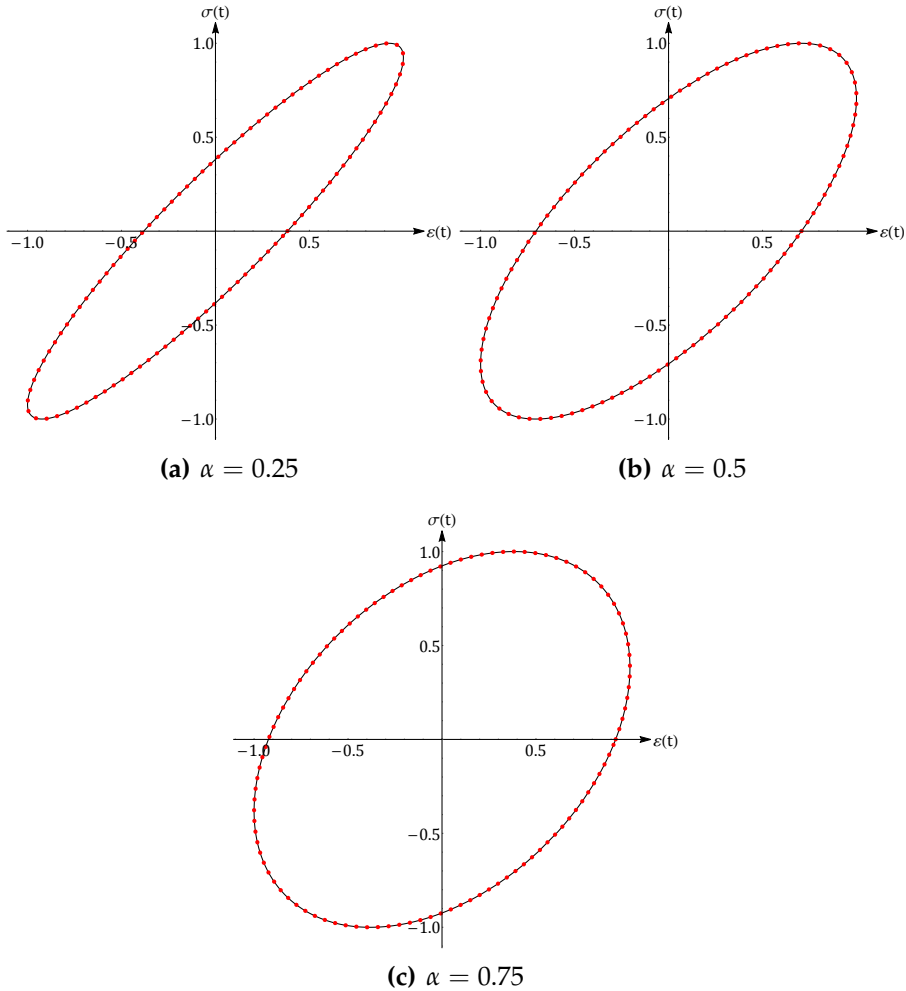


Figure 2.15: Hysteresis loop for harmonic excitation. Continuous line fractional model, dotted line equivalent Kelvin-Voigt model. $\omega = 1$ rad/s, $\epsilon_0 = 1$ and $E_\alpha = 1$.

Now, some useful considerations can be drawn by introducing some energetic concepts in the fractional and the equivalent viscoelastic model. The dissipation and the free energy for linear and nonlinear viscoelastic models were evaluated in several papers, e.g. [Breuer and Onat, 1964, Gurtin and Hrusa, 1988, Fabrizio and Morro, 1988, Fabrizio et al., 1994, Fabrizio et al., 1995]. A similar approach can be used also for the fractional viscoelastic model. In

this regard, according to the Staverman-Schwarzl formulation of the free energy (see [Deseri et al., 2014]), the dissipation rate of the fractional viscoelastic model is

$$\dot{\mathcal{D}}(t) = \frac{\alpha E_\alpha}{\Gamma(1-\alpha)} \int_{-\infty}^t \int_{-\infty}^t (2t - \tau_1 - \tau_2)^{-1-\alpha} \dot{\varepsilon}(\tau_1) \dot{\varepsilon}(\tau_2) d\tau_1 d\tau_2. \quad (2.49)$$

Such equation cannot be integrated in analytical form but can be solved numerically, and its time integral gives the exact solution of the dissipation energy of the fractional viscoelastic model. Instead, as it is shown in Eq. (2.48), the dissipated energy of the equivalent model is readily found and is given as

$$\mathcal{D}_e(t) = \mu_e \int_0^t \dot{\varepsilon}^2(t) dt = \frac{1}{4} \varepsilon_0^2 \mu_e \omega [2t\omega + \sin(2t\omega)]. \quad (2.50)$$

For the considered case in which the imposed strain history is the harmonic function in Eq. (2.27), at steady-state, a comparison between the two formulations of dissipated energy in Eq. (2.49) and in Eq. (2.50) is reported in Figure 2.17. Such Figure shows that the two time-evolution energies are different.

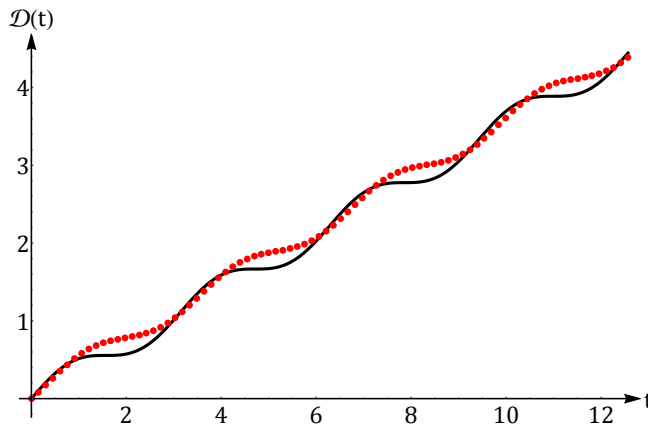


Figure 2.16: Staverman-Schwarzl dissipated energy of fractional viscoelastic model (dotted line) and dissipated energy of the classical equivalent model (continuous line).

However, the two functions coincide for $t = kT/2, \forall k \in \mathbb{N}^+$. This fact implies that the dissipated energy in a cycle and a half cycle of the fractional and the equivalent model are exactly the same.

Periodic excitation

As it has been done for the case of a harmonic excitation, the relation between E_e and μ_e with $E^*(i\omega)$, $E'(\omega)$ and $E''(\omega)$ has to be analyzed. By comparing Eq. (2.37) with Eq. (2.44), μ_e and E_e written in function of storage and loss moduli reads as

$$E_e = \frac{1}{\lambda_\varepsilon(0)} \sum_{j=1}^n E'(j\omega), \quad (2.51a)$$

$$\mu_e = \frac{1}{\lambda_\varepsilon(2)} \sum_{j=1}^n \omega_j E''(j\omega). \quad (2.51b)$$

As it has been demonstrated for pure harmonic excitation, for a periodic excitation the storage modulus is related to the elastic contribution and the loss modulus is linked to the viscous contribution.

By Eq. (2.46) the dissipated energy for both models is evaluated. For the fractional model the dissipated energy in one cycle is

$$\mathcal{D}(T) = E_\alpha \sum_{j=1}^n \pi (j\omega)^\alpha \varepsilon_j^2 \sin\left(\frac{\pi\alpha}{2}\right), \quad (2.52)$$

while for the equivalent model the dissipated energy results in

$$\mathcal{D}_e(T) = \mu_e \sum_{j=1}^n \pi j\omega \varepsilon_j^2. \quad (2.53)$$

From the substitution of the value μ_e obtained by Eq. (2.37a) in the dissipated energy for the equivalent model (Eq. (2.53)), it results that the two dissipated energies coincide, $\mathcal{D}(T) = \mathcal{D}_e(T)$. Thus, it is demonstrated that the dissipated energy in a cycle is exactly the same for both fractional and equivalent model. This is a very noteworthy result because despite the stress history and the hysteresis loop for the equivalent and for the fractional models do not coincide, the dissipated energy for one cycle is exactly the same.

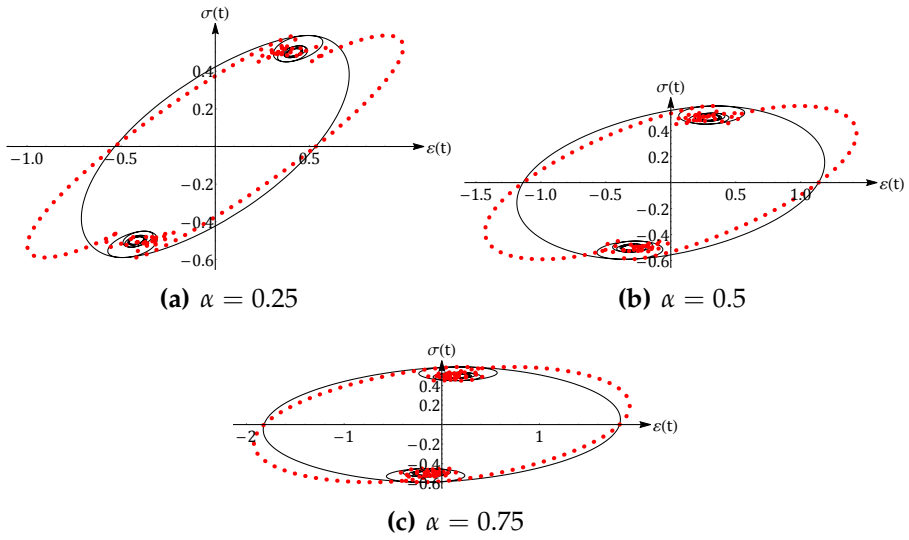


Figure 2.17: Hysteresis loop for Periodic excitation. Continuous line fractional model, dotted line equivalent Kelvin-Voigt model. $\omega = 0.5$ rad/s, $n = 15$ and $E_\alpha = 1$.

In Figure 2.14, the plots of the hysteresis loops, corresponding to the excitation depicted in Figure 2.17, for the fractional and for the equivalent model are displayed for different values of α .

2.5 Conclusions

In this chapter, the concepts of linear fractional viscoelasticity have been presented. It is well-known that for viscoelastic materials the creep and the relaxation functions are power laws rather than exponentials. Thus, generalised derivatives or integrals appear in the constitutive laws. In particular, the stress history is proportional to the Caputo's fractional time-derivative of order α of the strain history. Vice-versa the strain history is proportional to the Riemann-Liouville time-integral of the order α of the stress history. The order of such operators is $0 \leq \alpha \leq 1$. The two limit values of the fractional order, $\alpha = 0$ and $\alpha = 1$, correspond to the linear elastic relation and to the Newtonian viscous law, respectively. If the order is a non-integer value, the elastic and the viscous contribution may not be separated in the fractional stress-strain relation. Therefore, it cannot be distinguished between the solid and the viscous behaviour. On the contrary, in the classical viscoelastic units, such as the Kelvin-Voigt or Maxwell model, the two phases are immediately recognisable since the spring represents the solid part and the dashpot is related to the fluid phase.

Moreover, an equivalent classical model of the fractional stress-strain relation has been introduced in order to distinguish the elastic and the viscous contribution. In particular, if the imposed excitation is a strain history, the response is given in terms of stress history by the Caputo's fractional derivative, and the equivalent model is the Kelvin-Voigt unit. Vice-versa, if the stress history is imposed, the corresponding strain history is obtained by the Riemann-Liouville integral, and the proper equivalent model must be the Maxwell model. The parameters of the equivalent model have been found by an optimisation procedure once the imposed strain or stress history has been selected. In particular, the equivalent parameters have been calculated for two different classes of excitation, harmonic and periodic.

Chapter 3

Railway sub-ballast rubberised asphalt

This chapter discuss the use of *recycled rubber* in *asphalt mixtures*. The main problem on crumb rubber asphalt, using rubber of a certain size, is the compaction. It has been demonstrated experimentally that the void content increases after compaction. Thus, in this chapter an analytical approach is proposed to the mix design optimisation of bituminous mixtures containing crumb rubber using a gyratory compactor [Bressi et al., 2017]. The method takes into account the deformation release of the rubber after compaction for the analysis of the expected voids content. The analytical approach is validated by results of experimental tests.

3.1 The use of recycled rubber in asphalt mixtures

The disposal of waste tyres constitutes a problem with 275 million tyres being discarded per year in the US and 180 million in Europe [Issa and Salem, 2013]. Normally, some of the scrap tyres are reused (resold) [Heitzman, 1992] but for the most part they are piled in landfills. The environmental issues caused by this procedure and the lack of space have led to find other solutions. The recycling of scrap tyres began in the 60s of the last century, when pavement engineers started considering the use of crumb rubber as a modifier of bitumen for asphalt mixtures [McDonald, 1981, Scofield, 1989, Lo Presti, 2013].

The crumb rubber (CR) made by reprocessing end-of-life tyres (ELTs) finds different types of application in the production of asphalt mixtures. The pur-

pose is to improve the performance of asphalt mixtures. Indeed, tyres have a wider range of performance temperatures than bituminous mixtures, because they do not melt in the heat and they do not crack of cold temperatures. Two main different methods allow the addition of the rubber to asphalt mixtures: the wet and dry process. The wet process involves the dissolution of the crumb rubber in the bitumen as a modifying agent. The dry process involves the replacement of a small portion of aggregates with the same fraction of rubber grains. The asphalt produced following the “dry process” is called “rubberised asphalt” [Chesner et al., 1998]. Incorporating crumb rubber as an aggregate could enhance damping properties, because the rubber absorbs vibrations [D’Andrea et al., 2012]. For instance, D’Andrea et al. [D’Andrea et al., 2012], using 2D and 3D FEM models, have shown that the construction of a sub-ballast layer for a railway track bed (12 cm) with rubber (dry process) could produce a decrease in the effective levels of vibrations of approximately $4dB$, for frequencies in the $50 - 125Hz$ range, compared to track beds where a traditional bituminous mixture is used. Studies carried out on the mechanical properties of the crumb rubber mixtures (CRMs) report contradictory results. On one hand, the rubber increases the demand for bitumen and this could have a negative effect on the mechanical characteristics of the asphalt mixture. The resilient modulus of the rubberised asphalt decays and this implies an increase in layer thickness, compared with conventional mixtures [Chesner et al., 1998, D’Andrea et al., 2012, Maggiore et al., 2012, Moreno et al., 2011, Huang et al., 2007]. On the other hand, an interaction was observed between bitumen and rubber, the volatile components of bitumen are transferred to the rubber [López-Moro et al., 2013]. The absorption of lighter components (paraffin and maltenes) is part of the maturation process known as “maceration” [Hernández-Olivares et al., 2009, Dong et al., 2012]. It causes swelling of the crumb rubber particles and leads to a more viscous bitumen. As a consequence of this effect, the stiffness of the bitumen increases, thereby leading to higher performances of mixtures containing CR compared to conventional asphalt, in particular higher resistance to rutting [Dantas Neto et al., 2005]. Besides that, recent studies [Navarro et al., 2004, Rebala and Estakhri, 1995] showed that when the dry process is used to incorporate rubber in asphalt mixtures it is possible to obtain higher rutting resistance compared to mixtures based on the wet process. However, the use of the dry process cannot inhibit cracking at low temperature. It was found that the mechanical properties of rubberised asphalt largely depend on the dimensions of the rubber grains [Losa et al., 2011, Xiao et al., 2009]

The different mechanical properties, the crumb rubber gradation, the binder and rubber content, the mixing and compaction energies and the temperature are only some of the parameters that make the manufacturing process complex and unstable. Moreover, mixing time and temperature should be considered as additional factors that increase the number of variables to control during the fabrication process [Lee et al., 2008]. Moreover, some studies, using design of experiments, identified the most important parameters and the optimal conditions for manufacturing rubberised asphalt [Tortum et al., 2005].

3.1.1 Mix design of bituminous mixtures

When crumb rubber is added to asphalt mixtures, the compactability of the material is affected, because the rubber is an additional element involved in the mixture that has a different behaviour from the other components (bitumen, filler and aggregates). Recent studies [Pettinari and Simone, 2015] observed that the spring-back effect of the rubber causes an increase in the specimen volume after compaction and, this variation depends on the quantity of the rubber and grains size. The spring-back effect of the rubber raises the need to adjust the compaction method originally tailored to the traditional mixture. Indeed, when rubber is used, the mixing and compacting temperature may vary [Lee et al., 2008, Akisetty et al., 2011]. Despite the numerous efforts employed in improving the mix design system for bituminous mixtures, still certain limitations emerge when the traditional compaction technique is applied to CR mixtures. First, the rubber absorbs part of the bitumen, increasing its need in the mixture for a satisfactory workability [Moreno et al., 2011]. Moreover, the CR mixture needs a certain curing time to complete the swelling and stabilise [Pettinari and Simone, 2015]. This curing time is mainly influenced by temperature and the size of the rubber particles [Airey et al., 2003]. The swelling is partly due to the chemical interaction between rubber and bitumen [Dong et al., 2012] that leads to an increase in bitumen demand. Moreover, especially in the case of the dry process, the swelling after compaction is mostly due to the mechanical behaviour of the rubber.

3.1.2 Problem statement and objective

Crumb rubber could be approximately considered as an elastic material, significantly less stiff than aggregates. Therefore, when a stress is applied it is subjected to a deformation, but once the stress is removed, it returns to its

original configuration. Thus, crumb rubber releases the deformation accumulated during the compaction process. This may turn out in a non-negligible swelling of the asphalt mixture sample and can cause an increase in the amount of voids in the post-compaction phase, leading to an exceedence of the range of the admissible voids content for asphalt mixtures. Therefore, it is necessary to quantify the recovered deformation and the energy stored by the rubber to control this phenomenon by modifying adequately the compaction process. The objective of this chapter is to develop a mix design approach for rubberised asphalt (dry process) that takes into account the behaviour of crumb rubber during the compaction and post-compaction processes. An analytical approach to quantifying the recovered deformation of crumb rubber in the post-compaction phase has been developed in order to adjust the designed number of gyrations, with the final aim of meeting the requirements for voids content. Moreover, a mathematical relationship will be defined for computing the maximum allowable content of rubber in the mixture once the void content has been established. Finally, based on the results obtained, a full step-by-step protocol is proposed in order to fabricate and compact CR mixtures.

3.2 Mix design optimisation of bituminous mixtures with crumb rubber

The behaviour of the CR mixtures is analysed in three main phases:

1. Preliminary phase: quantification of the increase in bitumen demand when CR mixtures are fabricated.
2. Compaction phase: definition of a correction factor for increasing the compaction taking into account the elastic recovery of the rubber.
3. Post-compaction phase: thermal stabilisation, confinement and curing phase.

In the first step of the research it is necessary to understand how the demand for bitumen increases when the rubber is added to the mixture to obtain the same workability and compaction curve of the corresponding traditional mixture without the addition of rubber. A reference mixture without rubber and three with rubber were fabricated with different percentages of bitumen and they were compacted at the same percentage of voids or N_{design}

3.2 Mix design optimisation of bituminous mixtures with crumb rubber 63

used for the traditional mixture. The compaction curves obtained have been compared. In order to obtain the same workability in the mixtures, the aim of this preliminary phase is to identify the bitumen content in a CR mixture that allows its compaction curve to be similar to the one characterising the conventional mixture. This bitumen content was considered for further analysis. Having, at the end of the compaction phase, the same voids content for the traditional and CR mixtures allows the same starting point to be used for both mixtures when the post-compaction phase starts. This allows the contribution of the deformation release of the crumb rubber in increasing the voids content during the post-compaction phase to be isolated and highlighted.

This analysis leads to the definition of a coefficient (γ) for multiplying the standard number of gyrations in order to achieve, at the end of the curing time, the same voids content as that obtained for the traditional mixture. In other words, starting with the same voids content after compaction (traditional and CR mixtures), an analytical method is defined to calculate how the compaction should be increased for the CR mixtures given that after compaction, during the thermal stabilisation and curing phase, the rubber deformation release causes an increase in volume and additional voids. Figure 3.1 shows a schematic representation of the research steps.

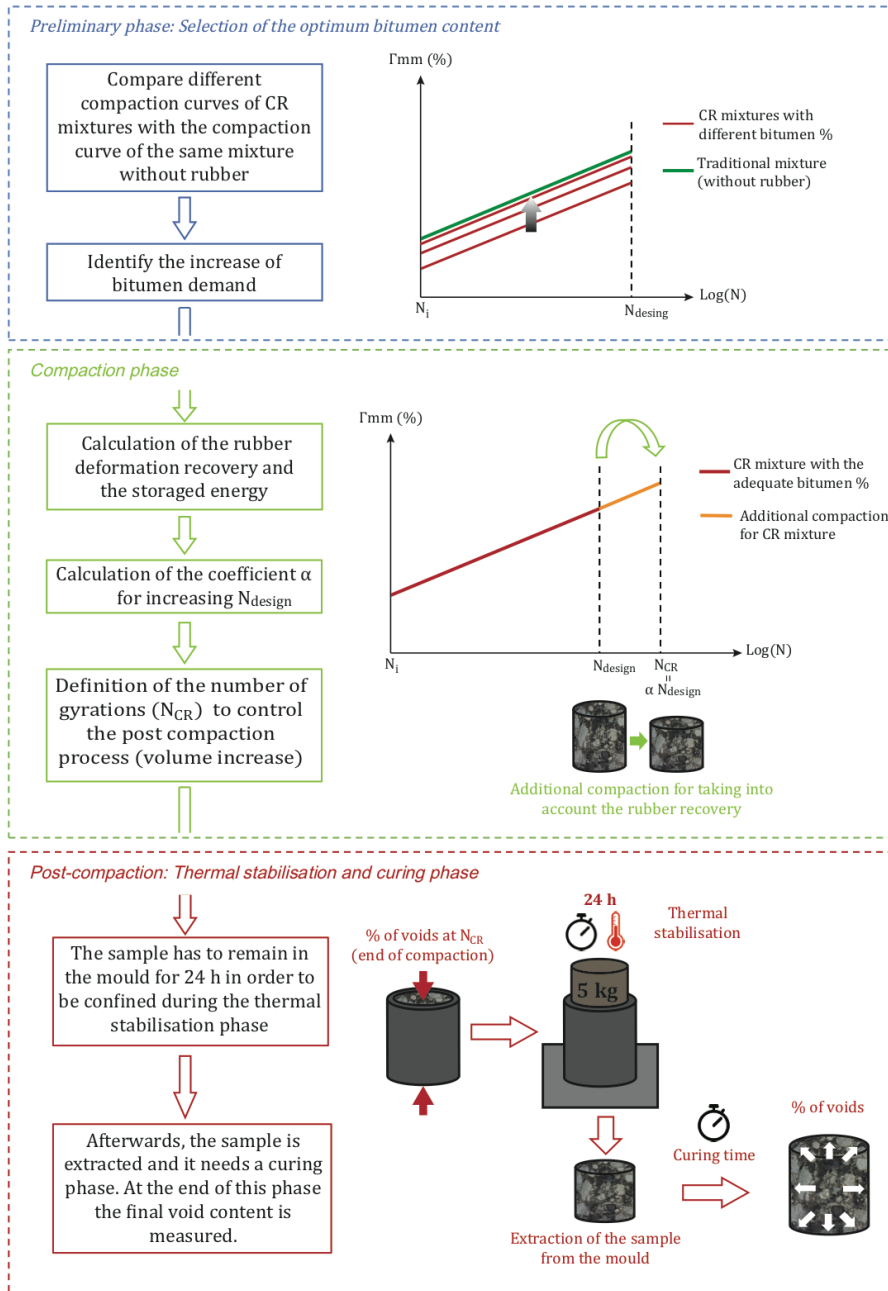


Figure 3.1: Schematic representation of the mix design of crumb rubber mixtures.

3.2.1 Analytical approach - Correction factor

In order to calculate a *correction factor* that adjusts the number of gyrations for CR asphalt mixtures, it is necessary to present a few considerations and hypotheses regarding the compaction process and the recovery of the rubber in the post-compaction phase.

Compaction is achieved by applying vertical stress (600KPa) via end plates. A known mass of asphalt mixture is placed into a mould between the two plates and completely confined. The plates are kept in parallel, but the longitudinal axis of the mould is rotated to a fixed angle equal to 1.25° . The mould rotates at 30 revolutions per minute and the load is continuously applied. This configuration increases the presence of shear stress applied to the sample. Nevertheless, the shear stress is considered negligible for the rubber deformation recovery, therefore in the framework of this work, only compression is taken into account in the calculation process.

Three main elements within the sample are considered in terms of volume: air voids (V_V), aggregates + bitumen (V_{A+B}) and rubber (V_R), as shown in Figure 3.2.

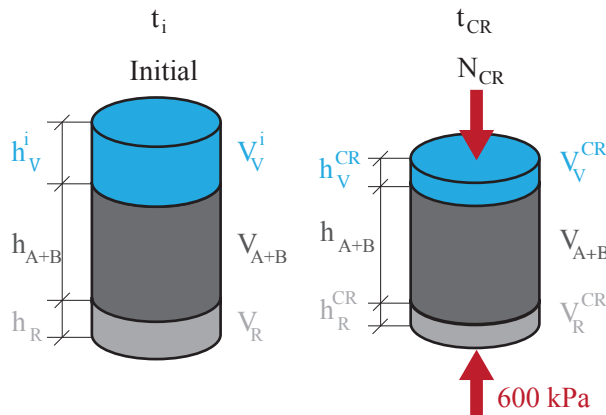


Figure 3.2: Compaction sample by layers.

The aggregates and bitumen are considered unique elements that do not recover after compaction. In fact, the bitumen is also subjected to a recovery after compaction, but this will be the same recovery as occurs in the traditional mixture. Thus, the difference between the recovery of traditional and CR mixtures can be attributed only to the presence of the rubber. Therefore,

the calculations below focus only on the rubber recovery.

After having defined the compaction condition, let the index i and N_{CR} denote, respectively, the initial and the final configuration of the CR asphalt sample at $t = t_i$ and at $t = t_{CR}$ (Figure 3.2). The surface area (A) at the base of the mould remains constant (100 or 150mm in diameter), while under the load applied by the gyratory compactor the height of the sample decreases. This corresponds to a volume reduction caused by the compression of the rubber and aggregate orientation that reduces the air voids content.

The difference between the compaction of a traditional and CR mixture is expressed using a correction factor for N_{design} denoted as γ . In the framework of this work, γ is defined as the coefficient that multiplies the design number of gyrations (N_{design}) necessary to compact a sample of traditional asphalt mixture to obtain the design number of gyrations required to compact a sample of CR mixture (N_{CR})

$$N_{CR} = \gamma \cdot N_{design}, \quad (3.1)$$

where γ is calculated as the ratio between the target voids expected for a sample of asphalt mixture without rubber ($\%voids$) at N_{design} . The percentages of the final voids achieved by the same asphalt mixture with crumb rubber ($\%voids_{CR}$) at N_{CR} follows from

$$\gamma = \frac{\%voids}{\%voids_{CR}}. \quad (3.2)$$

The percentage of the target voids ($\%voids$) is established at the beginning of the process. It should be defined as the design voids of the corresponding traditional asphalt mixture (without rubber), bearing in mind that the volumetric properties have an influence on the mechanical performance of the mixture (fatigue and rutting resistance).

On the other hand, the $\%voids_{CR}$ is the percentage of final voids obtained after the compaction in the CR mixture at $t = t_{CR}$ defined as

$$\%voids_{CR} = \frac{V_V^{CR}}{V_V^{CR} + V_{A+B} + V_R^{CR}} \quad (3.3)$$

where V_V^{CR} is the final volume of air voids at N_{CR} (at the end of the compaction), V_{A+B} is the volume of aggregates and bitumen that remains constant before and after the compaction, and V_R^{CR} is the final volume of the rubber at N_{CR} (at the end of compaction).

3.2 Mix design optimisation of bituminous mixtures with crumb rubber 67

The following calculations have the objective of identifying the unknown values V_V^{CR} , V_R^{CR} and V_{A+B} necessary for the determination of $\%voids_{CR}$ and therefore γ .

The final volume of air voids is calculated by subtracting the decrease in the rubber volume from the volume of the target voids. Thus, the final volume of air voids (V_V^{CR}) can be written as

$$V_V^{CR} = V_V - |\Delta V_R| = V_V - |V_R^{CR} - V_R| \quad (3.4)$$

where V_V is the volume of the target voids ($\%voids$), ΔV_R is the variation in the volume of rubber between the time $t = t_i$ and $t = t_{CR}$ because V_R is the volume of rubber at time $t = t_i$. Considering rubber as a pure elastic material and assuming normal compressive stress applied to the sample, it is possible to apply Hooke's law

$$\sigma = E_R \varepsilon_R = E_R \left| \frac{h_R^{CR} - h_R}{h_R} \right| \quad (3.5)$$

where E_R is Young's modulus of rubber, σ is the vertical stress (600KPa), and h_R and h_R^{CR} are respectively the initial and final height of the rubber layer (Figure 3.2). Thus, in order to obtain the final volume of the rubber it is necessary to calculate the final height of the rubber

$$h_R^{CR} = \left(\frac{\sigma}{E_R} + 1 \right) h_R. \quad (3.6)$$

Recalling that A as the area of the plate of the mould, writing V_R^{CR} as Ah_R^{CR} and substituting Eq. (3.6) in Eq. (3.4), it is possible to obtain the volume of voids at the end of compaction

$$V_V^{CR} = V_V - \left(V_R - A \left(\frac{\sigma}{E_R} + 1 \right) h_R \right) = V_V - \frac{\sigma}{E_R} V_R \quad (3.7)$$

This expression solved for V_V

$$\%voids = \frac{V_V}{V_V + V_{A+B} + V_R} \quad (3.8)$$

Thus, V_V can be isolated

$$V_V = \frac{\%voids (V_R + V_{A+B})}{1 - \%voids} \quad (3.9)$$

The volume of “aggregates + bitumen” and the initial volume of rubber can be obtained respectively as $V_{A+B} = \frac{M_A}{\rho_A} + \frac{M_B}{\rho_B}$ and $V_R = \frac{M_R}{\rho_R}$ where M_A , M_B and M_R are the masses of aggregates, bitumen and rubber and ρ_A , ρ_B and ρ_R are the densities of those three materials.

Once all the elements of Eq. (3.3), V_V^{CR} , V_{A+B} and V_R^{CR} , are known it is possible to write $\%voids_{CR}$ and γ as follows

$$\%voids_{CR} = \%voids + \frac{\sigma}{E_R} \frac{\frac{M_R}{\rho_R} (\%voids - 1)}{\frac{M_R}{\rho_R} + \frac{M_B}{\rho_B} + \frac{M_A}{\rho_A}} \quad (3.10)$$

$$\gamma = \frac{\%voids \left(\frac{M_R}{\rho_R} + \frac{M_B}{\rho_B} + \frac{M_A}{\rho_A} \right)}{\%voids \left(\frac{M_R}{\rho_R} + \frac{M_B}{\rho_B} + \frac{M_A}{\rho_A} \right) + \frac{\sigma}{E_R} \frac{M_R}{\rho_R} (\%voids - 1)} \quad (3.11)$$

Once γ is known N_{CR} can be calculated as defined in Eq. (3.1).

3.3 Maximum rubber content in asphalt mixtures

An additional step in the present methodology allows the maximum amount of rubber for a given recipe of asphalt mixture to be estimated. The limitations of the rubber content could come from different sources, a *physical/mathematical limit* or a *design limit*. The latter exists because the number of gyrations during the mix design procedure should simulate the compaction of the asphalt mixture in the field. For this reason the factor γ should have an upper limit, because N_{CR} should represent a reasonable number of gyrations for the compaction phase.

3.3.1 Physical or mathematical limit

Given the physical aspects, the volume of voids must be strictly positive, thus Eq. (3.7) can be rewritten as an algebraic inequality as follows

$$V_V > \frac{\sigma}{E_R} V_R \quad (3.12)$$

The percentage of volume of the rubber before compaction ($\%V_R$) can be written as

$$\%V_R = \frac{V_R}{V_V + V_R + V_{A+B}} \quad (3.13)$$

Therefore

$$V_R = (V_V + V_R + V_{A+B}) \cdot \%V_R \quad (3.14)$$

With Eqs. (3.8) and (3.14) substituted in Eq. (3.12) it is possible to obtain

$$\%V_R < \frac{E_R}{\sigma} \%voids \quad (3.15)$$

Eq. (3.15) defines the maximum upper limit of rubber content in the asphalt mixture. It can be seen that the maximum percentage of rubber depends proportionally on the target voids content.

The physical/mathematical limit should be interpreted as a theoretical threshold because the percentage of final voids cannot be equal to 0%. Nevertheless, it should be noted that the calculation above refers to the sample just after compaction, when the release of the rubber deformation has not yet occurred. Indeed, in the post-compaction phase the release of the deformation of the rubber causes the increase of the voids content of the asphalt mixture. Therefore, the required density should be measured once the volumetric stability of the sample is reached.

3.3.2 Design limit

The *physical/mathematical limit* analysed above should be combined with compaction limitations. N_{CR} should have an upper limit ($N_{CRlimit}$) defined by the engineers for conducting the compaction with a reasonable number of gyrations. Indeed, even if N_{CR} does not have a physical limit, the design of an asphalt mixture cannot envisage an infinite number of gyrations, because it should be compatible with the field compaction.

Therefore, the maximum possible number of gyrations ($N_{CRlimit}$) is introduced

$$N_{CRlimit} = \gamma_{Limit} \cdot N_{design} \quad (3.16)$$

where γ_{Limit} is the correction factor that corresponds to the selected $N_{CRlimit}$. γ_{Limit} is defined as

$$\gamma_{Limit} = \frac{\%voids}{\%voids_{CR}}; \quad \%voids_{CR} = \frac{\%voids}{\gamma_{Limit}} \quad (3.17)$$

From Eqs. (3.3) and (3.17) it is possible to obtain the following relationship

$$V_V^{CR} = \frac{1}{\gamma_{Limit}} V_V \frac{V_V^{CR} + V_{A+B} + V_R^{CR}}{V_V + V_{A+B} + V_R} \quad (3.18)$$

To simplify the calculation a variable substitution is used. Indeed, $Y = \frac{V_V^{CR} + V_{A+B} + V_R^{CR}}{V_V + V_{A+B} + V_R}$ is the ratio between the volumes of all the components at the end of the compaction and the target volume of the sample. Thus, Eq. (3.18) becomes

$$\frac{1}{\gamma_{Limit}} V_V \cdot Y = V_V^{CR} \quad (3.19)$$

Substituting V_V^{CR} as defined in Eq. (3.19) in Eq. (3.7) leads to

$$\frac{V_V}{\gamma_{Limit}} \cdot Y = V_V - \frac{\sigma}{E_R} V_R \quad (3.20)$$

Simplifying Eq. (3.20) and recalling Eq. (3.15) it is possible to obtain

$$\%V_R = \frac{E_R}{\sigma} \%voids \left(1 - \frac{1}{\gamma_{Limit}} \cdot Y \right) \quad (3.21)$$

Eq. (3.21) allows the maximum amount of rubber to be obtained, which depends on the γ_{Limit} combining then the physical and the design limit. Analysing Eq. (3.21) it is observed that

$$\%V_R = \frac{E_R}{\sigma} \%voids \left(1 - \frac{1}{\gamma_{Limit}} \cdot Y \right) < \frac{E_R}{\sigma} \%voids \quad (3.22)$$

because

$$\left(1 - \frac{1}{\gamma_{Limit}} \cdot Y \right) < 1 \quad (3.23)$$

Indeed, γ_{Limit} is always higher than 1 and $Y = \frac{V_V^{CR} + V_{A+B} + V_R^{CR}}{V_V + V_{A+B} + V_R}$ is always slightly lower than 1 because $V_R^{CR} < V_R$ just after compaction, and $V_V^{CR} < V_V$ because the compaction is higher in order to take into account the release of the rubber. Thus, as highlighted in Eq. (3.22), the maximum allowable amount of rubber determined by the *design limit* is always included in the range of the maximum allowable limit imposed by the *physical/mathematical limit*. Moreover, Y is slightly lower than 1 because the difference between the numerator and the denominator is small; for this reason Y could be considered equal to 1. This allows a further simplification of Eq. (3.22) and it is possible to arrive at the final formula for the maximum quantity of rubber allowable

$$\%V_R \leq \frac{E_R}{\sigma} \%V_V \left(1 - \frac{1}{\gamma_{Limit}} \right) \quad (3.24)$$

At this point, the maximum rubber content in an asphalt mixture may be calculated as a function of the desired compaction conditions.

3.4 Rubberised asphalt for railway sub-ballast

In this section, the analytical approximation presented in Sections 3.2 and 3.3 is validated through the experimental evidence. The experiments reported in this section have been performed in the facilities of IFSTTAR (Institut français des sciences et technologies des transports, de l'aménagement et des réseaux).

3.4.1 Materials description

The analytical approach presented in Section 3.2 consists on modifying (substituting part of the aggregates for crumb rubber) a reference mixture already designed for desired application (in this case as sub-ballast layer).

The bituminous sub-ballast is composed of a dense-graded bituminous mixture with a maximum aggregate size of 14-16 mm, similarly to the base course for road pavements [Rose et al., 2011]. In this case, discrete values of the granulometric curve of the sub-ballast reference asphalt are listed in Table 3.1. The bitumen content of this mixture is 4.8%.

Table 3.1: Discrete values of the granulometric curve of the reference asphalt.

Sieve [mm]	Target grading curve (passing material) [%]
16	100
14	94.40
12.5	81.76
10	58.29
8	49.04
6.3	43.80
5	38.32
4	33.91
3.15	32.88
2	32.20
1	23.33
0.5	17.24
0.25	12.83
0.125	9.98
0.063	7.60

Although the composition of the sub-ballast layer is similar to a base course,

typically the air voids content in the bituminous sub-ballast layer decreases to 1-3 % to ensure a higher impermeability of the layer [Rose et al., 2011]. For this reason, the target voids content for the mixtures, the reference and the crumb rubber, has been established as being equal to 3%.

The characteristics of the materials, bitumen and aggregates, used for the fabrication of the bituminous sub-ballast are summarised in Tables 3.2 and 3.3, respectively.

Table 3.2: Characteristics of the bitumen.

Property	Standard	Value
Penetration at 25C (pen. grade 35-50)	EN1426	≈ 40
Softening point [°C]	EN1427	≈ 52.6°
Bulk gravity [g/cm^3]	EN15326-A1	≈ 1.034

Table 3.3: Characteristics of the aggregates.

Property	Standard	Value
Los Angeles abrasion loss [%]	EN1097-2	10 to 13
Bulk specific gravity sand coarse aggregates [g/cm^3]	EN1097-6	0/2 2.859
		2/4 2.859
		4/6 2.910
		6/10 2.888
		10/14 2.89
Bulk specific gravity filler [g/cm^3]	EN1097-7	2.671

The crumb rubber used has been provided by “Aliapur”. Aliapur is the principal industry in charge of the valuation of used tires in France. The characteristics of the crumb rubber are reported in Table 3.4.

Table 3.4: Characteristics of the crumb rubber.

Property	Value
Fraction [mm]	0.8/2.4
Density [g/cm^3]	1.013

Discrete values of the granulometric curve of the crumb rubber are given in Table 3.5.

Table 3.5: Discrete values of the granulometric curve of crumb rubber.

Sieve [mm]	Target grading curve (passing material) [%]
3.15	100
2	69.5
1	7.3
0.5	0.7

Once the materials characteristics have been described, the quantity of crumb rubber and the compaction correction factor for the crumb rubber mixture may be calculated according to Eq (3.11).

3.4.2 Correction factor calculation and sample preparation

A preliminary study was conducted to determine the additional quantity of bitumen necessary during the compaction phase to obtain a compaction curve similar as much as possible with the reference mixture one. The reference mixture for bituminous sub-ballast was prepared and compacted with 4.8% of bitumen by the weight of the mixture and 3% of final voids. The real void content measured in the gamma bank (mean of several samples) is 3.27%.

The rubberised mixture has been obtained modifying the reference mixture. This modification consists on substituting the aggregates by crumb rubber of the same size fraction. The quantity of crumb rubber added to the mixture is 1.5% in volume. Several compaction test have been performed in order to obtain the optimum bitumen content for the rubberised mixture and it results in 5.83% by weight of the mixture.

At this point, the correction factor may be calculated by means of Eq (3.11) with the following material quantities $M_A = 7.317 \text{ kg}$, $M_B = 0.479 \text{ kg}$, $M_R = 0.240 \text{ kg}$, $\rho_A = 2.86 \text{ kg/m}^3$, $\rho_B = 1.03 \text{ kg/m}^3$, $\rho_R = 1.013 \text{ kg/m}^3$, $E_R = 1.50 \text{ MPa}$ and $\%voids = 3$.

The value obtained for the correction factor γ is equal to 1.69. In other words, the crumb rubber mixture has to be compacted 1.69 times more than the reference mixture, in order to overcome the rubber recovery after the compaction.

Once the correction factor for the gyratory compactor has been calculated, some considerations must be given for the sample preparation.

Sample preparation

The preparation of the samples was conducted following these steps:

- The aggregates were washed, dried and heated at 180 °C for at least 3 hours.
- The crumb rubber was kept at room temperature.
- The aggregates and the crumb rubber were mixed for 15 seconds in order to disperse the rubber homogeneously in the mixture.
- The bitumen (penetration grade 35/50) was heated at 150 °C for 1 hour. It was added to the aggregates and the crumb rubber into the mixture, and mixed for 1 minute.
- The mould was preheated at 150 °C, the asphalt mixture was poured into the mould and compacted with the gyratory compactor at 150 °C.
- Once the compaction was finished, the samples were kept confined in the mould for 24 hours. A load of approximately 5 kg was applied on the top of the specimens to confine them completely [Rahman, 2004]. The objective was to provide enough time for the asphalt mixture to reach thermal stability.

Probably, certain chemo-physical phenomena occur at high temperatures (mixing and compaction temperatures). Nevertheless, the analytical calculation developed in this chapter does not take temperature into account as a parameter and the possible chemical interactions between rubber and bitumen. For this reason the samples were kept confined until they reached room temperature and the calculation above was applied to determine the relaxation of the rubber when it achieves thermal equilibrium. Afterwards, the samples were left at room temperature for six days unconfined to allow the rubber to recover (curing time).

3.4.3 Results and observations

The results obtained are as expected. The real void content of the designed crumb rubber mixture, measured in the gamma bank (mean of several samples), is 3.52% (when for the reference mixture 3.27% was obtained). This is an optimum result, that allows to validate the proposed analytical approach presented in Section 3.2.

Some observations from the compaction experiments are now commented.

In Figure 3.3, there are 3 different samples with 1.5% of rubber in volume and different bitumen content.



Figure 3.3: Samples with different bitumen content.

In the picture of Figure 3.3, one broken sample is shown. This sample contains the same bitumen percentage as the reference mixture. This fact proves that on a crumb rubber mixture more bitumen has to be added than in the reference mixture probably due to the absorption of the lighter parts of the bitumen by the rubber particles.

Figure 3.4 shows two samples compacted in two different conditions. The one on the right has been compacted as based on the calculations on the analytical approach and the one on the left it has been compacted more. From Figure 3.4 it may be concluded that overcompacting may generate problems, since it seems that the rubber ties to go into the walls of the mould during the compaction.



Figure 3.4: Overcompaction problem in the gyratory compactor.

Slab compaction

The proposed procedure may be adopted in the laboratory using the gyratory compactor in a controlled environment. Certainly, the conditions may change if the compaction process is conducted at a construction site or even with a different laboratory sample shape (slab compaction).

It should be noticed that, in the case of the slab compaction (see Figure 3.5), it has been experimentally observed that it is not necessary to apply the correction factor proposed in Section 3.3 for the compaction. The void content obtained compacting under the same conditions as for the reference mixture is approximately the same.



Figure 3.5: Slab compaction.

3.5 Conclusions

This chapter proposes an analytical approach for the mix design optimisation of bituminous mixtures containing crumb rubber performed using a gyratory compactor. The method takes into account the deformation release of the rubber after compaction for the calculation of the expected voids content. Therefore, it is possible to estimate and control the final voids content by applying a correction factor that adjusts the number of gyrations based on the target voids to be achieved. The formula includes different input parameters such as the characteristics of the materials, the Young's modulus of the rubber and the target voids to achieve.

Based on the results, the analytical approach has been considered successfully in adjusting the required number of gyrations (or the final void content in the gyratory compactor) in order to compact asphalt mixtures containing rubber. The advantage of applying this methodology is that, by relying on theoretical calculation of the rubber deformation release, the method provides a base for estimating the increase of the compaction level when crumb rubber is added to the mixtures. The method can be used for every type of asphalt mixture, varying the content and types of aggregates and bitumen as input. Moreover, the target voids required by standards can be established at the beginning of the process.

Additionally, in terms of a physical/mathematical limit and/or a design limit, due to a correspondence between the number of gyrations and the compaction in the field, it is possible to calculate the maximum amount of rubber for the asphalt mixture of interest. Nevertheless, this study represents a first step in tailoring a mix design optimisation process to crumb rubber mixtures, and additional work is required for the findings to be accepted at the global level.

In conclusion, this study exploits the consolidated principles of the theory of elasticity for tailoring a rational methodology for the mix design optimisation of crumb rubber mixtures. It provides promising results for estimating the final voids content after thermal stabilisation and curing of asphalt mixtures with crumb rubber. The approach developed can be applied to every type crumb rubber mixture once the input parameters (Young's modulus of the rubber, mass and density of the materials involved and the target voids) have been established.

Chapter 4

3D fractional viscoelastic model for bituminous mixtures

The main aim and novelty in this Chapter arises on the validation of the 3D fractional viscoelasticity theory by means of experimental triaxial test on asphalt mixtures. Thus, this chapter starts with a brief introduction of the theory of the 3D fractional viscoelasticity and its relation with the fractional mechanical models presented in Chapter 2.

In order to study and to model the triaxial mechanical behaviour of the bituminous mixtures (reference asphalt and rubber asphalt) designed in Chapter 3, triaxial tests have been performed. Thus, the experimental set up used to perform the triaxial test for the asphalt mixtures is presented. Moreover, the mechanical behaviour of the reference asphalt and the rubber asphalt is compared by means of series of triaxial creep and cyclic tests. Finally, both asphalts are modelled as 3D fractional viscoelastic materials.

4.1 3D fractional viscoelasticity

The 3D constitutive model here introduced and proposed by [Alotta et al., 2016], and other authors [Makris, 1997, Freed and Diethelm, 2006, Hilton, 2012, Fukunaga and Shimizu, 2015], is obtained by means of a generalisation of Hooke's Law. In that case only two parameters are required to define the whole stiffness (or compliance) matrix of the material and these two parameters are Young's modulus and Poisson's ratio, or Young and shear modulus, or Bulk and shear modulus, or Lamé constants. Hereinafter, the relaxation

matrix is written in terms of the shear and Bulk (volumetric) contributions, for two main reasons: i) the terms of the relaxation (or creep) matrix can be expressed as a simple summation of the relaxation (or creep) volumetric and deviatoric functions, leading to simple and easy manageable governing equations; ii) the volumetric and deviatoric contributions have clear physical meanings and the relative relaxation (or creep) functions have to be measured experimentally. The relaxation matrix can be easily obtained by substituting in the stiffness matrix the shear modulus $G = \frac{E}{2(1+\nu)}$ and the Bulk modulus $K = \frac{E}{3(1-2\nu)}$, where E is the Young's modulus and ν is the Poisson's ratio, with the deviatoric relaxation function $G(t)$ and the volumetric relaxation function $K(t)$, respectively. In this way the relaxation matrix can be written as follows (see [Alotta et al., 2016])

$$R_{ijkh}(t) = \left(K_R(t) - \frac{2}{3}G_R(t) \right) \delta_{ij}\delta_{kh} + G_R(t)(\delta_{ik}\delta_{jh} + \delta_{ih}\delta_{jk}) \quad (4.1)$$

where δ_{ij} is the Kronecker symbol.

The relaxation function for the deviatoric and volumetric part have a power law shape that is analogous to the one-dimensional relaxation law of the spring-pot presented in Chapter 2. Thus

$$G_R(t) = G_\alpha \frac{t^{-\alpha}}{\Gamma(1-\alpha)} \quad (4.2a)$$

$$K_R(t) = K_\beta \frac{t^{-\beta}}{\Gamma(1-\beta)} \quad (4.2b)$$

where G_α , α , K_β and β are parameters of the deviatoric and volumetric relaxation functions, respectively. By assuming relaxation functions in the form of Eq. (4.2), a four parameters mechanical model is obtained. The strain-stress relationship can be obtained simply by applying the Boltzmann superposition principle

$$\sigma(t) = \int_0^t \mathbf{R}(t-\tau) \dot{\varepsilon} d\tau \quad (4.3)$$

where $\sigma(t) = [\sigma_{11} \sigma_{22} \sigma_{33} \tau_{12} \tau_{13} \tau_{23}]$ and $\varepsilon(t) = [\varepsilon_{11} \varepsilon_{22} \varepsilon_{33} \gamma_{12} \gamma_{13} \gamma_{23}]$ are the stress and strain vectors, respectively, and $\mathbf{R}(t)$ is the relaxation matrix (5). Since $\mathbf{R}(t)$ contains power law functions, the components of the stress vector $\sigma(t)$ depends on the fractional derivatives of the components of the strain vector $\varepsilon(t)$

$$\begin{aligned} \sigma_{ii}(t) = & \frac{4}{3}G_\alpha \left[D^\alpha \left(\varepsilon_{ii} - \frac{\varepsilon_{jj} + \varepsilon_{kk}}{2} \right) \right] (t) + \\ & + K_\beta \left[D^\beta (\varepsilon_{ii} + \varepsilon_{jj} + \varepsilon_{kk}) \right] (t) \quad i, j, k = 1, 2, 3; i \neq j \neq k \end{aligned} \quad (4.4a)$$

$$\tau_{ij}(t) = G_\alpha (D^\alpha \gamma_{ij})(t) \quad i, j = 1, 2, 3; i \neq j \quad (4.4b)$$

The inverse relationship of Eq. (4.3) is obtained by applying the dual form of Boltzmann's superposition principle, that is

$$\varepsilon(t) = \int_0^t \mathbf{C}(t - \tau) \dot{\sigma} d\tau \quad (4.5)$$

In order to use Eq. (4.5) it is necessary to obtain the creep matrix $\mathbf{C}(t)$ by using Eq. (2.7) (adapted for the 3D case). $\mathbf{C}(t)$ is evaluated by performing a Laplace transformation of the relaxation matrix and evaluating its inverse in the Laplace domain

$$\hat{\mathbf{C}}(s)\hat{\mathbf{R}}(s) = s^{-2} \quad (4.6)$$

By taking the inverse Laplace transform of $\hat{\mathbf{C}}(s)$ in Eq. (4.6) the creep matrix may be written as

$$C_{ijkh}(t) = \left(\frac{K_C(t)}{9} - \frac{G_C(t)}{6} \right) \delta_{ij}\delta_{kh} + G_C(t) \left(\delta_{ik}\delta_{jh} - \frac{\delta_{ih}\delta_{jk}}{2} \right) \quad (4.7)$$

where $K_C(t)$ and $G_C(t)$ are creep functions of the volumetric and deviatoric parts, that are written as follows

$$G_C(t) = \frac{t^\alpha}{G_\alpha \Gamma(1 + \alpha)} \quad (4.8a)$$

$$K_C(t) = \frac{t^\beta}{K_\beta \Gamma(1 + \beta)} \quad (4.8b)$$

It is observed that in Eqs. (4.1) and (4.7) the shear strain is considered as the engineering shear strain, that is $\gamma_{ij} = 2\varepsilon_{ij}$.

By substituting Eq. (4.8) in Eq. (4.5), the components of the strain vector $\varepsilon(t)$ depend on the fractional integrals of the components of the stress vector $\sigma(t)$, that is

$$\begin{aligned} \varepsilon_{ii}(t) = & \frac{1}{3G_\alpha} \left[I^\alpha \left(\sigma_{ii} - \frac{\sigma_{jj} + \sigma_{kk}}{2} \right) \right] (t) + \\ & + \frac{1}{9K_\beta} \left[I^\beta (\sigma_{ii} + \sigma_{jj} + \sigma_{kk}) \right] (t) \quad i, j, k = 1, 2, 3; i \neq j \neq k \end{aligned} \quad (4.9a)$$

$$\gamma_{ij}(t) = \frac{1}{G_\alpha} (I^\alpha \tau_{ij})(t) \quad i, j = 1, 2, 3; i \neq j \quad (4.9b)$$

Governing equations may be also obtained simply by writing separately the volumetric and deviatoric contribution and then summing them. It is emphasised that in the pure torsion case there is a perfect duality between the direct and the inverse constitutive laws. Such a duality is preserved in the three dimensional direct and inverse constitutive laws (see Eqs. (4.4a) and (4.9a)).

The 3D fractional viscoelastic model presented in this section may be represented as shown in Figure 4.1 and is governed by the tridimensional constitutive laws written in Eqs. (4.4) and (4.5).

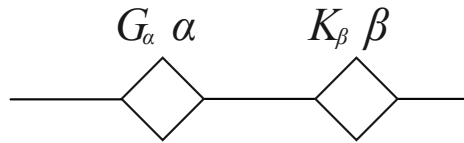


Figure 4.1: 3D fractional viscoelastic model.

As it may be observed, this mechanical model is quite similar (excepting from one spring) to the Huet model depicted in Figure 2.10(a).

The 3D fractional viscoelastic model presented in this section, has been analysed only in theoretical form. Thus, it has to be emphasised that in the next sections of this chapter it is shown how to determine the model parameters, and the 3D fractional viscoelastic model for bituminous mixtures is validated.

4.2 Triaxial tests for bituminous mixtures

The triaxial test have been performed in the facilities of IFSTTAR (Institut français des sciences et technologies des transports, de l'aménagement et des réseaux) with the apparatus used in [Sohm, 2011, Sohm et al., 2012].



Figure 4.2: Triaxial test set-up.

The triaxial apparatus is installed in an existing servo-hydraulic loading frame. The pressure cell, the temperature control system and the instrumentation have been developed specifically for triaxial tests on bituminous mixtures (Figure 4.2).

The apparatus is designed for specimens with a diameter of 80 mm and a height of 160 mm. The maximum axial load is 25 kN, the maximum confining pressure is 700 kPa and the temperature range is from 5°C to 60°C. Monotonic and cyclic axial loading can be applied, keeping a constant confining pressure. The maximum loading frequency is 10 Hz.

The loading frame is a SCHENCK frame with a load capacity of $\pm 100\text{kN}$ and an axial stroke of $\pm 100\text{mm}$. The loading frame is equipped with a monitoring control system, which allows to perform a large range of loading tests (monotonic or cyclic) with load or displacement control.

The triaxial cell for bituminous materials has been developed by GDS Instruments (Figure 4.2). It is made of aluminium, has an external diameter of 300 mm and can accept 80 or 100 mm diameter specimens. The confining fluid that is also used for temperature regulation can be water or air. The cell is equipped with an internal load transducer of 25 kN capacity, and a 1000 kPa pressure transducer, placed outside the cell, on the confining fluid supply circuit.

A double heating and cooling system (Figure 4.2) regulates the temperature in the triaxial cell. The first system consists of a coil, situated inside the triaxial cell, in which the heating and cooling fluid circulates (water with anti-freeze). This coil is connected with an external, removable heating and cooling system. To improve the control of the temperature in the cell, a thermal housing is added around the triaxial cell. A thermocouple placed inside the cell at mid-height of the specimen is used to control the temperature. To ensure stabilisation of temperature before testing, specimens are stored in the triaxial cell with thermal housing at the testing temperature for at least 4 hours prior to testing.

4.2.1 Measurement and loading

The axial and radial strains of the specimen are measured by a specific system of linear variable differential transformer (LVDT) sensors (Figure 4.3(a)) and strain gauges (Figure 4.3(b)).

The strain gauges (Figure 4.3(b)) used are the "HBM 1-LY41-50/120", which nominal resistance is 120 Ohms and the grid 50 mm. "Vishay's GA-2" adhesive is used to bond the gauges to the bituminous mixing test sample. This adhesive resists to large deformations (20% deformation after 40 hours at 24°C). The gauges normally measure deformations up to 6%. Bituminous mixtures are heterogeneous materials, with a deformable mastic and very rigid aggregates. When the asphalt is deformed, the deformations are located in the mastic and there is a displacement of the aggregates. These non-homogeneous deformations in the material lead to a gauge folding, and do not allow to correctly measure the deformations larger than about 1%. Each gauge is mounted in a 1/4 bridge circuit (2 resistors in the conditioners and a compensating resistor in the socket of the conditioner). The deformation values measured by the gauges are therefore independent of one another.

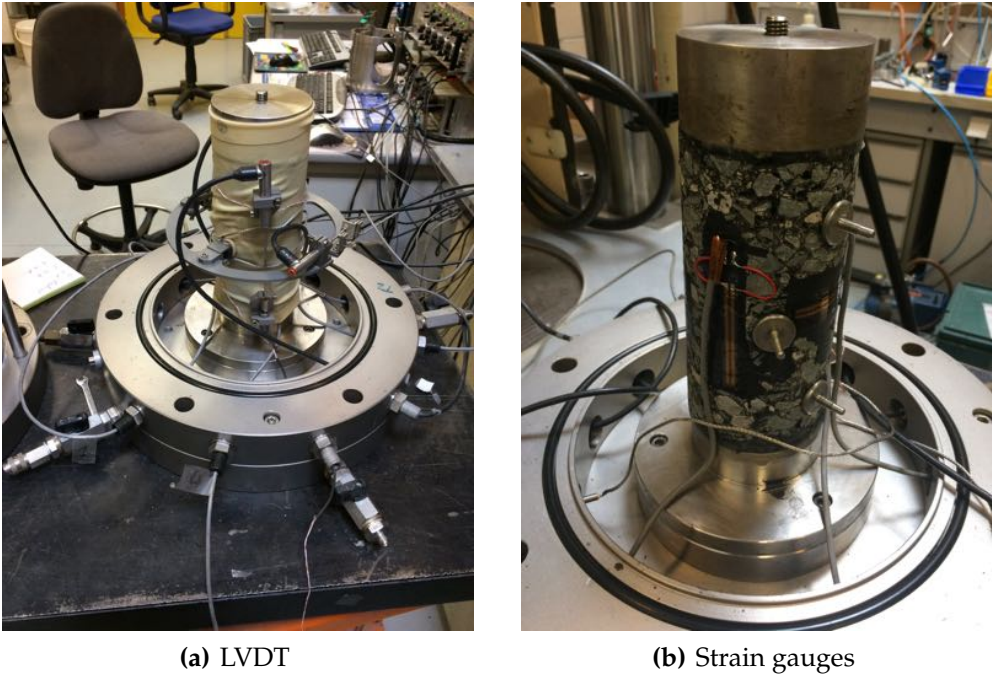


Figure 4.3: Strain measurement systems.

For the LVDT (Linear Variable Differential Transformer) measurements (Figure 4.3(a)), the axial strains are measured in the central part of the specimen using two LVDTs, placed vertically, on the opposite sides of the specimen. The average of the signals of the two sensors is used to calculate the axial strain. The homogeneity of the strain field is also checked by comparing the values given by each sensor. The radial strains are measured by an articulated ring, equipped with an LVDT, placed at mid-height of the specimen. The radial LVDT measures the opening of the ring, and thus the variations of the specimen diameter. The axial LVDTs and the articulated ring are attached to the specimen by metallic clamps, glued onto the specimen. The LVDTs have a measurement range of 5mm and a resolution of $1\mu\text{m}$.

The tests have been developed for different loading conditions. The notation for the loading conditions are depicted in Figure 4.4(a): σ_q denotes the vertical stress applied of both horizontal faces of the specimen (using the axial load of the press) and σ_c denotes the confinement pressure applied around the entire specimen (using pressured air).

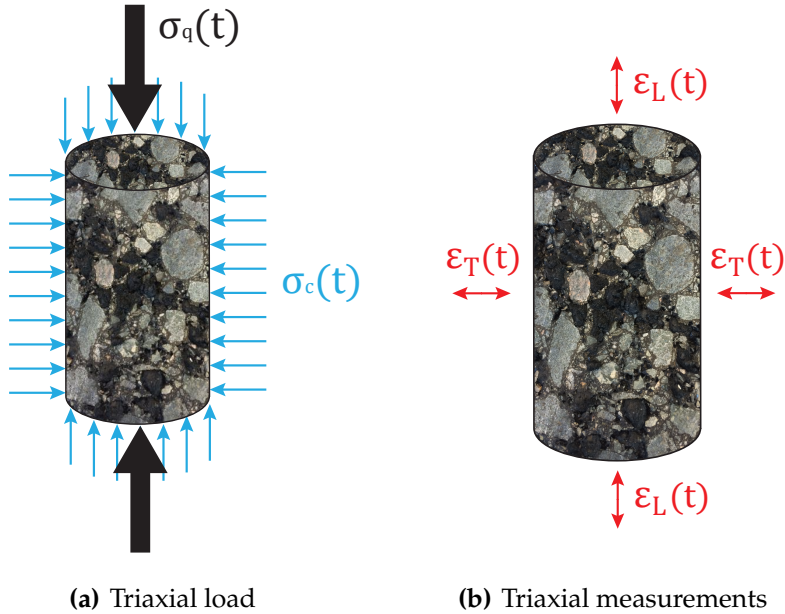


Figure 4.4: Triaxial test sample load and measurements.

The strain measurements are notated as shown in Figure 4.4(b), that is ϵ_L denotes the longitudinal strain and ϵ_T the transversal strain.

4.3 Creep-recovery and cyclic test with triaxial measurements

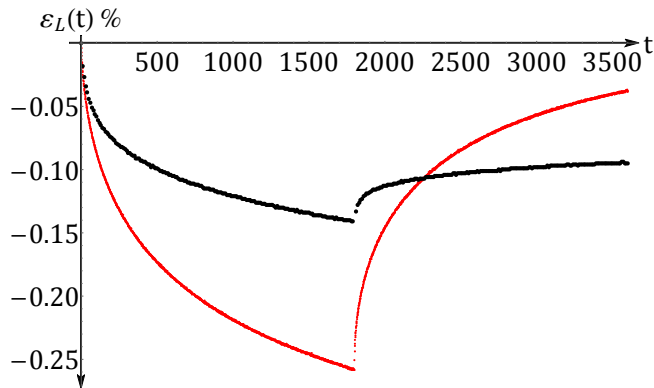
In order to understand the tridimensional behaviour of the asphalt mixtures presented in Chapter 3 and to define the capabilities of the crumb rubber asphalt, creep-recovery and cyclic test have been performed for the two mixtures. In this section, the results of creep recovery test and complex modulus are evaluated from a qualitative point of view.

4.3.1 Creep-recovery tests

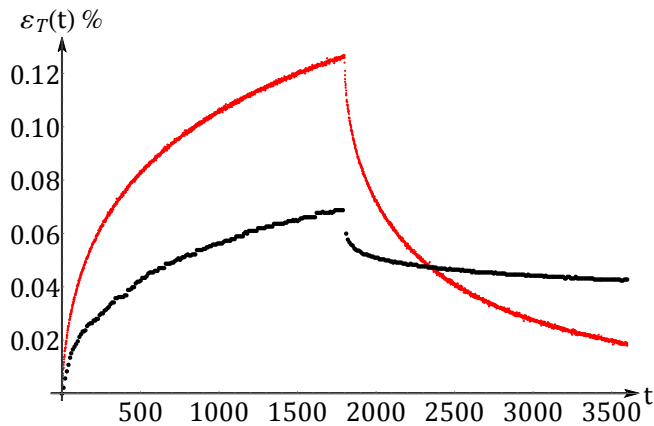
The creep-recovery tests have been developed for two different load conditions, the first one with only vertical stress load σ_q , and the second one with

combined vertical stress load σ_q and confinement load σ_c . The sign convention applied to represent the experimental results is negative if the sample is compressed and positive if it is extended.

The results of the first loading case, the creep-recovery test with $\sigma_q = 200kPa$ and $\sigma_c = 0kPa$, are represented in Figure 4.5. Figure 4.5(a) shows the longitudinal strain $\varepsilon_L(t)$, and Figure 4.5(b) shows the transversal strain $\varepsilon_T(t)$. In black the response of the reference asphalt is shown and in red the one of the crumb rubber asphalt.



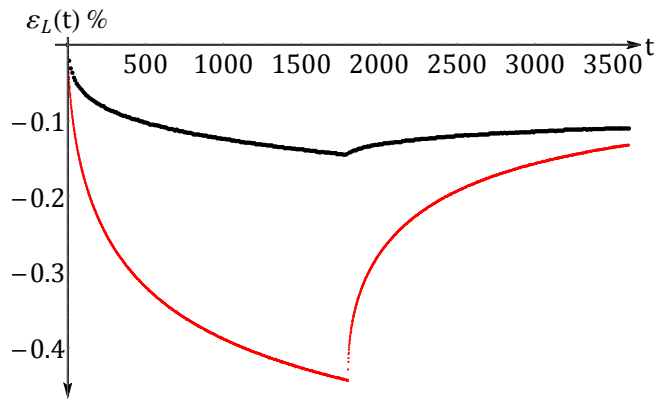
(a) Longitudinal strain measured, $\varepsilon_L(t)$.



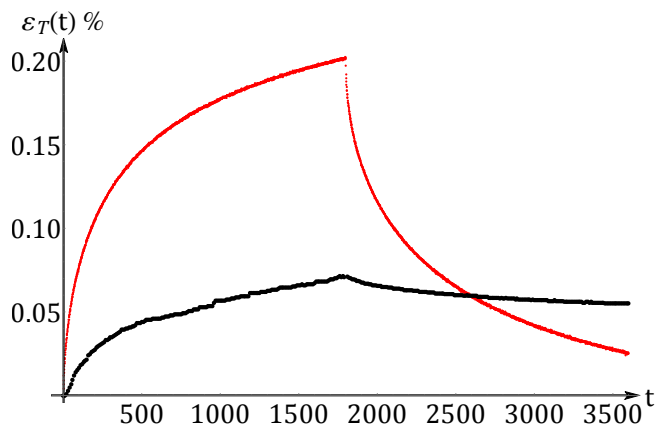
(b) Transversal strain measured, $\varepsilon_T(t)$.

Figure 4.5: Creep-recovery test $\sigma_q = 200kPa$ and $\sigma_c = 0kPa$.

As it may be observed from Figure 4.5, the response of the two mixtures is very different. During the creep phase the deformation of the crumb rubber mixture is approximately double of the reference mixture, and it may be seen as a negative aspect. On the other hand in the recovery phase, even if the deformation in the creep phase is higher for the crumb rubber mixture, the recovery is also higher for the mixture. Thus, the mechanical behaviour of the crumb rubber mixture shows higher deformations and huge recovery of these deformations.



(a) Longitudinal strain measured, $\varepsilon_L(t)$.



(b) Transversal strain measured, $\varepsilon_T(t)$.

Figure 4.6: Creep-recovery test $\sigma_q = 400kPa$ and $\sigma_c = 200kPa$.

The results of the second loading case, the creep-recovery test with $\sigma_q = 400kPa$ and $\sigma_c = 200kPa$, are depicted in Figure 4.6. In this case two times of the vertical load than in the first case is applied and confinement is added. Figure 4.6(a) shows the longitudinal strain $\varepsilon_L(t)$, and Figure 4.6(b) shows the transversal strain $\varepsilon_T(t)$. In black the response of the reference asphalt is shown and in red the one of the crumb rubber asphalt.

From Figure 4.6 it may be observed that the response of the two mixtures under this load conditions is again quite different. During the creep phase the deformations of the crumb rubber is four times larger compared to the reference asphalt for both longitudinal and transversal deformations. In the recovery phase, the longitudinal deformation recovery is approximately equal for both mixtures but in the transversal direction the recovery is higher for the crumb rubber mixture.

Comparing the results of the two loading cases, it may be concluded that the mechanical behaviour of the crumb rubber mixture designed allows higher deformations than the reference one, but the advantage is that the recovery is much higher.

4.3.2 Cyclic test

Cyclic tests have been performed for different loading conditions (as done for the creep recovery test) subjected to various temperatures and loading frequencies. The results of this test are represented in terms of the complex modulus (E^*) and loss angle (δ) against the loading frequency (ω). The considered temperatures are 10, 20 and 30 °C, and the frequencies are varied in the range from 0.1 to 10 Hz. Both the longitudinal and transversal behaviour is measured. The results of the mechanical behaviour under cyclic loading for the reference and crumb rubber mixtures are subsequently compared.

Cyclic loading without confinement

The amplitude of the vertical cyclic load σ_q is equal to $200kPa$ and there is not confinement stress σ_c . Figures 4.7 and 4.8 show the complex modulus and loss angle in this load condition for the longitudinal and transversal direction.

The complex modulus in the longitudinal direction shows that the reference mixture is stiffer than that of the crumb rubber mixture, see Figure 4.7(a). The difference is larger when the temperature increases.

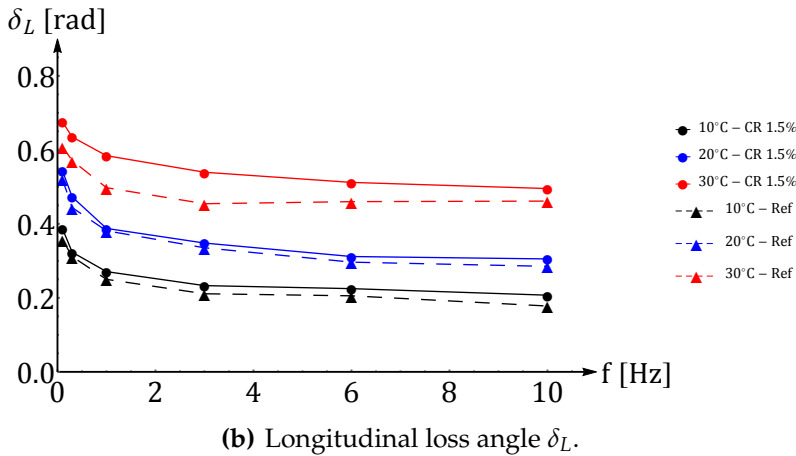
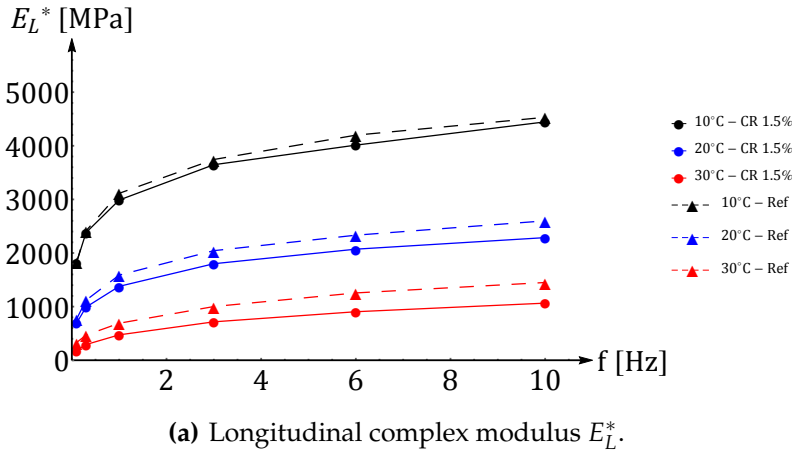


Figure 4.7: Longitudinal complex modulus and loss angle without confinement.

In Figure 4.7(b) the loss angle on longitudinal direction is depicted. From this the longitudinal loss angle response it may be concluded that the crumb rubber mixture is more viscous than the reference one.

The complex modulus on the transversal behaviour in Figure 4.8(a) shows that in the transversal direction the reference asphalt is again stiffer than the crumb rubber one.

On the other hand, as shown in Figure 4.8(b) the loss angle on the transversal direction of the crumb rubber mixture is less viscous than that of the reference asphalt.

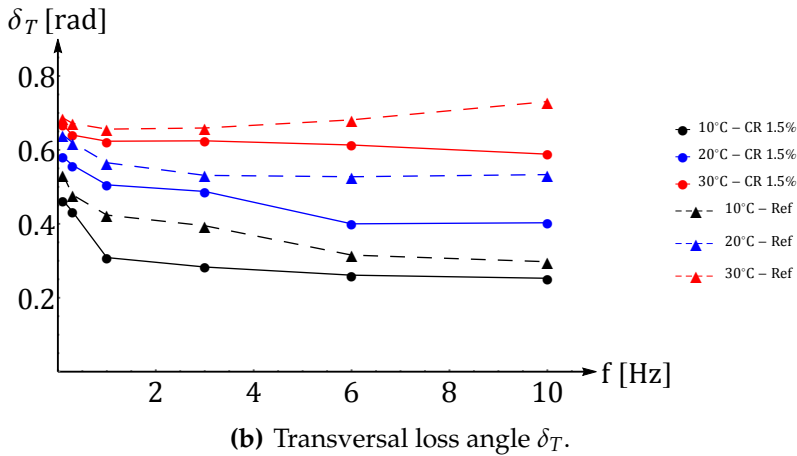
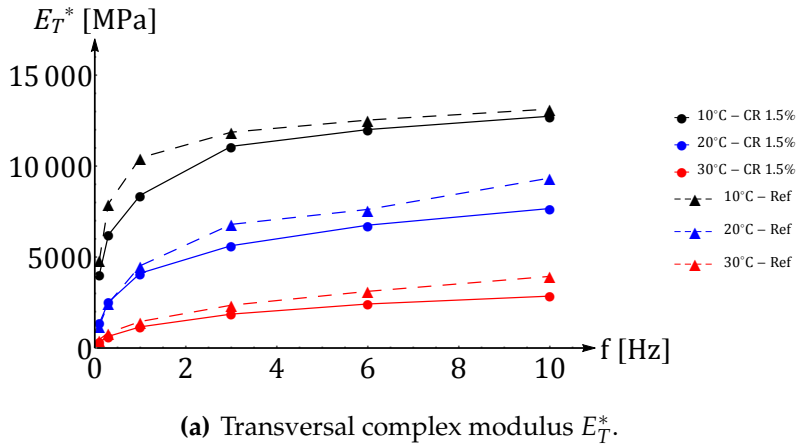


Figure 4.8: Transversal complex modulus and loss angle without confinement.

Cyclic loading with confinement

The amplitude of the vertical cyclic load σ_q is equal to $400kPa$ and the confinement constant load σ_c is equal to $200kPa$. Figures 4.9 and 4.10 show the complex modulus and loss angle for this load condition in the longitudinal and transversal direction.

As it is seen from Figure 4.9(a), for the complex modulus in the longitudinal direction, the reference mixture is stiffer than that the crumb rubber mixture. The difference becomes larger with increasing temperature.

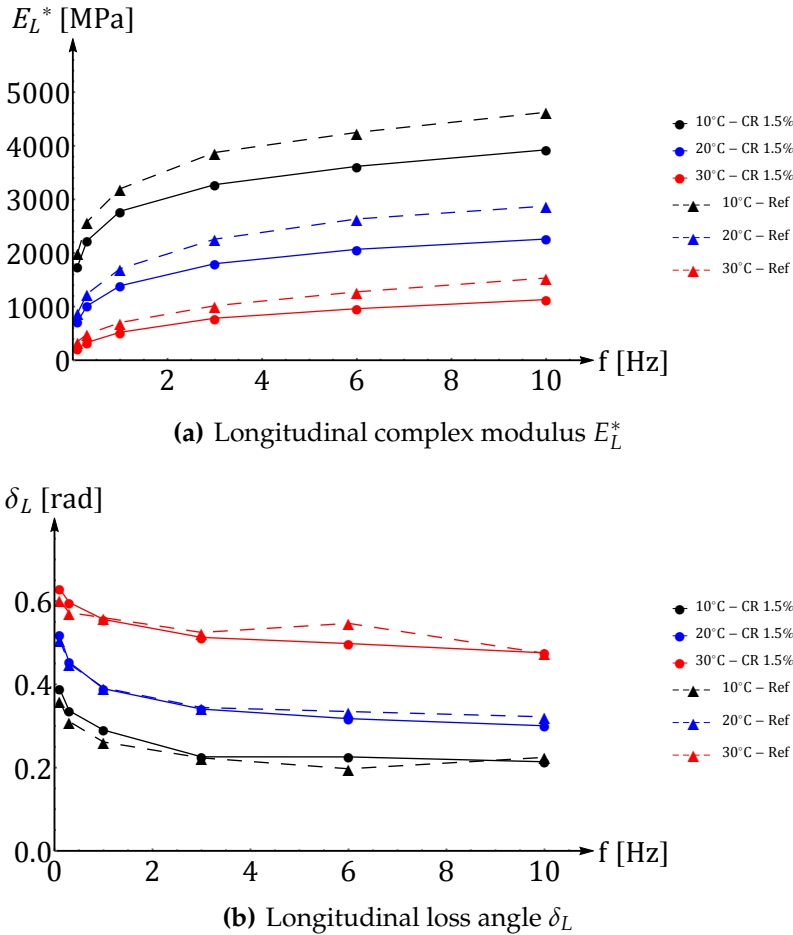


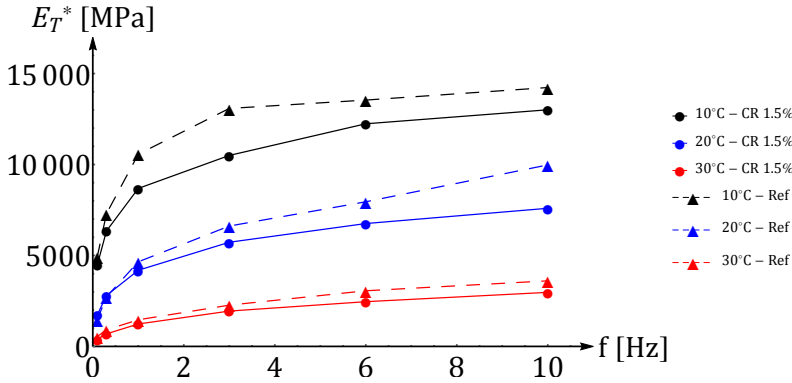
Figure 4.9: Longitudinal complex modulus and loss angle with confinement.

The loss angle in the longitudinal direction is very similar for both the reference and the crumb rubber mixtures, see Figure 4.9(b).

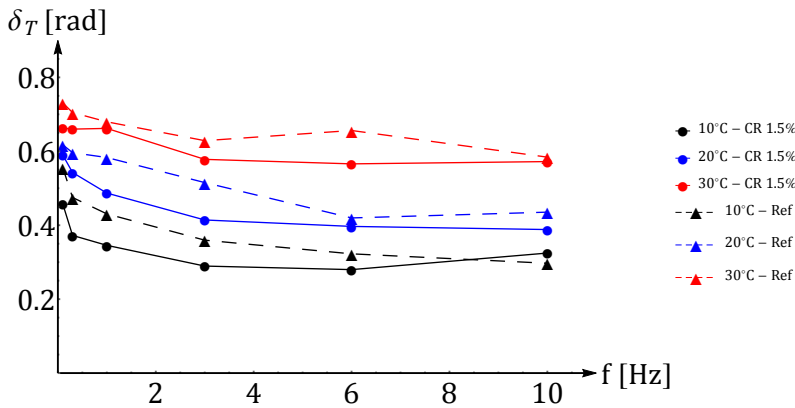
From the complex modulus results in the transversal direction, depicted in Figure 4.10(a), it may be observed that the transversal stiffness of the crumb rubber asphalt is lower than that of the reference one, and this difference becomes smaller when the temperature increases.

Figure 4.10(b) shows the loss angle in the transversal direction for this loading condition. It is seen that the transversal loss angle is lower for the crumb rubber mixture. In other words, the transversal behaviour of the refer-

ence mixtures is more viscous than that of the rubberised one.



(a) Transversal complex modulus E_T^*



(b) Transversal loss angle δ_T

Figure 4.10: Transversal complex modulus and loss angle with confinement.

The mechanical behaviour of the two asphalt mixtures have been evaluated through triaxial creep-recovery test and cyclic tests. From the presented results, it may be observed that the differences between the two mixtures are no so high. That means that the crumb rubber mixture designed is quite similar to the reference mixture.

4.4 3D fractional model for crumb rubber asphalt

In this section, the theory of 3D fractional viscoelasticity presented in Section 4.1 is used to model the tridimensional behaviour of the asphalt mixtures under study. The cyclic triaxial test have been used to obtain the model parameters. The procedure used to obtain the model parameters for the 3D fractional viscoelastic model is defined and explained.

The first step is define the compression stress load imposed to the sample, that is divided into two loads (the vertical axial load σ_q and the confinement load σ_c),

$$\sigma_q(t) = -\sigma_{q0} - \sigma_q \cos(\omega t + \phi) \quad (4.10a)$$

$$\sigma_c(t) = -\sigma_c U(t) \quad (4.10b)$$

In Figure 4.11 represents the compression vertical load $\sigma_q(t)$ applied to the sample, see Eq (4.10a).

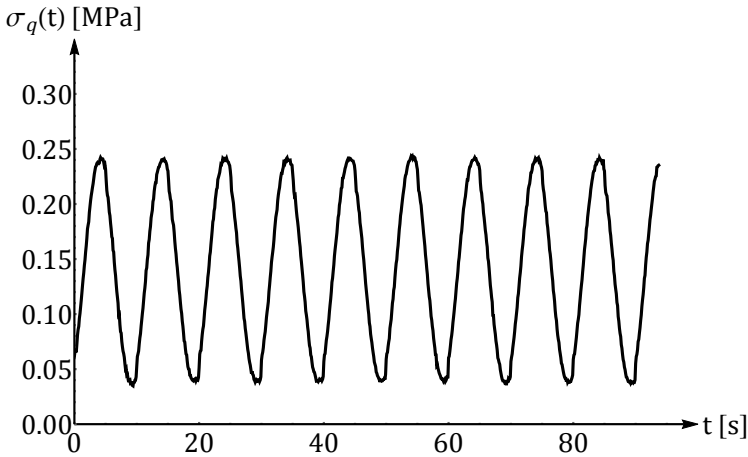


Figure 4.11: Imposed stress $\sigma_q(t)$.

The experimental results obtained from the tests are the measurements of the longitudinal and transversal strain, is respectively $\varepsilon_L(t)$ and $\varepsilon_T(t)$. For the imposed load shown in Figure 4.11 the resulting strain response is represented in Figure 4.12.

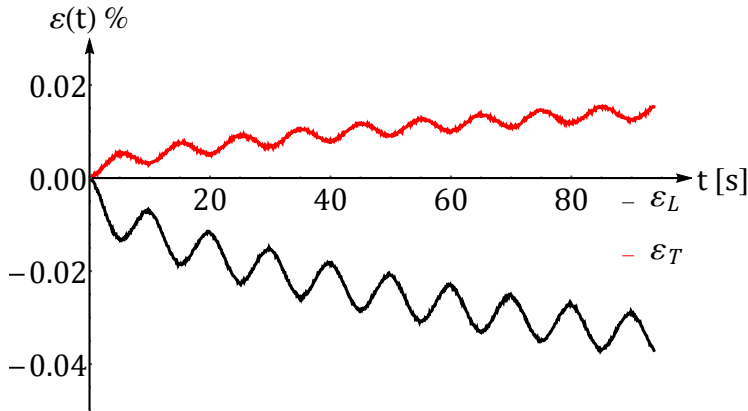


Figure 4.12: Longitudinal and transversal strain, $\varepsilon_L(t)$ and $\varepsilon_T(t)$, from triaxial measurements.

In order to calculate the longitudinal and transversal strain constitutive law it is necessary to know the correspondent creep functions (obtained from Eq. (4.7)) that are respectively

$$C_L(t) = \frac{1}{3} \frac{t^\alpha}{G_\alpha \Gamma(1 + \alpha)} + \frac{1}{9} \frac{t^\beta}{K_\beta \Gamma(1 + \beta)} \quad (4.11a)$$

$$C_T(t) = -\frac{1}{6} \frac{t^\alpha}{G_\alpha \Gamma(1 + \alpha)} + \frac{1}{9} \frac{t^\beta}{K_\beta \Gamma(1 + \beta)} \quad (4.11b)$$

For the load imposed in Eq. (4.10) the modelled longitudinal and the transversal strain history (obtained by introducing the stress history of Eq. (4.10) in Eq. (4.5)) are

$$\begin{aligned} \varepsilon_L(t) = & -\frac{\sigma_{q_0} t^\alpha}{3G_\alpha \Gamma(1 + \alpha)} - \frac{(\sigma_{q_0} + 3\sigma_c) t^\beta}{9K_\beta \Gamma(1 + \beta)} - \\ & - \sigma_q \left(\frac{\omega^{-\beta}}{9K_\beta} + \frac{\omega^{-\alpha}}{3G_\alpha} \right) \cos(\pi\beta/2 - \phi - t\omega) \end{aligned} \quad (4.12a)$$

$$\begin{aligned} \varepsilon_T(t) = & \frac{\sigma_{q_0} t^\alpha}{6G_\alpha \Gamma(1 + \alpha)} - \frac{(\sigma_{q_0} + 3\sigma_c) t^\beta}{9K_\beta \Gamma(1 + \beta)} - \\ & - \sigma_q \left(\frac{\omega^{-\beta}}{9K_\beta} - \frac{\omega^{-\alpha}}{6G_\alpha} \right) \cos(\pi\beta/2 - \phi - t\omega) \end{aligned} \quad (4.12b)$$

As it may be observed from Eq. (4.12), in both (longitudinal and transversal) constitutive laws it appears four parameters, two related with the volumetric contribution and two with the deviatoric. So, it becomes a difficult issue to obtain the coefficients by best fitting from the experimental results. To overcome this issue, the longitudinal and transversal strain may be split into deviatoric and volumetric strain, as show in Figure 4.13.

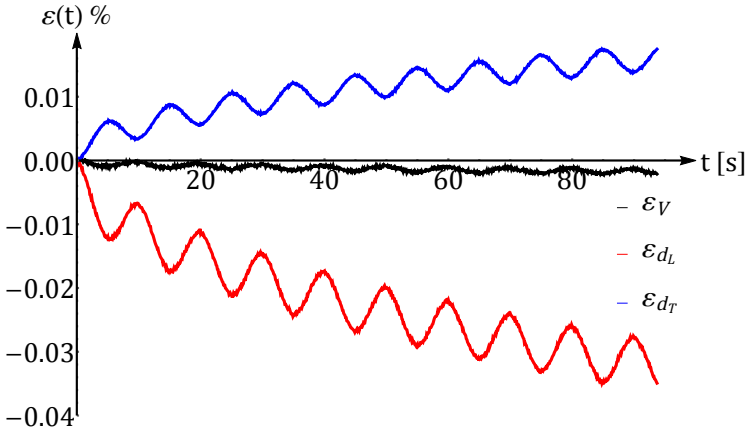


Figure 4.13: Volumetric and deviatoric decomposition of the strain.

The correspondent volumetric strain history for the 3D fractional viscoelastic model and for the stress load according to Eq. (4.10) results

$$\varepsilon_v(t) = -\frac{(\sigma_{q_0} + 3\sigma_c)t^\beta}{9K_\beta\Gamma(1+\beta)} - \sigma_q \frac{\omega^{-\beta}}{9K_\beta} \cos(\pi\beta/2 - \phi - t\omega) \quad (4.13)$$

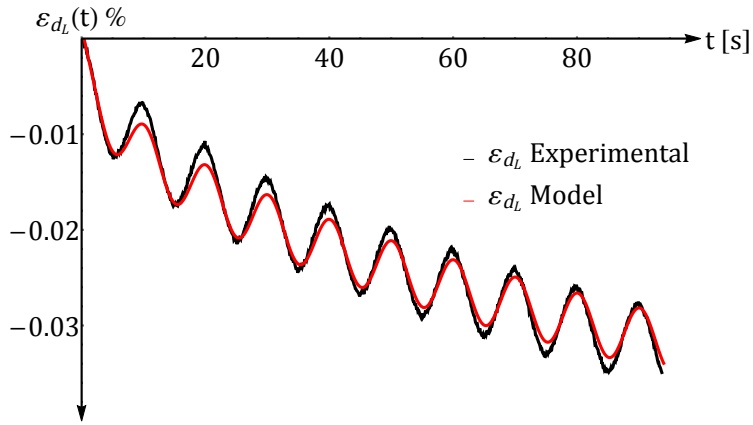
And correspondent longitudinal and transversal deviatoric strain histories for the 3D fractional viscoelastic model and for the stress load according to Eq. (4.10) read as

$$\varepsilon_{dT}(t) = -\frac{(\sigma_{q_0} + 3\sigma_c)t^\alpha}{6K_\alpha\Gamma(1+\alpha)} - \sigma_q \frac{\omega^{-\alpha}}{6G_\alpha} \cos(\pi\alpha/2 - \phi - t\omega) \quad (4.14a)$$

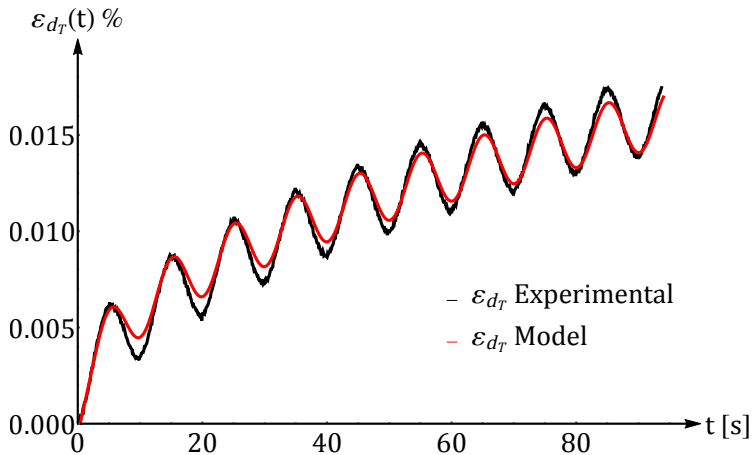
$$\varepsilon_{dL}(t) = \frac{(\sigma_{q_0} + 3\sigma_c)t^\alpha}{6K_\alpha\Gamma(1+\alpha)} + \sigma_q \frac{\omega^{-\alpha}}{6G_\alpha} \cos(\pi\alpha/2 - \phi - t\omega) \quad (4.14b)$$

At this point, the volumetric and deviatoric parameters are isolated and may be easily obtained by best fitting of the experimental results.

Figure 4.14 depicts the experimental results and the modelled longitudinal and transversal deviatoric strain histories.



(a) Longitudinal deviatoric strain, $\varepsilon_{d_L}(t)$.



(b) Transversal deviatoric strain, $\varepsilon_{d_T}(t)$.

Figure 4.14: Longitudinal and transversal deviatoric strain, $\varepsilon_{d_L}(t)$ and $\varepsilon_{d_T}(t)$.

Figures 4.15 shows the experimental results and the modelled volumetric strain history.

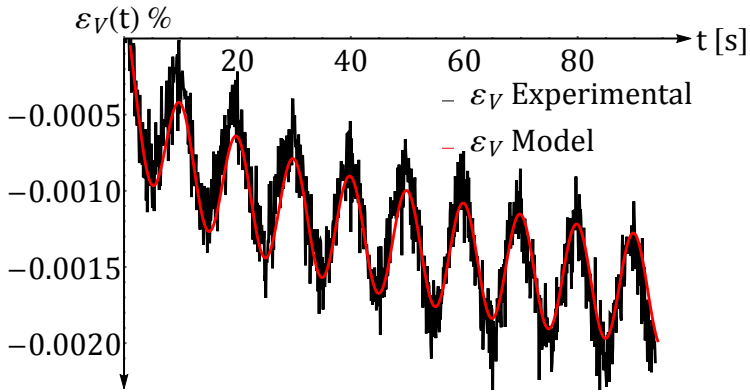


Figure 4.15: Volumetric strain, $\varepsilon_V(t)$.

Once the model parameters have been identified, the Poisson's ratio may be calculated as the rate between the transversal and the longitudinal strain history,

$$\nu(t) = \frac{\varepsilon_T(t)}{\varepsilon_L(t)} \quad (4.15)$$

As it may be observed in Figure 4.16, the outcome model agree with the experimental results.

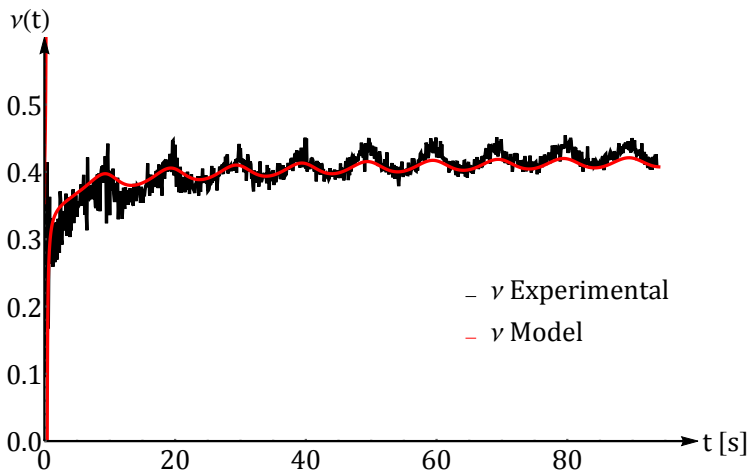
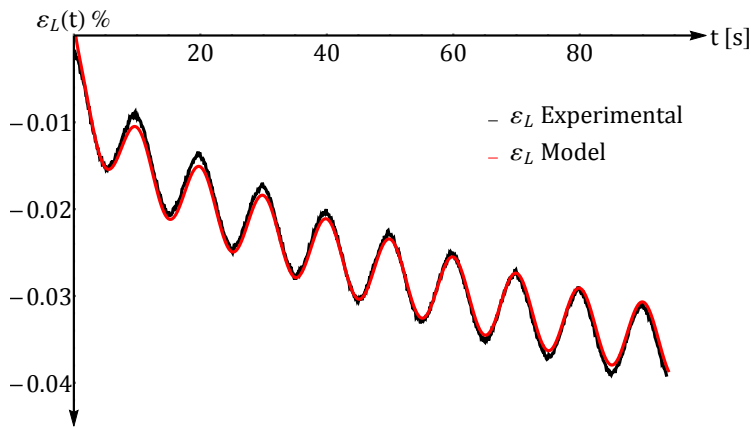


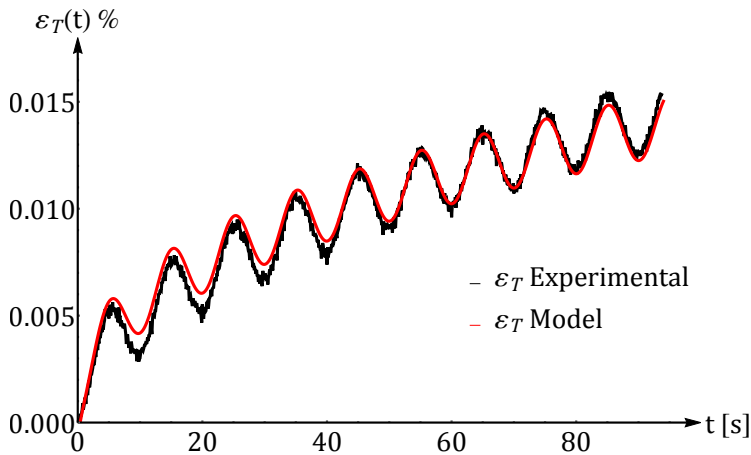
Figure 4.16: Poisson's ratio, $\nu(t)$.

Figure 4.17 shows the longitudinal and transversal strain, $\varepsilon_L(t)$ and $\varepsilon_T(t)$. The experimental results are plotted in black and the modelled response in red, with the coefficients obtained from the best fitting of the volumetric and deviatoric strains.

As it may be observed from Figure 4.17, the model suits well the experimental results.



(a) Longitudinal strain, $\varepsilon_L(t)$.



(b) Transversal strain, $\varepsilon_T(t)$.

Figure 4.17: Experimental versus modelled longitudinal and transversal strain, $\varepsilon_L(t)$ and $\varepsilon_T(t)$.

4.4.1 Model parameter fitting

The model parameters obtained using the presented methodology at different temperature levels are summarised for the reference and the crumb rubber mixtures respectively in Tables 4.1 and 4.2.

Table 4.1: Model parameters for reference asphalt.

Temperature [C°]	α	G_α [MPas $^\alpha$]	β	K_β [MPas $^\beta$]
10	0.34	38	0.23	69
20	0.37	19	0.31	47
30	0.41	5	0.39	24

Table 4.2: Model parameters for crumb rubber asphalt 1.5%.

Temperature [C°]	α	G_α [MPas $^\alpha$]	β	K_β [MPas $^\beta$]
10	0.37	34	0.25	60
20	0.44	14	0.32	35
30	0.48	4	0.41	18

From the parameters obtained in Tables 4.1 and 4.2, some observations have to be remarked. From parameters α and β it is concluded that the crumb rubber mixture is more viscous than the reference one. On the other hand, from parameters G_α and K_β it is observed that the reference asphalt is stiffer than the crumb rubber one. Note that, the same conclusion have been obtained from the cyclic test reported on Subsection 4.3.2.

This model parameters will be used in Chapter 5 to analyse the mechanical response of the two bituminous mixtures (reference and crumb rubber asphalts) as sub-ballast layer under temperature variations.

4.5 Conclusions

In this chapter, the theory of the 3D fractional viscoelasticity has been introduced and its relationship with the fractional mechanical models have been introduced.

The mechanical behaviour of the two asphalt mixtures presented in Chapter 3 (reference and crumb rubber asphalt) has been analysed and modelled. It has been observed that the creep-recovery properties of the crumb rubber mixture allow larger deformations. It recovers more than the reference mixture does. The cyclic test have shown that the crumb rubber mixture is less stiff and more viscous than the reference one. The parameters of the 3D fractional viscoelastic model for both mixtures have been obtained at various temperatures.

The theory of the 3D fractional viscoelasticity has been validated by means of experimental triaxial test performed on the two considered asphalt mixtures.

Chapter 5

Temperature effect on railway sub-ballast rubberised asphalt

This chapter is focused on the temperature effect on viscoelastic materials. The chapter starts with the introduction of the Time-Temperature Superposition Principle, this principle deals with the strong relationship that time and temperature have in most of the viscoelastic materials. Once the Time-Temperature Superposition Principle is introduced, its mathematical inconsistency when fractional elements appear in the mechanical model is demonstrated.

Furthermore, the mechanical response of the bituminous mixtures presented and characterised in the previous Chapters 3 and 4 is evaluated taking into account the temperature effect, using a methodology inspired by the work of [Colinas-Armijo et al., 2017b]. To conclude, the response of the two bituminous mixtures (reference and crumb rubber) as railway sub-ballast is compared using the discrete fractional operators presented in Chapter 1.

5.1 Time temperature superposition principle

It is well known, from the experimental and theoretical point of view, that the properties of viscoelastic materials are strongly influenced by temperature and time.

In the decade of the 1950's the so called Time Temperature Superposition Principle (TTSP) [Williams et al., 1955] was experimentally observed in a study of the viscoelastic behaviour of polymers. This principle defines the

relationship between time or frequency and temperature in the mechanical properties of the viscoelastic materials under constant or dynamic stress conditions.

TTSP only may be applied to thermorheologically simple materials [Ferry, 1980, Tschoegl, 2012]. Thermorheological simplicity requires that all characteristic times depend identically on temperature. The *shift factor* $a(T, T_0)$ defines the concept of thermorheologically simplicity and is defined as (see [Tschoegl et al., 2002])

$$a(T, T_0) = \frac{\tau(T)}{\tau(T_0)} \quad (5.1)$$

where $\tau(T)$ and $\tau(T_0)$ are the characteristic times at the temperatures T and T_0 , respectively. If a material is thermorheologically simple all the $a(T, T_0)$ have to remain constant for all the different characteristic times.

Thermorheological simplicity may also be analysed through the Cole-Cole plot or the Wicket (also called Van Gurp-Palmer) plot, see [Tschoegl et al., 2002, Van Gurp and Palmen, 1998]. The Cole-Cole plot represents the storage magnitude versus the loss magnitude at several temperatures. If the Cole-Cole plot is temperature independent the material is referred to as thermorheologically simple. The Wicket plot is the representation of the loss tangent versus the complex magnitude. When the Wicket plot is temperature independent, it also referred to as the material is thermorheologically simple.

For thermorheologically simple materials it is possible to build the so called *master curve*, for a given reference temperature, a mechanical property (i. e. creep or relaxation functions, complex modulus,...) may be predicted for any other temperature by shifting the time scale, see [Christensen, 1971, Ferry, 1980]. The master curve is readily obtained by using the shift factor of Eq. (5.1) and mainly consists of an acceleration or deceleration in the time (or frequency) scale according to

$$t_0 = a(T, T_0)t; \quad f_0 = a(T, T_0)f; \quad (5.2)$$

where t_0/f_0 is the time/frequency scale at the reference temperature and t/f is the time/frequency scale at any temperature. Thus, the shift factor $a(T, T_0)$ modifies the time (or frequency) scale of each mechanical property as shown in Eq. (5.2).

Once the applicability of the TTSP with respect to the thermorheologically simple behaviour has been proved, a master curve at the desired reference temperature is modelled. This master curve is very useful to predict the long-range effects of stress respectively strain application, and the effects of low

respectively high frequency application of stress cycles on mechanical properties of linear viscoelastic materials. To construct this master curve it is necessary to select the most suitable technique of data shifting. This master curve can be represented in the time or frequency domain. Different shifting techniques exist. These techniques are mathematical relationships that define empirical relations between time and temperature effect of stress and strain on some mechanical properties.

The shift factor $a(T, T_0)$, defined in Eq. (5.1), modifies the time/frequency axis and usually is referred to as horizontal shift factor. In some cases it has been demonstrated that horizontal shifting is not significant. Consequently, in order to overcome this issue, some authors have proposed additional vertical shift factor $b(T, T_0)$.

The next part of this section is dedicated to review the classical shifting techniques (horizontal and vertical).

5.1.1 Classical horizontal shifting

Since the 1950s, dozens of formulas had been proposed to link the shift factors of a master curve to its reference temperature. The most commonly used shift factor techniques are here reported and may be found in different references as for example [Christensen, 1971, Ferry, 1980, Tschoegl et al., 2002, Dealy and Plazek, 2009].

The numerical technique is a non-functional method in which no equation is used to determinate the shift factors. The temperature shift factors and the master curve model coefficients are simultaneously determined by the method of least square optimisation.

The log-linear technique arises from the Doolittle equation [Doolittle and Doolittle, 1957], and is defined as

$$\log(a(T, T_0)) = C \left(\frac{1}{T} - \frac{1}{T_0} \right) \quad (5.3)$$

where C is a constant determined by the experimental data, T_0 is the reference temperature and T is the temperature of the test. This technique

The Williams-Landel-Ferry (WLF) technique [Williams et al., 1955] is defined by the following equation

$$\log(a(T, T_0)) = \frac{-C_1(T - T_0)}{C_2 + (T - T_0)} \quad (5.4)$$

where C_1 and C_2 are the constants that can be obtained through analysis of the experimental data, T_0 is the reference temperature and T is the testing temperature. Note that this method is based on the assumption that the fractional free volume of polymers increases with temperature.

The modified Kaelble technique [Kaelble, 1985] is based on the WLF technique, see equation (5.4), with a modification of the denominator

$$\log(a(T, T_0)) = \frac{-C_1(T - T_0)}{C_2 + |T - T_0|}. \quad (5.5)$$

The Arrhenius technique (see [Dealy and Plazek, 2009]) is formulated as follows

$$\log(a(T, T_0)) = \frac{\Delta H_a}{R} \left(\frac{1}{T} - \frac{1}{T_0} \right) \quad (5.6)$$

where ΔH_a is the activation or relaxation energy associated with the compliance or relaxation transition, R is the universal gas constant ($R = 8,314$ J/KmolK), T_0 is the reference temperature and T is the test temperature.

5.1.2 Classical vertical shifting

The classically applied TTSP involves only horizontal shifting coefficients $a(T, T_0)$, and gives an equivalence between the mechanical properties measured at a frequency f (or a time t), a temperature T and the mechanical properties at a reduced frequency f_0 (or a reduced time t_0) of a reference temperature T_0 .

The vertical shift factor is a translation along the vertical axes, the axis that defines the mechanical property which is needed to build the master curve. The vertical shift factor $b(T, T_0)$ modifies the values of the mechanical property that it has been evaluated,

$$\text{MechanicalProperty}_0 = b(T, T_0) \text{MechanicalProperty}. \quad (5.7)$$

As there are different shifting factor techniques for the horizontal shifting, let's define those which also consider the possibility of vertical shifting. These are WLF and Arrhenius techniques.

For the WLF vertical shifting technique, first the Bouche-Rouse theory for linear viscoelasticity [Bueche, 1954] needs to be introduced. The Bouche-Rouse theory says that the complex compliance or relaxation is proportional to the density and the temperature. Since the vertical shift coefficients reflect

the temperature dependance of the mechanical property (compliance/relaxation) of the viscoelastic material, b can be model as

$$b(T, T_0) = \frac{T_0 \rho_0}{T \rho} \quad (5.8)$$

where ρ_0 is the density of the material at the reference temperature and ρ is the density at the test temperature. Assuming that the mass material remains constant, Eq. (5.8) can be rewritten as

$$b(T, T_0) = \frac{T_0}{T} [1 + \alpha(T - T_0)]^3 \quad (5.9)$$

in which α is the thermal expansion coefficient.

In the case of the Arrhenius shifting model the vertical shifting is defined as

$$\log(b(T, T_0)) = \frac{\Delta H_b}{R} \left(\frac{1}{T} - \frac{1}{T_0} \right) \quad (5.10)$$

where ΔH_b is the activation or retardation energy.

5.2 Mathematical inconsistency of classical shifting in fractional viscoelasticity

The use of Time-Temperature Superposition Principle in viscoelastic materials is very important, it simplifies the models and reduces the number of experimental test to characterise a viscoelastic material.

The starting point to reconsider the definition of shift factor for fractional viscoelastic models has been the definition of the shift factor according to Eq. (5.1). The main difficulty of this formula is the calculation of the characteristic times. For this reason in the Chapter 2 and in [Colinas-Armijo et al., 2016], a methodology has been proposed to calculate the fractional characteristic times. In order to evaluate the shifting technique based on the characteristic times, some works, studying the temperature effect on polymers, have been proposed [Badagliacco et al., 2016, Colinas-Armijo et al., 2017a].

Even changing the formulation of the shift factor, from a mathematical point of view some incongruences have been found, and are presented in the next subsection.

5.2.1 Mathematical inconsistency of classical shifting in fractional viscoelasticity

From a mathematical point of view the shift factors presented in Section 5.1 are inconsistent when the materials are modelled by fractional constitutive laws. This is due to the fact that these horizontal shift factors are designed for constitutive laws that contain exponential functions instead of power law ones.

For this reason, here a new shifting technique is proposed that uses element shifting. So, each element has to be shifted by knowing its characteristics, the element parameters, at each temperature. Below, it is explained how each element (spring, dashpot and springpot) should be shifted, in order to obtain a coherent result from a mathematical point of view.

Spring

The spring element is characterised by a creep function of the type

$$C(t) = \frac{1}{E} \quad (5.11)$$

being E the stiffness of the spring.

On the other hand, the relaxation function of the spring is equal to

$$R(t) = E. \quad (5.12)$$

Obviously time is not involved in the creep and relaxation functions, and also the spring is not a viscoelastic element. However, if the spring stiffness varies with the temperature, and thus it may be written

$$\frac{1}{E_j} = b_{E_C}(T_j, T_0) \frac{1}{E_0}, \quad (5.13)$$

where $b_{E_C}(T_j, T_0)$ is the vertical shift factor for the spring. Then, from Eq. (5.13) it follows that the vertical shift is $b_{E_C}(T_j, T_0) = E_0/E_j$. In contrast, for the relaxation function the shift factor is $b_{E_R}(T_j, T_0) = E_j/E_0$.

Dashpot

The dashpot element is characterised by a creep function of the type

$$C(t) = \frac{1}{\mu} t \quad (5.14)$$

being μ the viscosity of the dashpot.

On the other hand, the relaxation function of the dashpot reads as

$$R(t) = 0. \quad (5.15)$$

For the dashpot element the time is involved in the creep function, but not in the relaxation function. If the dashpot viscosity is temperature dependent, it follows that

$$\frac{1}{\mu_j} t_j = b_{\mu_C}(T_j, T_0) \frac{1}{\mu_0} t_0, \quad (5.16)$$

where $b_{\mu_C}(T_j, T_0)$ is the vertical shift factor for the dashpot. Then, from Eq. (5.16) it follows that the vertical shift factor is $b_{\mu_C}(T_j, T_0) = \mu_0/\mu_j$. The shift factor of the relaxation function in contrast is not necessary since the relaxation function is zero.

Springpot

The springpot element is characterised by a creep function of the type

$$C(t) = \frac{t^\alpha}{E_\alpha \Gamma(1 + \alpha)}, \quad (5.17)$$

and the relaxation function of the dashpot reads as

$$R(t) = \frac{E_\alpha t^{-\alpha}}{\Gamma(1 - \alpha)}. \quad (5.18)$$

In the case of the springpot element, both vertical and horizontal shifting are involved, and may be written as follows

$$\frac{t_j^\alpha}{E_{\alpha_j} \Gamma(1 + \alpha_j)} = b_{\alpha_C}(T_j, T_0) \frac{t^{\alpha_0} a_{\alpha_C}(T_j, T_0)}{E_{\alpha_0} \Gamma(1 + \alpha_0)}, \quad (5.19)$$

where $b_{\alpha_C}(T_j, T_0)$ is the vertical creep shift factor and $a_{\alpha_C}(T_j, T_0)$ is the horizontal creep shift factor for the spring-pot. Then, from Eq. (5.19) that the vertical creep shift is $b_{\alpha_C}(T_j, T_0) = (E_{\alpha_0} \Gamma(1 + \alpha_0)) / (E_{\alpha_j} \Gamma(1 + \alpha_j))$ and the vertical shift factor for the relaxation function the is the contrary, that is $b_{\alpha_R}(T_j, T_0) = (E_{\alpha_j} \Gamma(1 - \alpha_0)) / (E_{\alpha_j} \Gamma(1 - \alpha_j))$.

By the other hand, the horizontal shift factor $a_{\alpha_C}(T_j, T_0)$ is equal for both the creep and the relaxation and it is equal to $a_{\alpha_C}(T_j, T_0) = b_{\alpha_R}(T_j, T_0) = \alpha_j/\alpha_0$. It has to be remarked that, in the case of the springpot, the time axes has to be modified raising to the power of the horizontal shift factor.

5.3 Temperature effect on 3D fractional viscoelasticity

In this section it is studied how can be modelled the effect of the temperature in the 3D fractional constitutive laws by means of the Riemann-Liouville and Grünwald-Letnikov discrete fractional operators presented in Chapter 1.

The Time Temperature Superposition Principle approach, introduced in Section 5.1, and the step material parameters variation with temperature, are also evaluated.

5.3.1 Time Temperature Superposition Principle approach

As discussed before, the main advantage of the TTSP approach is that, by shifting in the time axis, a mechanical property at different temperatures may be calculated. Thus, if the shift factor it is known, knowing a mechanical property for a reference temperature, the same mechanical property may be obtained by means of the shift factor. Consequently, in this subsection the formulation of the TTSP approach is evaluated, for the longitudinal and transversal response, considering both the Riemann-Liouville and Grünwald-Letnikov operators.

Riemann-Liouville operator

Using the Riemann-Liouville discrete operators presented in Section 1.4, see Eq. (1.47), the longitudinal and transversal strain according to Eq. (4.5), may be rewritten as

$$\begin{aligned} \varepsilon_{LN} = & \frac{\Delta t^{\alpha_0}}{3G_{\alpha_0}\Gamma(1+\alpha_0)} S_{\alpha N} V_N(\alpha_0) \sigma_{qN} \\ & + \frac{\Delta t^{\beta_0}}{9K_{\beta_0}\Gamma(1+\beta_0)} S_{\beta N} V_N(\beta_0) (\sigma_{qN} + 3\sigma_{cN}) \end{aligned} \quad (5.20a)$$

$$\begin{aligned} \varepsilon_{TN} = & -\frac{\Delta t^{\alpha_0}}{6G_{\alpha_0}\Gamma(1+\alpha_0)} S_{\alpha N} V_N(\alpha_0) \sigma_{qN} \\ & + \frac{\Delta t^{\beta_0}}{9K_{\beta_0}\Gamma(1+\beta_0)} S_{\beta N} V_N(\beta_0) (\sigma_{qN} + 3\sigma_{cN}) \end{aligned} \quad (5.20b)$$

where subscript N stands for the number of discrete steps, σ_{qN} and σ_{cN} are respectively the axial and confinement stress, and subscript 0 refers to the reference temperature. The matrixes $V_N(\alpha_0)$ and $V_N(\beta_0)$ are defined as

$$\mathbf{V}_N(\alpha_0) = \begin{bmatrix} 1 & 0 & \dots & 0 & 0 \\ -2^{\alpha_0} & 1 & \dots & 0 & 0 \\ 0 & -2^{\alpha_0} & \dots & 0 & 0 \\ \vdots & \vdots & \ddots & \vdots & \vdots \\ 0 & 0 & \dots & 1 & 0 \\ 0 & 0 & \dots & -2^{\alpha_0} & 1 \end{bmatrix} \quad (5.21a)$$

$$\mathbf{V}_N(\beta_0) = \begin{bmatrix} 1 & 0 & \dots & 0 & 0 \\ -2^{\beta_0} & 1 & \dots & 0 & 0 \\ 0 & -2^{\beta_0} & \dots & 0 & 0 \\ \vdots & \vdots & \ddots & \vdots & \vdots \\ 0 & 0 & \dots & 1 & 0 \\ 0 & 0 & \dots & -2^{\beta_0} & 1 \end{bmatrix} \quad (5.21b)$$

and the matrixes $\mathbf{S}_{\alpha N}$ and $\mathbf{S}_{\beta N}$ are written as

$$\mathbf{S}_{\alpha N} = \begin{bmatrix} a(T_1, T_0)^{\alpha_0} & 0 & \dots & 0 \\ 0 & a(T_2, T_0)^{\alpha_0} & \dots & 0 \\ 0 & 0 & \dots & 0 \\ \vdots & \vdots & \ddots & \vdots \\ 0 & 0 & \dots & (T_N, T_0)^{\alpha_0} \end{bmatrix} \quad (5.22a)$$

$$\mathbf{S}_{\beta N} = \begin{bmatrix} a(T_1, T_0)^{\beta_0} & 0 & \dots & 0 \\ 0 & a(T_2, T_0)^{\beta_0} & \dots & 0 \\ 0 & 0 & \dots & 0 \\ \vdots & \vdots & \ddots & \vdots \\ 0 & 0 & \dots & a(T_N, T_0)^{\beta_0} \end{bmatrix} \quad (5.22b)$$

where $a(T_i, T_0)$ is the shift factor at the i -th step.

Grünwald-Letnikov operator

using the Grünwald-Letnikov discrete operators presented in Section 1.2.3, see Eq. (1.19), the longitudinal and transversal strain according Eq. (4.5) may be rewritten as

$$\begin{aligned}\boldsymbol{\varepsilon}_{LN} &= \frac{\Delta t^{\alpha_0}}{3G_{\alpha_0}\Gamma(1+\alpha_0)} \mathbf{S}_{\alpha N} \mathbf{B}_N(\alpha_0) \boldsymbol{\sigma}_{qN} \\ &+ \frac{\Delta t^{\beta_0}}{9K_{\beta_0}\Gamma(1+\beta_0)} \mathbf{S}_{\beta N} \mathbf{B}_N(\beta_0) (\boldsymbol{\sigma}_{qN} + 3\boldsymbol{\sigma}_{cN})\end{aligned}\quad (5.23a)$$

$$\begin{aligned}\boldsymbol{\varepsilon}_{TN} &= -\frac{\Delta t^{\alpha_0}}{6G_{\alpha_0}\Gamma(1+\alpha_0)} \mathbf{S}_{\alpha N} \mathbf{B}_N(\alpha_0) \boldsymbol{\sigma}_{qN} \\ &+ \frac{\Delta t^{\beta_0}}{9K_{\beta_0}\Gamma(1+\beta_0)} \mathbf{S}_{\beta N} \mathbf{B}_N(\beta_0) (\boldsymbol{\sigma}_{qN} + 3\boldsymbol{\sigma}_{cN})\end{aligned}\quad (5.23b)$$

where $\boldsymbol{\sigma}_{qN}$ and $\boldsymbol{\sigma}_{cN}$ are respectively the axial and confinement stress. The matrixes $\mathbf{B}_N(\alpha_0)$ and $\mathbf{B}_N(\beta_0)$ read as

$$\mathbf{B}_N(\alpha_0) = \begin{bmatrix} 1 & 0 & \dots & 0 \\ \omega_1(-\alpha_0) & 1 & \dots & 0 \\ \vdots & \vdots & \ddots & \vdots \\ \omega_{N-1}(-\alpha_0) & \omega_{N-2}(-\alpha_0) & \dots & 1 \end{bmatrix}\quad (5.24a)$$

$$\mathbf{B}_N(\beta_0) = \begin{bmatrix} 1 & 0 & \dots & 0 \\ \omega_1(-\beta_0) & 1 & \dots & 0 \\ \vdots & \vdots & \ddots & \vdots \\ \omega_{N-1}(-\beta_0) & \omega_{N-2}(-\beta_0) & \dots & 1 \end{bmatrix}\quad (5.24b)$$

and matrices $\mathbf{S}_{\alpha N}$ and $\mathbf{S}_{\beta N}$ are the same that in the case of the Riemann-Liouville operator, see Eq. (5.22).

In both cases, Riemann-Liouville and Grünwald-Letnikov, the change at each step is represented by the diagonal matrixes $\mathbf{S}_{\alpha N}$ and $\mathbf{S}_{\beta N}$, which depend on the reference temperature selected and the actual temperature at each step.

5.3.2 Step-by-step material parameter variation with temperature

Subsequently, the temperature effect, knowing the value of the parameters at each time step, for the longitudinal and transversal response is evaluated, using both the Riemann-Liouville and Grünwald-Letnikov operators.

Riemann-Liouville operator

The longitudinal and transversal strain, calculated in Eq. (4.5), and using the Riemann-Liouville discrete operators presented in Section 1.4, see Eq. (1.47), may be rewritten as

$$\varepsilon_{LN} = \frac{1}{3} \tilde{V}_{\alpha N} \sigma_{qN} + \frac{1}{9} \tilde{V}_{\beta N} (\sigma_{qN} + 3\sigma_{cN}) \quad (5.25a)$$

$$\varepsilon_{TN} = -\frac{1}{6} \tilde{V}_{\alpha N} \sigma_{qN} + \frac{1}{9} \tilde{V}_{\beta N} (\sigma_{qN} + 3\sigma_{cN}) \quad (5.25b)$$

where the subindex N stands for the number of discrete steps, σ_{qN} and σ_{cN} are respectively the axial and confinement stress and the matrixes $\tilde{V}_{\alpha N}$ and $\tilde{V}_{\beta N}$ are defined as

$$\tilde{V}_{\alpha N} = \begin{bmatrix} \frac{\Delta t^{\alpha_1}}{\Gamma(1+\alpha_1)G_{\alpha_1}} & 0 & \dots & 0 & 0 \\ -2^{\alpha_2} \Delta t^{\alpha_2} & \frac{\Delta t^{\alpha_2}}{\Gamma(1+\alpha_2)G_{\alpha_2}} & \dots & 0 & 0 \\ \frac{\Delta t^{\alpha_1}}{\Gamma(1+\alpha_1)G_{\alpha_1}} & \frac{\Delta t^{\alpha_2}}{\Gamma(1+\alpha_2)G_{\alpha_2}} & \dots & 0 & 0 \\ 0 & \frac{-2^{\alpha_3} \Delta t^{\alpha_3}}{\Gamma(1+\alpha_3)G_{\alpha_3}} & \dots & 0 & 0 \\ \vdots & \vdots & \ddots & \vdots & \vdots \\ 0 & 0 & \dots & \frac{\Delta t^{\alpha_{N-1}}}{\Gamma(1+\alpha_{N-1})G_{\alpha_{N-1}}} & 0 \\ 0 & 0 & \dots & \frac{-2^{\alpha_N} \Delta t^{\alpha_N}}{\Gamma(1+\alpha_N)G_{\alpha_N}} & \frac{\Delta t^{\alpha_N}}{\Gamma(1+\alpha_N)G_{\alpha_N}} \end{bmatrix} \quad (5.26a)$$

$$\tilde{V}_{\beta N} = \begin{bmatrix} \frac{\Delta t^{\beta_1}}{\Gamma(1+\beta_1)K_{\beta_1}} & 0 & \dots & 0 & 0 \\ -2^{\beta_2} \Delta t^{\beta_2} & \frac{\Delta t^{\beta_2}}{\Gamma(1+\beta_2)K_{\beta_2}} & \dots & 0 & 0 \\ \frac{\Delta t^{\beta_1}}{\Gamma(1+\beta_1)K_{\beta_1}} & \frac{\Delta t^{\beta_2}}{\Gamma(1+\beta_2)K_{\beta_2}} & \dots & 0 & 0 \\ 0 & \frac{-2^{\beta_3} \Delta t^{\beta_3}}{\Gamma(1+\beta_3)K_{\beta_3}} & \dots & 0 & 0 \\ \vdots & \vdots & \ddots & \vdots & \vdots \\ 0 & 0 & \dots & \frac{\Delta t^{\beta_{N-1}}}{\Gamma(1+\beta_{N-1})K_{\beta_{N-1}}} & 0 \\ 0 & 0 & \dots & \frac{-2^{\beta_N} \Delta t^{\beta_N}}{\Gamma(1+\beta_N)K_{\beta_N}} & \frac{\Delta t^{\beta_N}}{\Gamma(1+\beta_N)K_{\beta_N}} \end{bmatrix} \quad (5.26b)$$

Grünwald-Letnikov operator

The longitudinal and transversal strain calculated according to Eq. (4.5) using the Grünwald-Letnikov discrete operators presented in Section 1.2.3, see Eq. (1.19), may be rewritten as

$$\varepsilon_{LN} = \frac{1}{3} \tilde{\mathbf{B}}_{\alpha N} \sigma_{qN} + \frac{1}{9} \tilde{\mathbf{B}}_{\beta N} (\sigma_{qN} + 3\sigma_{cN}) \quad (5.27a)$$

$$\varepsilon_{TN} = -\frac{1}{6} \tilde{\mathbf{B}}_{\alpha N} \sigma_{qN} + \frac{1}{9} \tilde{\mathbf{B}}_{\beta N} (\sigma_{qN} + 3\sigma_{cN}) \quad (5.27b)$$

where σ_{qN} and σ_{cN} are respectively the axial and confinement stress and the matrixes $\tilde{\mathbf{B}}_{\alpha N}$. The $\tilde{\mathbf{B}}_{\beta N}$ are defined as

$$\tilde{\mathbf{B}}_{\alpha N} = \begin{bmatrix} \frac{\Delta t^{\alpha_1}}{\Gamma(1+\alpha_1)K_{\alpha_1}} & 0 & \dots & 0 \\ \frac{\omega_1(-\alpha_2)\Delta t^{\alpha_2}}{\Gamma(1+\alpha_2)K_{\alpha_2}} & \frac{\Delta t^{\alpha_2}}{\Gamma(1+\alpha_2)K_{\alpha_2}} & \dots & 0 \\ \vdots & \vdots & \ddots & \vdots \\ \frac{\omega_{N-1}(-\alpha_N)\Delta t^{\alpha_N}}{\Gamma(1+\alpha_N)K_{\alpha_N}} & \frac{\omega_{N-2}(-\alpha_N)\Delta t^{\alpha_N}}{\Gamma(1+\alpha_N)K_{\alpha_N}} & \dots & \frac{\Delta t^{\alpha_N}}{\Gamma(1+\alpha_N)K_{\alpha_N}} \end{bmatrix} \quad (5.28a)$$

$$\tilde{\mathbf{B}}_{\beta N} = \begin{bmatrix} \frac{\Delta t^{\beta_1}}{\Gamma(1+\beta_1)K_{\beta_1}} & 0 & \dots & 0 \\ \frac{\omega_1(-\beta_2)\Delta t^{\beta_2}}{\Gamma(1+\beta_2)K_{\beta_2}} & \frac{\Delta t^{\beta_2}}{\Gamma(1+\beta_2)K_{\beta_2}} & \dots & 0 \\ \vdots & \vdots & \ddots & \vdots \\ \frac{\omega_{N-1}(-\beta_N)\Delta t^{\beta_N}}{\Gamma(1+\beta_N)K_{\beta_N}} & \frac{\omega_{N-2}(-\beta_N)\Delta t^{\beta_N}}{\Gamma(1+\beta_N)K_{\beta_N}} & \dots & \frac{\Delta t^{\beta_N}}{\Gamma(1+\beta_N)K_{\beta_N}} \end{bmatrix} \quad (5.28b)$$

It may be observed that the formulation of the Riemann-Liouville and Grünwald-Letnikov operators is quite similar, except from the matrixes $\tilde{\mathbf{V}}_N$ and $\tilde{\mathbf{B}}_N$. It has to be emphasised that the use of the Riemann-Liouville operator is more interesting from a computational point of view, since the matrixes $\tilde{\mathbf{V}}_{\alpha N}$ and $\tilde{\mathbf{V}}_{\beta N}$ are two diagonal matrixes and the matrixes $\tilde{\mathbf{B}}_{\alpha N}$ and $\tilde{\mathbf{B}}_{\beta N}$ are triangular matrixes.

5.4 Evaluation of the creep response and the temperature effect on railway sub-ballast rubberised asphalt

In this section, the effect of the temperature on the creep response of the railway sub-ballast modelled by means of the theory of 3D fractional viscoelasticity is evaluated.

5.4.1 Material parameters variations with temperature

The two bituminous mixtures presented in Chapters 3 and 4 are considered. In Figures 5.1 and 5.2 the model parameters obtained in Section 4.4.1 are graphically displayed as function of temperature.

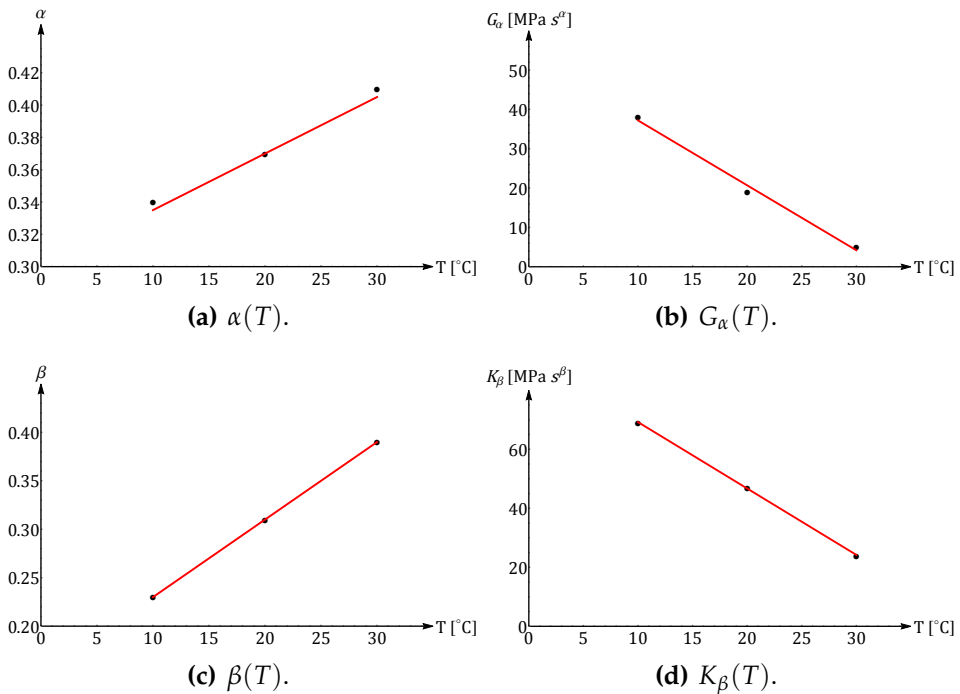


Figure 5.1: Parameter variation with temperature $\alpha(T)$, $G_\alpha(T)$, $\beta(T)$ and $K_\beta(T)$ for the reference asphalt.

Figure 5.1 shows the model parameters α , G_α , β and K_β for the reference asphalt. Linear regression of these parameters with respect to the temperature

T lead to the following relations

$$\alpha(T) = 0.004 T + 0.323 \tag{5.29a}$$

$$G_\alpha(T) = -1.650 T + 53.725 \tag{5.29b}$$

$$\beta(T) = 0.008 T + 0.149 \tag{5.29c}$$

$$K_\beta(T) = -2.250 T + 91.715 \tag{5.29d}$$

The model parameters for the crumb rubber mixture with respect to the temperature T is shown Figure 5.2.

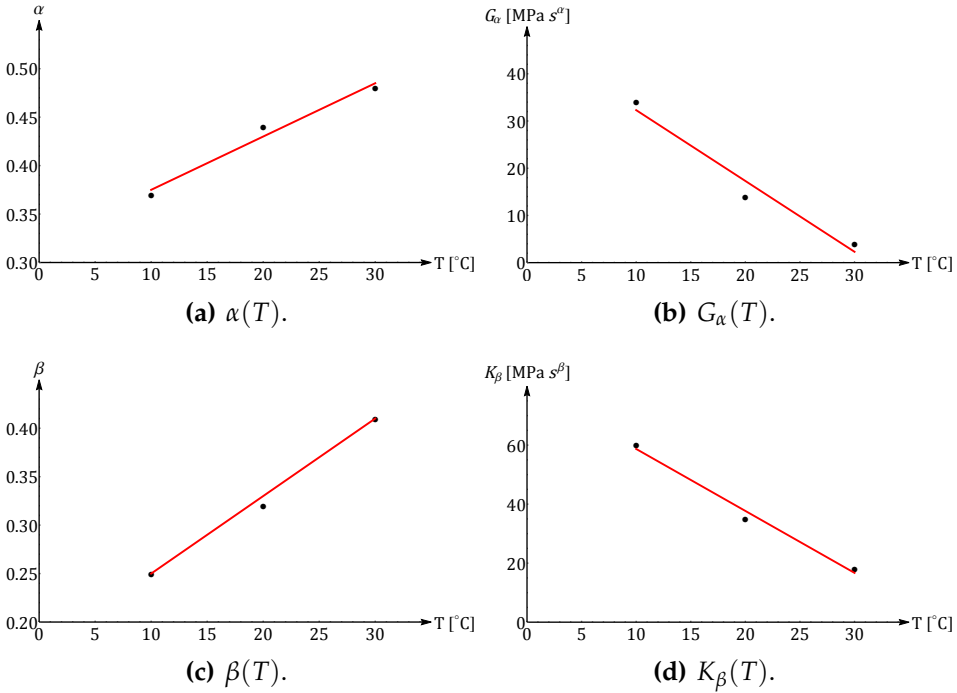


Figure 5.2: Parameter variation with temperature $\alpha(T)$, $G_\alpha(T)$, $\beta(T)$ and $K_\beta(T)$ for the crumb rubber asphalt.

The regression equations for the crumb rubber mixture are reported are the following

$$\alpha(T) = 0.0055T + 0.32 \tag{5.30a}$$

$$G_\alpha(T) = -1.5T + 47.3 \tag{5.30b}$$

$$\beta(T) = 0.008T + 0.17 \tag{5.30c}$$

$$K_\beta(T) = -2.1T + 79.7 \tag{5.30d}$$

As observed from Figures 5.1 and 5.2, the parameters α and β increase with the temperature but the parameters G_α and K_β decrease.

5.4.2 Creep response and temperature effect on railway sub-ballast made of bituminous mixtures

Now the creep response of the railway sub-ballast made of bituminous mixtures with respect the temperature effect is evaluated. In particular, the reference asphalt and the rubberised asphalt presented in Chapters 3 and 4 are evaluated.

The step-by-step material parameter variation presented in Subsection 5.3.2 is used to assess the creep response when the material is subjected to a time dependant temperature history.

The creep has been evaluated for load conditions of $\sigma_q = 200kPa$ and $\sigma_c = 100kPa$. This loading conditions have been selected since it has been calculated with the software ViscoRail 2.0 that for a high speed train the vertical stress that arrives to the sub-ballast layer is equal to $200kPa$. ViscoRail 2.0, developed by IFSTTAR (see [Chupin et al., 2014]), is a numerical program designed to solve the equations of motion for semi-infinite layered media excited by loads moving at constant speed.

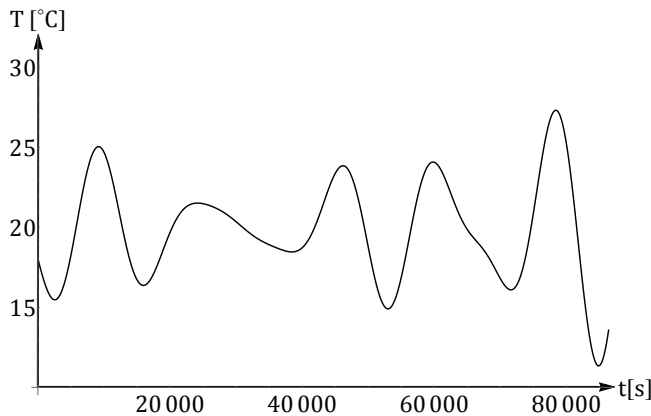
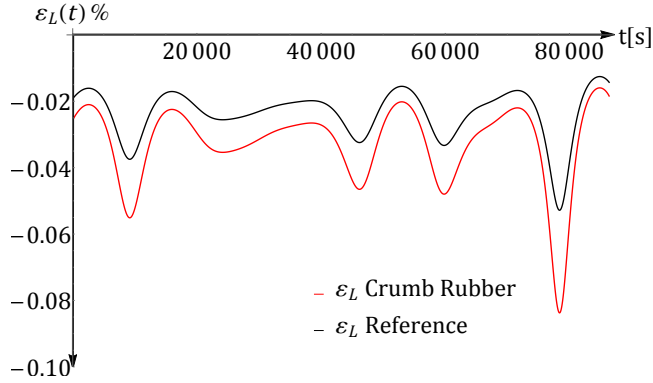


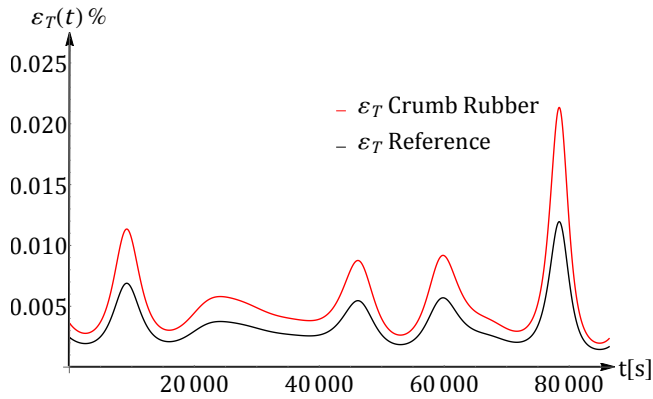
Figure 5.3: Temperature variations with time.

Figure 5.3 represents the applied temperature history.

Based on the temperature history $T(t)$ of Figure 5.3, the longitudinal and transversal strain, $\varepsilon_L(t)$ and $\varepsilon_T(t)$ is calculated according to Eq. (5.25). The longitudinal and transversal strain response, $\varepsilon_L(t)$ and $\varepsilon_T(t)$ are depicted in Figure 5.4.



(a) Longitudinal strain, $\varepsilon_L(t)$



(b) Transversal strain, $\varepsilon_T(t)$

Figure 5.4: Longitudinal and transversal strain response under the temperature history $T(t)$ reported in Figure 5.3.

From Figure 5.4, it is readily observed that the mechanical behaviour of the crumb rubber mixture shows higher deformations than the reference one but the recovery is also much higher, as discussed in Chapter 4. Furthermore, it has been shown the importance of temperature influence on the mechanical response of the bituminous mixtures under study.

5.5 Conclusions

In this chapter the temperature effect on viscoelastic materials has been discussed. In particular, the Time-Temperature Superposition Principle, the principle that deals with the relationship between time and temperature in viscoelastic materials, has been introduced. Then, its mathematical inconsistency has been demonstrated when fractional elements appear in the fractional constitutive laws.

Moreover, the mechanical behaviour of the 3D fractional viscoelastic model under varying temperature conditions has been evaluated using the discrete fractional operators presented in Chapter 1.

Finally the triaxial behaviour of the two bituminous mixtures (reference and crumb rubber), presented and characterised in Chapters 3 and 4, as railway sub-ballast are compared. Consequently, the creep behaviour has been simulated taking into account the temperature effect.

Concluding remarks

The most important conclusions obtained from this PhD thesis are here summarised.

The first chapter presents the basic concepts of fractional calculus including its most relevant properties. The manuscript starts introducing Fractional Calculus since fractional operators are necessary to understand and model the fractional viscoelastic behaviour. Furthermore, an approach based on the definition of the Riemann-Liouville fractional operators is proposed in order to provide a different discretisation technique as alternative to the Grünwald-Letnikov operator. This approach is used in the last chapter to model the viscoelastic behaviour under temperature effect.

The second chapter introduces linear fractional viscoelasticity. The basic concepts of linear viscoelasticity are presented in order to introduce the theory of linear fractional viscoelasticity. A review of mechanical models (focusing on mechanical models for asphalt mixtures) is done in order to better understand how they are related to the theory of 3D fractional viscoelasticity. Moreover, a methodology to distinguish the elastic and the viscous contribution and to calculate the fractional characteristic times has been proposed.

The third chapter proposes an analytical approach to the mix design optimisation of crumb rubber bituminous mixtures. This approach aims to design a crumb rubber mixture by modifying a reference bituminous mixture with a certain void content. The proposed methodology takes into account the deformation recovery of the rubber after compaction to obtain the desired void content in the mixture. Based on the experimental results, the analytical approach proposed is successful since it allows to design a crumb rubber mixture with the desired void content. Moreover, this approach permits to estimate the maximum rubber content that on a bituminous mixtures depending on a target void content.

The fourth chapter deals with the mechanical characterisation and the 3D

fractional viscoelastic model of the two asphalt mixtures (reference and crumb rubber asphalt) design in the previous chapter. The chapter starts with the theory of the 3D fractional viscoelasticity. From the creep-recovery test it has been observed that the crumb rubber mixture allows larger deformations but it recovers more than that of the reference asphalt. The cyclic test and the 3D fractional viscoelastic model have shown that the crumb rubber mixture is less stiff and more viscous than the reference one.

The last chapter deals with the temperature effect on bituminous mixtures for railway sub-ballast. The chapter starts with the introduction of the Time-Temperature Superposition Principle, this principle studies the relationship between time and temperature in viscoelastic materials. The mechanical behaviour of the 3D fractional viscoelastic model under varying temperature conditions has been evaluated using the discrete fractional operators presented in first chapter. The model parameters at different temperatures have been obtained through the triaxial test performed in the fourth chapter. Finally the triaxial behaviour of the two bituminous mixtures (reference and crumb rubber), presented and characterised in the two previous chapters as railway sub-ballast are compared.

Bibliography

- [Airey et al., 2003] Airey, G., Rahman, M., and Collop, A. (2003). Absorption of bitumen into crumb rubber using the basket drainage method. *International Journal of Pavement Engineering*, 4(2):105–119.
- [Akisetty et al., 2011] Akisetty, C., Xiao, F., Gandhi, T., and Amirkhanian, S. (2011). Estimating correlations between rheological and engineering properties of rubberized asphalt concrete mixtures containing warm mix asphalt additive. *Construction and Building Materials*, 25(2):950–956.
- [Alotta et al., 2016] Alotta, G., Barrera, O., Cocks, A., and Di Paola, M. (2016). On the behavior of a three-dimensional fractional viscoelastic constitutive model. *Meccanica*, pages 1–16.
- [Badagliacco et al., 2016] Badagliacco, D., Colinas-Armijo, N., Di Paola, M., and Valenza, A. (2016). Evaluation of the temperature effect on the fractional linear viscoelastic model for an epoxy resin. *AIP Conference Proceedings*, 1736(1):020089.
- [Bressi et al., 2017] Bressi, S., Colinas-Armijo, N., and Di Mino, G. (2017). Analytical approach for the mix design optimisation of bituminous mixtures with crumb rubber. *Materials and Structures*, page (Under Review).
- [Breuer and Onat, 1964] Breuer, S. and Onat, E. (1964). On the determination of free energies in linear viscoelastic solids. *Materials & Design*, 15:184–191.
- [Bueche, 1954] Bueche, F. (1954). The viscoelastic properties of plastics. *Journal of Chemical Physics*, 22:603–609.
- [Caputo, 1967] Caputo, M. (1967). Linear models of dissipation whose q is almost frequency independent-ii. *Geophysical Journal Royal Astronomic Society*, 13:529–539.

- [Caputo, 1969] Caputo, M. (1969). *Elasticità e Dissipazione*. Zanichelli.
- [Chesner et al., 1998] Chesner, W. H., Collins, R. J., and MacKay, M. H. (1998). User guidelines for waste and by-product materials in pavement construction. Technical report, No. FHWA-RD-97-148.
- [Christensen, 1971] Christensen, R. M. (1971). *Theory of viscoelasticity: An introduction*. New York: Academic Press.
- [Chupin et al., 2014] Chupin, O., Martin, A., Piau, J. M., and Hicher, P. Y. (2014). Calculation of the dynamic response of a viscoelastic railway structure based on a quasi-stationary approach. *International Journal of Solids and Structures*, 51(13):337–343.
- [Colinas-Armijo and Di Paola, 2017] Colinas-Armijo, N. and Di Paola, M. (2017). Step by step integration for fractional operators. *Communications in Nonlinear Science and Numerical Simulation*, (Under-Review).
- [Colinas-Armijo et al., 2017a] Colinas-Armijo, N., Di Paola, M., Badagliacco, D., and Valenza, A. (2017a). Time-temperature superposition principle through fractional characteristic times: experimental evidence on epoxy resin. *Mechanics of materials*, (Under-Review).
- [Colinas-Armijo et al., 2017b] Colinas-Armijo, N., Di Paola, M., and Di Matteo, A. (2017b). Fractional viscoelastic behaviour under stochastic temperature process. *Probabilistic Engineering Mechanics*, (In Press).
- [Colinas-Armijo et al., 2016] Colinas-Armijo, N., Di Paola, M., and Pinnola, F. (2016). Fractional characteristic times and dissipated energy in fractional linear viscoelasticity. *Communications in Nonlinear Science and Numerical Simulation*, 37:14–30.
- [D’Andrea et al., 2012] D’Andrea, A., Loprencipe, G., and Xhixha, E. (2012). Vibration Induced by Rail Traffic: Evaluation of Attenuation Properties in a Bituminous Sub-ballast Layer. *Procedia - Social and Behavioral Sciences*, 53:245–255.
- [Dantas Neto et al., 2005] Dantas Neto, S. A., de Farias, M. M., Mello, L. G. R., Pereira, P. A. A., and Pais, J. C. (2005). The use of crumb rubber in asphalt mixtures using the dry process. *2005 international symposium on pavement recycling são paulo*.

- [Dealy and Plazek, 2009] Dealy, J. and Plazek, D. (2009). Time-temperature superposition - a users guide. *Rheology Bulletin*, 78:Pages 16–31.
- [Deseri et al., 2014] Deseri, L., Di Paola, M., and Zingales, M. (2014). Free energy and states of fractional-order hereditariness. *International Journal of Solids and Structures*, 51:3156–3167.
- [Di Paola et al., 2013a] Di Paola, M., Pinnola, F. P., and Zingales, M. (2013a). A discrete mechanical model of fractional hereditary materials. *Meccanica*, 48(7):1573–1586.
- [Di Paola et al., 2013b] Di Paola, M., Pinnola, F. P., and Zingales, M. (2013b). Fractional differential equations and related exact mechanical models. *Computers and Mathematics with Applications*, 66:608–620.
- [Di Paola and Zingales, 2012] Di Paola, M. and Zingales, M. (2012). Exact mechanical models of fractional hereditary materials. *Journal of Rheology*, 56(5):983–1004.
- [Dong et al., 2012] Dong, D., Huang, X., Li, X., and Zhang, L. (2012). Swelling process of rubber in asphalt and its effect on the structure and properties of rubber and asphalt. *Construction and Building Materials*, 29:316–322.
- [Doolittle and Doolittle, 1957] Doolittle, A. and Doolittle, D. (1957). Studies in newtonian flow. further verification of the free-space viscosity equation. *Journal of Applied Physics*, 28:901–905.
- [Fabrizio et al., 1994] Fabrizio, M., Giorgi, C., and Morro, A. (1994). Free energies and dissipation properties for systems with memory. *Archive for Rational Mechanics and Analysis*, 125:341–373.
- [Fabrizio et al., 1995] Fabrizio, M., Giorgi, C., and Morro, A. (1995). Internal dissipation, relaxation property, and free energy in materials with fading memory. *Journal of Elasticity*, 40:107–122.
- [Fabrizio and Morro, 1988] Fabrizio, M. and Morro, A. (1988). Viscoelastic relaxation functions compatible with thermodynamics. *Journal of Elasticity*, 19:63–75.
- [Ferry, 1980] Ferry, J. (1980). *Viscoelastic properties of polymers*. John Wiley & Sons.

- [Flügge, 1967] Flügge, W. (1967). *Viscoelasticity*. Blaisdell Publishing Company.
- [Freed and Diethelm, 2006] Freed, A. D. and Diethelm, K. (2006). Fractional calculus in biomechanics: a 3d viscoelastic model using regularized fractional derivative kernels with application to the human calcaneal fat pad. *Biomechanics and modeling in mechanobiology*, 5(4):203–215.
- [Fukunaga and Shimizu, 2015] Fukunaga, M. and Shimizu, N. (2015). Fractional derivative constitutive models for finite deformation of viscoelastic materials. *Journal of Computational and Nonlinear Dynamics*, 10(6):061002.
- [Gurtin and Hrusa, 1988] Gurtin, M. and Hrusa, W. (1988). On energies for nonlinear viscoelastic materials of single-integral type. *Quarterly of Applied Mathematics*, 46:381–392.
- [Heitzman, 1992] Heitzman, M. (1992). Design and construction of asphalt paving materials with crumb rubber modifier. *Transportation Research Board, Washington, DC*, 1339.
- [Hernández-Olivares et al., 2009] Hernández-Olivares, F., Witoszek-Schultz, B., Alonso-Fernández, M., and Benito-Moro, C. (2009). Rubber-modified hot-mix asphalt pavement by dry process. *International Journal of Pavement Engineering*, 10(4):277–288.
- [Hilton, 2012] Hilton, H. H. (2012). Generalized fractional derivative anisotropic viscoelastic characterization. *Materials*, 5(1):169–191.
- [Huang et al., 2007] Huang, Y., Bird, R. N., and Heidrich, O. (2007). A review of the use of recycled solid waste materials in asphalt pavements. *Resources, Conservation and Recycling*, 52(1):58–73.
- [Huet, 1963] Huet, C. (1963). *Etude par une méthode d'impédance du comportement viscoélastique des matériaux hydrocarbonés*. PhD thesis, Faculté des Sciences de l'université de Paris.
- [Issa and Salem, 2013] Issa, C. A. and Salem, G. (2013). Utilization of recycled crumb rubber as fine aggregates in concrete mix design. *Construction and Building Materials*, 42:48–52.
- [Kaelble, 1985] Kaelble, D. H. (1985). *Computer aided design of polymers and composites*, volume 7. CRC Press.

- [Kilbas et al., 2006] Kilbas, A., Srivastave, H., and Trujillo, J. (2006). *Theory and applications of fractional differential equations*. Elsevier, Amsterdam.
- [Lee et al., 2008] Lee, S., Amirkhani, S., and Kwon, S. (2008). The effects of compaction temperature on crm mixtures made with the sgc and the marshall compactor. *Construction and Building Materials*, 22(6):1122–1128.
- [Lo Presti, 2013] Lo Presti, D. (2013). Recycled Tyre Rubber Modified Bitumens for road asphalt mixtures: A literature review. *Construction and Building Materials*, 49:863–881.
- [López-Moro et al., 2013] López-Moro, F. J., Moro, M. C., Hernández-Olivares, F., Witoszek-Schultz, B., and Alonso-Fernández, M. (2013). Microscopic analysis of the interaction between crumb rubber and bitumen in asphalt mixtures using the dry process. *Construction and Building Materials*, 48:691–699.
- [Losa et al., 2011] Losa, M., Leandri, P., and Bacci, R. (2011). Mix design and performance evaluation of crm-modified asphalt concrete mixtures. *5th International Conference Bituminous Mixtures and Pavements*.
- [Maggiore et al., 2012] Maggiore, C., Mino, G. D., Liberto, M. D., and Airey, G. (2012). Mechanical characterisation of dry asphalt rubber concrete for base layers by means of the four bending point tests. *Proceedings of the 3rd Conference on Four-Point Bending*, 123.
- [Makris, 1997] Makris, N. (1997). Three-dimensional constitutive viscoelastic laws with fractional order time derivatives. *Journal of Rheology*, 41(5):1007–1020.
- [McDonald, 1981] McDonald, C. H. (1981). Recollections of early asphalt-rubber history. *National Seminar on Asphalt-Rubber*.
- [Miller and Ross, 1993] Miller, K. S. and Ross, B. (1993). *An Introduction to the Fractional Calculus and Fractional Differential Equations*. Wiley-InterScience, New York.
- [Moreno et al., 2011] Moreno, F., Rubio, M., and Martinez-Echevarria, M. (2011). Analysis of digestion time and the crumb rubber percentage in dry-process crumb rubber modified hot bituminous mixes. *Construction and Building Materials*, 25(5):2323–2334.

- [Navarro et al., 2004] Navarro, F. J., Partal, P., Martínez-Boza, F., and Gallegos, C. (2004). Thermo-rheological behaviour and storage stability of ground tire rubber-modified bitumens. *Fuel*, 83(14-15):2041–2049.
- [Nutting, 1921] Nutting, P. G. (1921). A new general law of deformation. *Journal of The Franklin Institute*, 191:679–685.
- [Oeser and Pellinien, 2012] Oeser, M. and Pellinien, T. (2012). Computational framework for common visco-elastic models in engineering based on the theory of rheology. *Computers and Geotechnics*, 42:145–156.
- [Olard and Di Benedetto, 2003] Olard, F. and Di Benedetto, H. (2003). General “2S2P1D” model and relation between the linear viscoelastic behaviours of bituminous binders and mixes. *Road materials and pavement design*, 4(2):185–224.
- [Oldham and Spainer, 1974] Oldham, K. B. and Spainer, J. (1974). *The Fractional Calculus: Theory and applications of differentiation and integration to arbitrary order*. Academic Press, New York.
- [Pettinari and Simone, 2015] Pettinari, M. and Simone, A. (2015). Effect of crumb rubber gradation on a rubberized cold recycled mixture for road pavements. *Materials & Design*, 85:598–606.
- [Podlubny, 1998] Podlubny, I. (1998). *Fractional differential equations: an introduction to fractional derivatives, fractional differential equations, to methods of their solution and some of their applications*. Academic press.
- [Rahman, 2004] Rahman, M. (2004). *Characterisation of dry process crumb rubber modified asphalt mixtures*. PhD thesis, University of Nottingham.
- [Rebala and Estakhri, 1995] Rebala, S. R. and Estakhri, C. K. (1995). Laboratory evaluation of crumb rubber modified mixtures designed using TxDOT mixture design method. *Transportation Research Record*, 1515:1–10.
- [Rose et al., 2011] Rose, J., Teixeira, P., and Veit, P. (2011). International design practices, applications, and performances of asphalt/bituminous railway trackbeds. *GEORAIL 2011–International*, pages 19–20.
- [Samko et al., 1993] Samko, G. S., Kilbas, A. A., and Marichev, O. I. (1993). *Fractional Integrals and Derivatives: Theory and Applications*. Gordon and Breach, New York.

- [Sayegh, 1965] Sayegh, G. (1965). *Contribution à l'étude des propriétés viscoélastiques des bitumes purs et des bétons bitumineux*. PhD thesis, Faculté des Sciences de l'université de Paris.
- [Schofield, 1989] Schofield, L. (1989). The history, development, and performance of asphalt rubber at adot: Special report. Technical report, No. AZ-SP-8902.
- [Scott Blair, 1966] Scott Blair, G. W. (1966). The subjective assessment of the consistency of materials in relation to physical measurements. *Journal of the Society of Cosmetic Chemists*, 17(1):45–56.
- [Scott Blair, 1974] Scott Blair, G. W. (1974). Psychorheology: links between the past and the present. *Journal of Texture studies*, 5(1):3–12.
- [Scott Blair and Caffyn, 1949] Scott Blair, G. W. and Caffyn, J. E. (1949). Vi. an application of the theory of quasi-properties to the treatment of anomalous strain-stress relations. *The Philosophical Magazine and Journal of Science*, 40(300):80–94.
- [Sohm, 2011] Sohm, J. (2011). *Prédiction des déformations permanentes des matériaux bitumineux*. PhD thesis, Ecole Centrale de Nantes.
- [Sohm et al., 2012] Sohm, J., Gabet, T., Hornych, P., Piau, J. M., and Di Benedetto, H. (2012). Creep tests on bituminous mixtures and modelling. road materials and pavement design. *Road Materials and Pavement Design*, 13(4):832–849.
- [Tortum et al., 2005] Tortum, A., Çelik, C., and Aydin, A. (2005). Determination of the optimum conditions for tire rubber in asphalt concrete. *Building and Environment*, 40(11):1492–1504.
- [Tschoegl, 2012] Tschoegl, N. (2012). *The phenomenological theory of linear viscoelastic behavior: an introduction*. Springer Science & Business Media.
- [Tschoegl et al., 2002] Tschoegl, N., Knauss, W., and Emri, I. (2002). The effect of temperature and pressure on the mechanical properties of thermo- and/or piezorheologically simple polymeric materials in thermodynamic equilibrium—a critical review. *Mechanics of Time-Dependent Materials*, 6(1):53–99.

- [Van Gorp and Palmen, 1998] Van Gorp, M. and Palmen, J. (1998). Time-temperature superposition for polymeric blends. *Rheology Bulletin*, 67(1):58.
- [Williams et al., 1955] Williams, M., Landel, R., and Ferry, J. (1955). The temperature dependence of relaxation mechanisms in amorphous polymers and other glass-forming liquids. *Journal of American Chemical Society*, 77:3701–3707.
- [Xiao et al., 2009] Xiao, F., Amirkhanian, S., Shen, J., and Putman, B. (2009). Influences of crumb rubber size and type on reclaimed asphalt pavement (rap) mixtures. *Construction and Building Materials*, 23(2):1028–1034.

Acknowledgements

I am immensely grateful to Prof. Mario Di Paola for his time, his patient, his teachings, his advices and his wise guide. It has been an honour having him as supervisor.

I appreciate the support, time and advices from Prof. Gaetano Di Mino, Prof. Giuseppe Muscolino, Prof. Antonina Pirrotta, Prof. Laura Inzerillo and Prof. Antonino Valenza.

I would like to thank IFSTTAR (Institut français des sciences et technologies des transports, de l'aménagement et des réseaux) where I spend 6 months of this PhD that allowed me to perform the experimental results reported in this manuscript. Specially, I am really grateful to Thomas, Olivier and Jean-Michel for their warm welcoming, their time, availability and kindness.

I have been really fortunate to having colleagues and friends like Sara, Edwina, Francesco, Pietro, Emma, Gioacchino, Mohsen, Salvo, Alberto and Dionisio. Thanks to my SUP&R friends and supervisors, without you this experience would not have been the same.

Thank you Palermo and the Marie curie experience, this three years living in such particular place and conditions have made me grow and open my mind.

I have not words to explain how grateful I am with all my family and friends. Thank you mama and papa for supporting me even if you could not understand my motivations and feelings. Thank you Zurbi for loving me as I am and for your unconditional support. Finally I have to express my gratitude to my granddad Gabino, even if you left us a long time ago, I could not have arrived here without all the love and teachings that I have received from you during the fourteen year that I shared with you.

Natalia Colinas-Armijo
Palermo, September 2017

